

1998

Paramagnetic Nuclear Magnetic Resonance (NMR) Studies on the Calcium Binding Site of [Alpha]- Lactalbumin

Thomas Kurt Ritter
Portland State University

Follow this and additional works at: https://pdxscholar.library.pdx.edu/open_access_etds

 Part of the [Chemistry Commons](#)

Let us know how access to this document benefits you.

Recommended Citation


Ritter, Thomas Kurt, "Paramagnetic Nuclear Magnetic Resonance (NMR) Studies on the Calcium Binding Site of [Alpha]-Lactalbumin" (1998). *Dissertations and Theses*. Paper 6372.
<https://doi.org/10.15760/etd.3518>

This Thesis is brought to you for free and open access. It has been accepted for inclusion in Dissertations and Theses by an authorized administrator of PDXScholar. Please contact us if we can make this document more accessible: pdxscholar@pdx.edu.

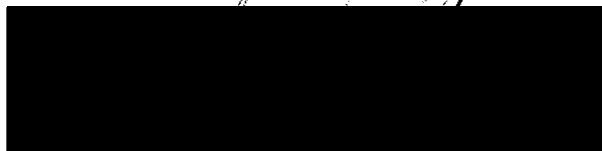
THESIS APPROVAL

The abstract and thesis of Thomas Kurt Ritter for the Master of Science in Chemistry were presented June 29, 1998, and accepted by the thesis committee and the department.

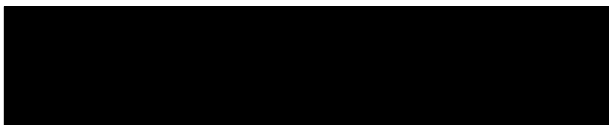
COMMITTEE APPROVALS:



David H. Peyton, Chair



Dirk Iwata-Reuyl

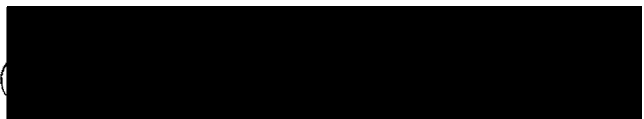


Jie Lin



Pavel R. Smejtek
Representative of the Office of Graduate Studies

DEPARTMENT APPROVAL:



David H. Peyton, Chair
Department of Chemistry

ABSTRACT

An abstract of the thesis of Thomas Kurt Ritter for the Master of Science in Chemistry presented June 29, 1998.

Title: Paramagnetic Nuclear Magnetic Resonance (NMR) Studies on the Calcium Binding Site of α -Lactalbumin.

Paramagnetic NMR has drawn interest as a technique for extending the range of systems that can be investigated. The purpose of this study was to determine whether a combination of paramagnetic two-dimensional and relaxation techniques allows for assigning resonances corresponding to residues forming the metal binding site of proteins in which the metal is coordinated exclusively by amino acid side chains and which have been previously inaccessible to assignment.

α -Lactalbumin (LA) is a calcium binding protein with relatively broad NMR signals; this broadness has prevented complete assignment. LA has been the subject of many studies, because it can form a molten globule state which is closely related to one of the intermediates in protein folding. The assignment of LA's resonances could therefore serve as basis for experiments investigating protein folding.

In a first approach, calcium was exchanged for gadolinium, which enhances relaxation. However, the properties of gadolinium turned out to be too strong to allow for discrimination between resonances. In a second approach, calcium was exchanged for ytterbium, which has strong hyperfine-shifting properties. The melting point of ytterbium LA was determined by observing the change in NMR peak intensities with temperature. Hyperfine-shifted resonances were assessed as completely as possible by one-dimensional NMR experiments, connected into spin-systems by two-dimensional

NMR experiments, and their spin-lattice and spin-spin relaxation times were determined. Assignment of the residues constituting the metal binding site was then sought with the help of LA's crystal structure and exchange experiments. Although the combined experimental data suggests one model of resonance assignments, they must be seen as tentative for three reasons. First, the crystal and solution structures of the metal binding site might differ significantly. Second, the relaxation enhancing properties of ytterbium might be strong enough to broaden the resonances of the closest protons to such an extent that they become invisible in the NMR spectrum. Third, different mechanisms of the protons closest to the metal binding site and those further away might govern relaxation which would complicate systematic interpretation of the data.

PARAMAGNETIC NUCLEAR MAGNETIC RESONANCE (NMR) STUDIES
ON THE CALCIUM BINDING SITE OF α -LACTALBUMIN

by

THOMAS KURT RITTER

A thesis submitted in partial fulfillment of the
requirements for the degree of

MASTER OF SCIENCE

in

CHEMISTRY

Portland State University

1998

ACKNOWLEDGMENTS

I would like to take this opportunity to express my appreciation and gratitude to those who offered support and encouragement during the two years I spent at Portland State University.

First and foremost I wish to acknowledge my advisor Dr. David Peyton for his guidance throughout this work. Without his help the successful completion of this thesis would not have been possible.

I would like to thank Drs. Dirk Iwata-Reuyl, Jie Lin, and Pavel Smejtek for serving on the committee and the time they spent reading my thesis.

Many thanks go out to all my friends that I have met in the past two years, you guys greatly enriched my stay here in Portland. I am especially grateful to the other members of the Peyton group, Ayna Alfadhli, Jane Kelly, and Run Zhang, for their support, encouragement, and the great working atmosphere they provided.

I would also like to acknowledge the financial support granted by the Oregon/Baden-Württemberg exchange program and Portland State University without which it would not have been possible for me to study abroad.

Finally, I wish to express my gratitude to my parents in Germany for their never ending support and the patience they had and still have with their son who keeps on extending his stay in the United States.

TABLE OF CONTENTS

Acknowledgments.....	i
Table of Contents.....	ii
List of Tables	iv
List of Figures	v
List of Abbreviations.....	vii
1. Introduction.....	1
1.1 Lactalbumin Function and Structure.....	1
1.2 LA folding and the Molten Globule State.....	5
1.3 Previous NMR Studies on Lactalbumin	7
1.4 Paramagnetic NMR.....	9
1.5 Scope of this study	14
2. Materials and Methods.....	17
2.1 Materials	17
2.2 Instrumentation	18
2.3 Titrations.....	19
2.4 1D NMR Experiments on Yb-LA.....	20
2.5 2D NMR Experiments on Yb-LA.....	21
2.6 T_1 and T_2 Determination	22
2.7 2D Exchange Experiments.....	23
3. Results and Discussion.....	24
3.1 Studies on Gd-LA	24
3.2 Studies on Yb-LA	26
3.2.1 Temperature Stability	26

3.2.2 Assessment of Hyperfine Shifted Resonances	29
3.2.3 Two-dimensional Connectivities	34
3.2.4 Measurement of Relaxation Times	39
3.2.5 Correlation to the Crystal Structure	42
3.2.6 Exchange Studies	47
4. Conclusion.....	49
Tables.....	51
Figures.....	57
References.....	88
Appendix A	93
Appendix B	95

LIST OF TABLES

1. Summary of One-Dimensional NMR Experiments.....	51
2. Summary of Two-Dimensional NMR Experiments.....	52
3. Complete Listing of the Hyperfine Shifted Peaks Detected in the 1D Spectra of Yb-LA.....	53
4. T_1 and T_2 Values of the Hyperfine Shifted Resonances in the 1D NMR Spectrum of Yb-LA.....	54
5. Distances between Ca^{2+} and nearby Protons in the Crystal Structure of Bovine LA.....	55
6. Modification of Table 5 by Taking the Average Distances for Equivalent Methyl and Ring Protons.....	56

LIST OF FIGURES

1. Primary Structures of Guinea Pig, Human and Bovine LA.....	57
2. Ribbon Diagram of the Crystal Structure of Bovine LA.....	58
3. The Ca ²⁺ Binding Site of Bovine LA	59
4. Superposition of the Ca ²⁺ Binding Loops of Human and Bovine LA	60
5. The “Calcium Elbow” in LA.....	61
6. Titration of Ca-LA with Gd ³⁺	62
7. Superposition of Three COSY Spectra in ANSIG	63
8. Temperature Dependence of the 1D NMR Spectrum of Ca-LA	64
9. Temperature Dependence of Peak Intensities in the 1D NMR Spectra of Calcium and Ytterbium LA.....	65
10. Temperature Dependence of the 1D NMR Spectrum of Yb-LA	66
11. Titration of Ca ²⁺ Depleted LA with Yb ³⁺	67
12. 1D Spectra of Yb-LA with Short Recycle Delays	68
13. SUPERWEFT of Yb-LA in D ₂ O.....	69
14. SUPERWEFT of Yb-LA in H ₂ O.....	70
15. 1D Spectra of Yb-LA with different solvent suppression	71
16. 1D Spectra of Yb-LA at 90 and 500 MHz.....	72
17. 1D Spectra of Human and Bovine Yb-LA	73
18. Extrapolation of the temperature behavior of the hyperfine shifted resonances	74
19. COSY Spectrum of Yb-LA	75
20. NOESY Spectrum of Yb-LA (Mixing Time 80 ms)	76
21. Upfield Region of Figure 20.....	77
22. Downfield Region of Figure 20	78

23. NOESY Spectrum of Yb-LA (Mixing Time 20 ms).....	79
24. 1D NOE Spectra of Yb-LA.....	80
25. 1D NOE Spectra of Yb-LA.....	81
26. Summary of Cross Signals between Hyperfine Shifted Resonances in the 2D NMR Spectra of Yb-LA	82
27. T_1 IR Experiment of Yb-LA (transmitter at 4.76 ppm).....	83
28. T_1 IR Experiment of Yb-LA (transmitter at 57.4 ppm).....	84
29. T_1 IR Experiment of Yb-LA (transmitter at 37.3 ppm).....	85
30. Linear Regression of Peak Intensities of Some Resonances of Yb-LA for T_1 Determinations by Inversion Recovery	86
31. Peak Simulations of Some Resonances of Yb-LA for T_2 Determinations from Linewidths.....	87

LIST OF ABBREVIATIONS AND SYMBOLS

1D	One-dimensional
2D	Two-dimensional
β	Electron Bohr magneton
γ_I	Nuclear gyromagnetic ratio
δ	Chemical shift
δ_{DIA}	Diamagnetic chemical shift
δ_{FC}	Fermi contact shift
δ_{PC}	Pseudo contact shift
η	Viscosity
φ	Spherical coordinate
θ	Spherical coordinate
τ_C	Total correlation time
τ_M	Mixing time and exchange correlation time
τ_R	Rotational correlation time
τ_S	Electron spin correlation time
Ω	Chemical shift offset
ω_I	Nuclear Larmor frequency
ω_S	Electron Larmor frequency
a	Molecular radius including hydration layer
ANSIG	Assignment of NMR Spectra by Interactive Graphics
B_0	External magnetic field
Ca-LA	Lactalbumin with Ca^{2+} in the Calcium Binding Site
COSY	Correlated Spectroscopy

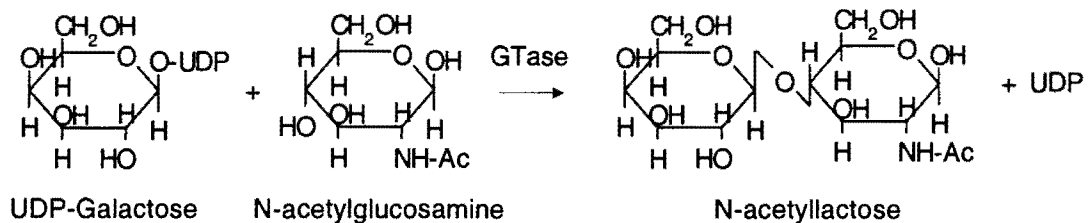
DQF-COSY	Double Quantum Filtered-Correlation Spectroscopy
DSS	2,2-dimethyl-2-silapentane-5-sulfonate
EDTA	Ethylenediaminetetraacetate
EXSY	Exchange Spectroscopy
FID	Free Induction Decay
FWHH	Full width at half height
Gd-LA	Lactalbumin with Gd ³⁺ in the Calcium Binding Site
g_j	Landé g factor
GlcNAc	N-Acetylglucosamine
GTase	Galactosyltransferase
I	Peak intensity
J	Total angular momentum
k	Boltzman's constant
K_d	Dissociation constant
K_M	Michaelis-Menten constant
LA	Lactalbumin
M_0	Magnitude of equilibrium magnetization
m_p	Melting point
NMR	Nuclear Magnetic Resonance
NOE	Nuclear Overhauser Effect
NOESY	Nuclear Overhauser Effect Spectroscopy
PAGE	Polyacrylamide Gel Electrophoresis
pdb	Protein Data Bank
POV	Persistence of Vision
r	Spherical coordinate

R_1	Spin-lattice relaxation rate constant
R_2	Spin-spin relaxation rate constant (theoretical)
R_2^*	Spin-spin relaxation rate constant (experimental)
$R_{2,\text{inhom}}$	Spin-spin relaxation rate constant (from field inhomogeneities)
S/N	Signal to Noise Ratio
super-WEFT	“Super”-Water Eliminated Fourier Transform Spectroscopy
SW	Spectral Window
T_1	Spin-lattice relaxation time
$T_{1\chi}$	Curie spin contribution to the spin-lattice relaxation time
T_{1e}	Longitudinal electron spin relaxation time
T_{1M}	Dipolar contribution to the spin-lattice relaxation time
T_2	Spin-spin Relaxation Time
$T_{2\chi}$	Curie spin contribution to the spin-spin relaxation time
T_{2e}	Transversal electron spin relaxation time
T_{2M}	Dipolar contribution to the spin-spin relaxation time
TOCSY	Total Correlated Spectroscopy
TPPI	Time proportional phase-incrementation
UDP	Uridine Diphosphate
WEFT	Water Eliminated Fourier Transform Spectroscopy
Yb,Ca-LA	Lactalbumin with Yb ³⁺ and Ca ²⁺ in the Calcium Binding Site
Yb-LA	Lactalbumin with Yb ³⁺ in the Calcium Binding Site

1. Introduction

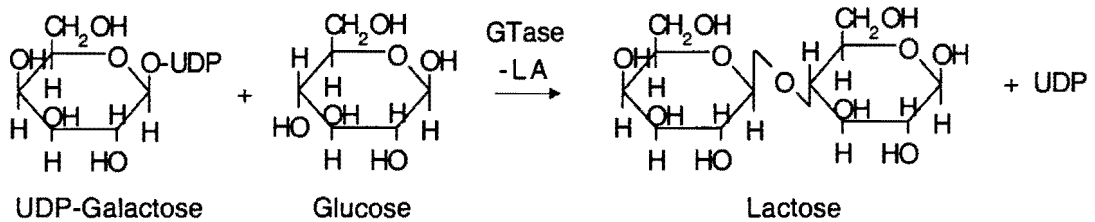
1.1 Lactalbumin Function and Structure

α -Lactalbumin (from the Latin “lacteum album”, meaning a white substance from milk) was one of the first proteins to be isolated, probably as early as in the late 19th century. This is not surprising if one considers its origin: it comprises some 15% of milk whey proteins of most mammalian species (Jenness, 1971). Lactalbumin (LA) can be isolated easily by salting out with ammonium sulfate in the presence of dilute acid (Widman, 1899). In spite of this early availability, it took many years to establish LA’s function other than serving as nutrient for young mammals. In 1966, lactose synthase was resolved into two protein components (Brodbeck & Ebner, 1966), one of which turned out to be identical to LA (Brodbeck et al., 1967). The second component of lactose synthase is galactosyltransferase (GTase). GTase is ubiquitous in cells, it is involved in the biosynthesis of glycoproteins by catalyzing the reaction



During lactation, however, LA is synthesized in the mammary gland. It binds to GTase, thereby decreasing the K_M (Michaelis-Menten constant) of GTase for glucose by approximately three orders of magnitude, while inhibiting the reaction involving N-

Acetylglucosamine (GlcNAc) as an acceptor (Hill & Brew, 1975). Consequently, after LA binding GTase transfers UDP-galactose no longer to GlcNAc but to glucose:



Although there has been considerable interest in how this modulation of catalytic activity of GTase by LA is achieved, there is little unambiguous information available. Understanding of the interaction between the two proteins depends on insights into their structure. This is not easy in the case of GTase since it is an integral trans-Golgi protein. Liberation of proteins from the membrane is often only possible under harsh conditions, and once released from their natural environment they often aggregate and precipitate from aqueous solution.

Structural investigations on LA have proved to be more fruitful. The primary structure of LAs from a wide variety of species have been elucidated (Figure 1). They are all of virtually the same size, with the exception of rat LA which has a 17 residue carboxyl terminal extension (Prasad et al., 1982). Comparison between the primary structure of LA and lysozyme yielded 40% identity. This confirmed a long-cherished assumption: LA and lysozyme are thought to be derived from the same ancestral protein (Shewale et al., 1984). They function on the same type of bond, though in opposite directions: lysozyme hydrolyzes glycosidic bonds in bacterial cell walls, while LA participates in the formation of glycosidic bonds as described above. Moreover,

lysozyme catalyses a reaction, whereas LA only changes the substrate specificity of another enzyme.

Up to now the X ray structures of LAs of several species have been solved (Figure 2): baboon at 1.7 Å resolution (Acharya et al., 1989), human at 1.7 Å resolution (Acharya et al., 1991), guinea pig at 1.9 Å, goat at 2.3 Å, and bovine at 2.3 Å resolution (Pike et al., 1996). Comparison between the three-dimensional structures of LA and lysozyme corroborates their relatedness.

The LA molecule is composed of two domains, an α -helical domain (residues 1-34 and 86-123, the numbering corresponds to the primary structure of bovine LA) and a β -sheet domain (residues 35-85). LA is roughly ellipsoidal in shape with dimensions of 23 Å x 26 Å x 40 Å. It contains four α -helices (residues 5-11, 23-34, 86-98, and 105-110) and three 3_{10} -helices (residues 18-20, 77-80, and 115-118). The single anti-parallel β -sheet is comprised of three strands (residues 41-44, 47-50, and 55-56). Four disulfides stabilize the protein structure (residues 6-120, 28-111, 61-77, and 73-91).

Further, LA features at least two metal binding sites. This property is shared by just a handful of the evolutionarily related lysozymes. LA has been shown to bind numerous metal ions, and this binding has been studied intensively especially by Berliner and co-workers (Berliner et al., 1983, Berliner et al., 1987, Musci & Berliner, 1985, Musci et al., 1986). Identification of two distinct binding sites, however, became possible only after successful crystallization of human LA in the presence of both Ca^{2+} and Zn^{2+} (Ren et al., 1993). The two sites bind metals with different affinities; the high-affinity binding site has been termed the Ca^{2+} site, while the low-affinity binding site has been termed the Zn^{2+} site. The Zn^{2+} site is rather flexible, with the metal ion coordinated by two glutamic acid residues (49 and 116) and two water molecules. Zn^{2+} binds with a dissociation constant (K_d) of 5 μM . The Zn^{2+} site also

accommodates a wide variety of other metal ions such as Mg^{2+} , Sn^{2+} , Hg^{2+} , Co^{2+} , Cu^{2+} , and Tl^{3+} .

The Ca^{2+} site is far more rigid. Ca^{2+} binds with a K_d of 0.1-0.01 μM over a pH range from 6.6 to 8.4 (Eberhard & Erne, 1991); it can be replaced by the lanthanides which bind with stronger affinity. Other metal ions that bind with weaker affinity to the Ca^{2+} site include Sr^{2+} , Cd^{2+} , Pb^{2+} , Ba^{2+} , and Sc^{2+} (Aramini et al., 1996). The metal ions in the Ca^{2+} site are coordinated by Asp 82, Asp 87, and Asp 88 via the side chain carboxylates, by Lys 79 and Asp 84 via backbone carbonyl groups, and by two water molecules (Figure 3). The geometry of the Ca^{2+} binding site is related to the so-called EF hand found in many other Ca^{2+} binding proteins such as carp parvalbumin and calmodulin. However, while the overall coordination in the EF hand is a distorted octahedron, Ca^{2+} in crystalline LA is coordinated by a pentagonal bipyramid. This unique binding motif in LA is referred to as the “calcium binding elbow” (Stuart et al., 1986). The elbow consists of a tight loop of five residues flanked by two nearly orthogonal helical segments, a short 3_{10} - and a long α -helix (Figures 4 and 5).

LA, as generally isolated, contains a single bound Ca^{2+} (Hiraoka et al., 1980), the role of which has yet to be established. The region of contact between LA and GTase has been identified by differential kinetic labeling (Richardson & Brew, 1980): LA in the free state and in a 1:1 complex with GTase was acetylated with trace amounts of [3H]-acetic anhydride and the reactivity of the lysine amino groups in both samples were compared. The distance between the region of contact between the two proteins and the Ca^{2+} site is too great for the Ca^{2+} to participate directly in the formation of the lactose synthase complex or in the catalysis. Several observations make a structural role of Ca^{2+} seem most likely: its abstraction from LA with EDTA decreases the protein's stability (Hiraoka et al., 1980). Further, refolding of LA from the reduced, denatured

state into its native form with a high level of activity and accurately arranged disulfides depends on the presence of Ca^{2+} (Rao & Brew, 1989).

1.2 LA folding and the Molten Globule State

One of the most interesting features of LA is its folding behavior. Most globular proteins, including lysozyme, follow the two-state model. They unfold cooperatively into a totally denatured state under conditions of high temperature or extreme pH, or in the presence of chaotropic reagents (Tanford, 1968). LA, however, changes its conformation among at least three states when exposed to denaturing conditions (Kuwajima, 1989):



Moderate denaturing conditions cause a cooperative unfolding of the native protein into an intermediate state. Unfolding of the intermediate state occurs uncooperatively and only in the presence of high concentrations of denaturants (Shimizu et al., 1993). The intermediate state can be induced by acidic conditions (A-state) or by elevated temperatures (T-state) (Dolgikh et al., 1985). The A- and T-states have been shown to be structurally closely related (Improta et al., 1995). They are actually compact, heterogeneous states. Their α -helical domain is structured with the β -domain being significantly unfolded. Although extensive stretches of well-defined secondary structure are present, a specific and stable tertiary structure is missing.

The properties of the intermediate states resemble those of the so-called molten globules. Their existence has been proposed as a solution to the Levinthal paradox (Levinthal, 1968): it would take proteins a very long time to fold into their native structure, if they had to find an energy minimum through random exploration of all available conformations. Yet, many proteins fold into their native conformation in a matter of a few seconds. This rapid folding cannot be caused exclusively by other proteins such as proline cis/trans isomerases and chaperones, since refolding of most proteins happens in the absence of folding supporting proteins *in vitro* on the same fast time-scale. Protein folding is therefore thought to occur via a multi-stage process (Ptitsyn, 1991).

In the first stage short stretches of secondary structure are formed and fall apart in short time intervals. These so-called nuclei exist for less than a millisecond. Nuclei with structures resembling the native state grow, because their stability is high as compared to non-native like folds. They become even more stable as their size increases and start to build up domains. Within a second after folding has been initiated, the domains join into a larger entity which is called the molten globule. The molten globule is characterized by extensive secondary structure, but disordered tertiary structure. From this conformation the protein gets into its native state by small adjustments. Folding via an organized pathway is much more efficient than systematic exploration of all possible conformations. The peptide chain drifts very quickly into its energetically minimum structure. Unfortunately, not much is known about the properties of the folding intermediates, because folding occurs in a matter of seconds.

Since the intermediate states of LA denaturation share structural properties with the molten globule, they are often referred to as molten globule states. Their stability over a relatively wide temperature and pH range facilitates the investigation of their

structure. Although one has to be aware of the differences between the molten globule, which is a kinetic intermediate, and the thermodynamically stable A- and T-states, it is probably valid to draw conclusions about the molten globule from the properties of the intermediate states. Investigation of their structures might therefore lead to insights into the process of protein folding.

1.3 Previous NMR Studies on Lactalbumin

Although several NMR studies have been aimed at elucidating the structure of LA, complete assignment of all resonances turned out to be impossible. This can be rationalized by a combination of several factors. First, the size of LA (14.2 kDa) is at or above the upper limit of the sequential assignment method (Wüthrich, 1986). Second, NMR spectra of LA feature relatively broad signals. This may be attributed to LA's high conformational flexibility especially in the C-terminal region, an observation that is also related to the poor electron density in the X ray crystal structure (Acharya et al., 1991). Third, the sequence of LA contains many amino acids with complex spin systems, whereas the number of readily identifiable (unique) spin systems is relatively low. In bovine LA, for example, out of a total of 122 residues eight are isoleucines and thirteen are leucines, whereas the number of alanines, glycines, threonines, and valines is only three, six, seven, and six, respectively.

Several studies by the Dobson group led to partial assignment. The aromatic regions were solved by comparing the two-dimensional spectra of LA of several different species (Alexandrescu et al., 1992). Small differences in the primary structure were used as a starting point in the interpretation. For example, guinea pig LA lacks

Trp 60, and Trp 26 is missing from human LA. Their spectra were compared to those of bovine LA which features both Trp 60 and Trp 26. Signals present in the bovine spectra, but missing in the spectra of the two other species were assigned to the two Trp residues. Once a few spin systems in the aromatic region were identified, it became relatively easy to assign the remaining aromatic resonances, especially since the aromatic side chains in LA are organized into two separate clusters. Nuclear Overhauser effects (NOEs) in cluster I connect Tyr 36, Phe 31, His 32, and Trp 118, while Phe 53, Trp 104, Trp 26, Tyr 103, and Trp 60 give rise to interresidue NOEs in cluster II.

Apart from the aromatic region, 19 of the 26 slowly exchanging amides giving detectable cross peaks in the correlated spectroscopy (COSY) spectrum of guinea pig LA have been identified by interpretation of connectivities between spin systems (Chyan et al., 1993). Those comprise residues 26-31 (B helix), 89-98 (C helix), 42 (β sheet), 61-62 and 74-75. In spite of those successes, complete assignment has been prevented by low spectral resolution. In particular, resonances corresponding to the residues that form the metal binding site could not be identified.

Resolution in the NMR spectra of the A- and T- states is even worse than that in the spectrum of native LA, because of the lack of an organized long-range tertiary structure. Methods rely therefore on correlations between the poorly resolved spectrum of the molten globule state and the somewhat better resolved spectra of the native protein. Magnetization transfer experiments, for example, under conditions where the two states are interconverting have been performed (at pH 7.8 and above 65°C), leading to the assignment of some of the aromatic resonances in the T-state spectrum of guinea pig LA (Baum et al., 1989). In the same study protons that are protected from exchange in both the molten globule and the native state were identified: the protein was

desolved in deuterated water and the A-state was induced by lowering the pH; protons that are accessible to the solvent molecules exchanged with deuterium. The native state was restored by raising the pH again. Identification of signals that are missing in the NMR spectrum of such treated LA as compared to the spectrum of natural LA indicates protons that are exchangeable in the A-state, but are protected from exchange in the native state.

1.4 Paramagnetic NMR

Before the arrival of two-dimensional techniques, detailed NMR spectroscopy was generally limited to small to medium sized molecules. Spectra of molecules with a large number of magnetically nonequivalent protons were simply too crowded for interpretation. In 1969, a method was introduced which could potentially deal with this problem. McDonald and Phillips showed that the addition of Co^{2+} , a paramagnetic ion, to a solution of hen egg-white lysozyme leads to the resolution of previously overlapping peaks by differential shifting in the upfield region of the protein (McDonald & Phillips, 1969). This was the beginning of paramagnetic biological NMR.

The magnetism of a substance is defined by the direction of the field that is induced by an external magnetic field. In diamagnetic substances the induced field is opposite to the external field. As a consequence, they tend to move from the stronger part of the field to the weaker part. In paramagnetic substances the behavior is opposite. All pure substances are inherently diamagnetic; even paramagnetic materials also exhibit diamagnetism and correction for this property must be made in a precise measurement of a permanent magnetic moment. Paramagnetism results when the

magnetic effects of the individual electrons are not mutually neutralized. This is the case in particles which contain at least one unpaired electron such as organic radicals and many metal ions. The lanthanides turned out to be especially valuable in biological NMR spectroscopy. Their radii are comparable to those of metal ions found ligated to natural proteins. Similar radii facilitate the exchange of metal ions against one another.

Paramagnetic ions have two major effects on NMR spectra. First, they can shift resonances into the far upfield and downfield regions, a property also referred to as hyperfine shifting. Second, they enhance relaxation. Different lanthanides exhibit the two effects to different extents. Ytterbium (Yb^{3+}), for example, acts mainly as shift reagent, whereas gadolinium (Gd^{3+}) exclusively enhances relaxation. Other lanthanides cause a mixture of both effects.

The total chemical shift of nuclei in a lanthanide complex is a combination of a diamagnetic contribution (δ_{DIA}) and two paramagnetic contributions, a through-bond effect (the Fermi contact shift δ_{FC}) and a through-space effect (the dipolar or pseudo-contact shift δ_{PC}) (Gansow et al., 1976). Thus, the total shift δ_{tot} is given by

$$\delta_{tot} = \delta_{DIA} + \delta_{PC} + \delta_{FC} \quad (1)$$

In the immediate vicinity of the metal binding site the diamagnetic contribution can be relatively small compared to the shift induced by the paramagnetic effects, and can in a first approximation be neglected. The Fermi contact contribution is due to the small but finite unpaired electron spin density present on the nucleus. The dipolar or pseudo-contact term arises from interaction between the two magnetic moments associated with the nuclear and the electron spin. This dipolar shift can be described by (Bleany, 1972)

$$\delta_{PC} = D_1 \left(\frac{3 \cos^2(\theta) - 1}{r^3} \right) + D_2 \left(\frac{\sin^2(\theta) \cos(2\phi)}{r^3} \right) \quad (2)$$

where D_1 and D_2 are constants depending on the temperature and the nature of the lanthanide, and r , θ , and ϕ are the spherical polar coordinates of the nucleus being observed in the principal magnetic axis system of the magnetic susceptibility tensor of the paramagnetic center. Equation 2 can theoretically be used to obtain structural information about a lanthanide complex, if the complexing lanthanide causes only small contact shifts compared to the pseudo-contact shifts. From experimental data, it has been determined that Yb^{3+} fulfills this requirement (Gansow et al., 1976). The differences between the shifts calculated from equation 2 and the observed shifts are considered to be sufficiently small to justify neglect of δ_{PC} in Yb^{3+} complexes.

Unfortunately, even in Yb^{3+} complexes it is not trivial to obtain geometry information from hyperfine shifts due to this effect's anisotropy. Only in cases of axial symmetry ($D_2=0$) the interpretation becomes relatively straightforward:

$$\frac{\delta_{PC}^i}{\delta_{PC}^j} = \frac{(3 \cos^2 \theta_i - 1)r_j^3}{(3 \cos^2 \theta_j - 1)r_i^3} \quad (3)$$

However, axial symmetry cannot generally be assumed, and for complex biological molecules it is usually not valid.

To circumvent the complications associated with anisotropy effects, researchers interested in biological molecules have concentrated on the effect of paramagnetic agents on relaxation. Nuclei that are close to the paramagnetic agent experience relaxation from two sources: other nuclei and the paramagnetic metal. For protons that are very close

to the metal binding site, the dipolar relaxation caused by other nuclei is much weaker than the relaxation caused by the unpaired electron and can therefore be neglected.

The paramagnetic contribution to relaxation is a combination of three factors: scalar or contact interactions, dipolar or pseudo-contact interactions, and the susceptibility or “Curie spin” contribution. For the lanthanides the contact interactions are usually neglectable, because 4f electrons are not highly delocalized (at least compared to 3d electrons). This assumption can be justified most easily for Yb^{3+} which causes the smallest contact interactions (Reuben, 1973).

With the assumption that the longitudinal and transverse electron spin relaxation times are equal ($T_{1e} = T_{2e} \equiv \tau_s$), the dipolar contribution to the spin-lattice (T_1) and spin-spin (T_2) relaxation times can be expressed by (Solomon, 1955)

$$\frac{1}{T_{1M}} = \frac{2}{15} \frac{g_j^2 \beta^2 \gamma_l^2 J(J+1)}{r^6} \left(\frac{3\tau_c}{1 + \omega_l^2 \tau_c^2} + \frac{7\tau_c}{1 + \omega_s^2 \tau_c^2} \right) \quad (4)$$

$$\frac{1}{T_{2M}} = \frac{1}{15} \frac{g_j^2 \beta^2 \gamma_l^2 J(J+1)}{r^6} \left(4\tau_c + \frac{3\tau_c}{1 + \omega_l^2 \tau_c^2} + \frac{13\tau_c}{1 + \omega_s^2 \tau_c^2} \right) \quad (5)$$

where g_j is the Landé g factor, β the electron Bohr magneton, γ_l the nuclear gyromagnetic ratio, ω_s and ω_l are the electron and nuclear Larmor frequencies ($\omega_s = 657 \omega_l$), and J is the total angular momentum. τ_c , the total correlation time, is determined by several processes:

$$\frac{1}{\tau_c} = \frac{1}{\tau_R} + \frac{1}{\tau_S} + \frac{1}{\tau_M} \quad (6)$$

τ_R is the rotational correlation time of the complex. It describes the tumbling rate of the molecule in the solvent and can be approximated by the Stokes-Einstein equation (Banci et al., 1991)

$$\tau_R = \frac{4\pi a^3 \eta}{3kT} \quad (7)$$

where η and a are the viscosity of the solvent and the radius of the molecule under investigation including a hydration layer. τ_M , the exchange correlation time, has to be considered if the inverse of the lifetime of the complex is smaller than any of the paramagnetically induced shifts. In large paramagnetic molecules τ_s , the electron correlation time, is usually the smallest of the three factors, and as such determines τ_C .

The Curie relaxation takes into account that the electron spins are distributed between spin levels according to the Boltzmann law. The excess of spins in the lower energy level gives rise to a static magnetic moment. Nuclear relaxation can be induced by this static magnetic moment. This interaction cannot be modulated by τ_s , because the static magnetic moment is already time averaged over the electron spin states. The Curie relaxation is given by (Guéron, 1975, Vega & Fiat, 1976)

$$\frac{1}{T_{1X}} = \frac{2}{5} \frac{\omega_I^2 g_I^4 \beta^4 J^2 (J+1)^2}{r^6 (3kT)^2} \left(\frac{3\tau_R}{1 + \omega_I^2 \tau_R^2} \right) \quad (8)$$

$$\frac{1}{T_{2X}} = \frac{1}{5} \frac{\omega_I^2 g_I^4 \beta^4 J^2 (J+1)^2}{r^6 (3kT)^2} \left(4\tau_R + \frac{3\tau_R}{1 + \omega_I^2 \tau_R^2} \right) \quad (9)$$

At first sight, this set of equations does not look much simpler than the shift equations. However, the lanthanides give rise to dipolar and Curie relaxation to varying

degrees. In many T_1 and T_2 calculations only one of the two effects has to be considered. In lanthanide complexes of parvalbumin, for example, it has been shown that at high field strengths T_{1M} and $T_{2\chi}$ contribute to the relaxation the most (Lee & Sykes, 1980a). In the case of Gd^{3+} , there is no “Curie spin” contribution, therefore T_1 and T_2 are equal to T_{1M} and T_{2M} , respectively.

Paramagnetic NMR has been used for structural investigations in a variety of biological systems. For example, tryptophan resonances in the one-dimensional NMR spectrum of lysozyme were assigned by interpretation of Gd^{3+} induced relaxation enhancement (Campbell et al., 1975). Lee and Sykes carried out a very detailed study of parvalbumin (Lee & Sykes, 1980a, Lee & Sykes, 1980b, Lee & Sykes, 1980c, Lee & Sykes, 1980d, Lee & Sykes, 1981, Lee & Sykes, 1982, Lee & Sykes, 1983). They exchanged one of the two calcium ions in parvalbumin for Yb^{3+} . By combining relaxation enhancement data with the atomic coordinates from the crystal structure, they were able to determine the anisotropy tensor of Yb^{3+} in parvalbumin.

1.5 Scope of this study

General interest in paramagnetic NMR almost vanished with the development of two techniques that are standard today: two-dimensional NMR and C^{13}/N^{15} labeling of proteins. Labeling became possible through advances in molecular biology. Two-dimensional NMR experiments of diamagnetic systems are easier to perform and more generally applicable than their paramagnetic counterparts. Detection of heteronuclei and two-dimensional techniques have provided two whole new levels of resolution. Further, with the constant development of ever larger magnets, resolution enhancement

through paramagnetic shifts seemed not to be required any longer. Unfortunately, there does not seem to be a linear correlation between field strength and cost, but an exponential one. Today, 600 MHz instruments, though expensive, are standard in larger laboratories. 800 MHz instruments are commercially available, but hardly affordable for most single institutions. The development of a 900 MHz instrument at Pacific Northwest National Laboratory is now almost complete after years of intensive work. However, a practical upper limit of what is economically and technically feasible by current materials in terms of magnetic field strengths may be almost reached.

On the other hand, the general availability of two-dimensional NMR made many structural biologists adopt those techniques. A huge amount of work has been invested into structure elucidation by NMR. Many of the interesting small-sized protein structures are solved today. In order to expand the scope of NMR structure investigations to larger proteins, alternative techniques have to be developed. For this reason, paramagnetic NMR has become a "hot topic" again in the early nineties, after resting almost completely for a decade. With today's high-field instruments, it has become possible to detect cross-signals in two-dimensional spectra between hyperfine shifted peaks. To date only a few studies have combined the new paramagnetic two-dimensional techniques with the older methods of determining the extent of relaxation enhancement by paramagnetic agents. The few that have, usually dealt with heme proteins, for example, metmyoglobin (Luo, 1996). Heme proteins are a very special case: the protons in their prosthetic group are not comparable to the protons of amino acid residues. The aim of this study was to assess the potential of combining the two levels of information, paramagnetic two-dimensional and relaxation enhancement experiments, in an investigation of a metalloprotein which has its metal ion bound to the amino acids of the protein, not a prosthetic group.

LA seemed to be the ideal system to test this approach. It contains a metal binding site which can accommodate paramagnetic ions. Conventional NMR has failed in providing a solution structure. Besides serving as a model system, the structure of the metal binding site is of interest by itself for reasons described above: LA features an unusual folding behavior and Ca^{2+} seems to be of importance in this process. The crystal structure of LA has already been solved. It can serve as tool in the interpretation of NMR data as well as a control for our new results. Assignment of residues in the close neighborhood of the metal binding site might serve as a basis for future studies aimed at elucidating the role of Ca^{2+} in the folding process.

2. Materials and Methods

2.1 Materials

Calcium depleted bovine LA (containing up to 0.3 equivalents Ca^{2+}) and the Ca^{2+} form of human LA were purchased as lyophilized powders from Sigma and used without further purification (bovine LA is according to the catalog “approximately 85% pure by polyacrylamide gel electrophoresis (PAGE)”, and human LA “at least 90% by electrophoresis”). Yb(III) and Gd(III) were obtained from Aldrich as chloride hexahydrates and were of the highest quality (99.999%). Calcium chloride dihydrate was from Mallinckrodt, St. Louis, Missouri. The salts were dissolved in D_2O and lyophilized at least twice before use.

Human Yb-LA was prepared by addition of ten times excess Yb^{3+} to a solution of human LA. The excess Yb^{3+} was removed by dialysis (molecular weight cut-off 6,000 - 8,000 g/mol). Metal complexes of bovine LA were prepared by addition of one equivalent of metal ions to a solution of calcium depleted LA. The bovine Yb-LA sample whose spectra were compared to those of human Yb-LA was also prepared by the dialysis procedure. No differences between the spectra of bovine Yb-LA prepared by the two different methods were observed. Samples were exchanged with D_2O by lyophilizing at least two times. “ H_2O ” samples were dissolved in 90% H_2O /10% D_2O (the D_2O was included in order to obtain a lock signal). The pH values of all samples were measured with a Radiometer Copenhagen pH meter 26 and an Ingold electrode, and adjusted to approximately 6.8 with NaOH/HCl or NaOD/DCl, not corrected for the isotope effect. Unless mentioned otherwise, the experiments described in the following sections were performed on bovine samples.

2.2 Instrumentation

Proton NMR spectra were recorded on Jeol JNM-FX90Q and Bruker AMX 400 spectrometers, and a Nicolet NM-500 spectrometer modified with a Tecmag interface. The two high field instruments were equipped with 5 mm ^1H probes, but the 90 MHz instrument with a 10 mm ^1H probe. All chemical shifts were referenced to 2,2-dimethyl-2-silapentane-5-sulfonate (DSS) through the residual water resonance. The carrier frequency was set to the resonance frequency of water protons in all acquisitions on the two high field instruments. The residual HDO signal was usually suppressed with a long, low-powered presaturation pulse (Wider et al., 1983).

Data processing was performed with MacNMR (version 5.5, Tecmag Inc.) or SwaN-MR (Balacco, 1994) on a PowerMacintosh, or with NMR Pipe (Delaglio et al., 1995) on a SiliconGraphics INDY computer. One-dimensional spectra were typically apodized with an exponential function (line-broadening factor 5.0 Hz), two-dimensional spectra with a phase-shifted sine bell square function. Two-dimensional spectra were compared with the help of ANSIG (assignment of NMR spectra by interactive graphics (Kraulis, 1989)).

The programs MOLMOL (molecule analysis and molecule display (Karadi et al., 1996)) and Swiss-Pdb Viewer (Guex & Peitsch, 1997) were used for the interpretation of crystal structures. Figures generated with the Swiss Pdb Viewer were further optimized with the Persistence of Vision (POV) Ray-Tracer (version 3.0.2a, Hallam Oaks Pty. Ltd.). Additionally, a FORTRAN program (Appendix A) allowed for systematic assessment of metal ion-proton and proton-proton distances from the Brookhaven protein data bank (Bernstein et al., 1977) files 1hfz (bovine LA (Acharya et al., 1991)) and 1hml (human LA (Pike et al., 1996)).

2.3 Titrations

Ca-LA with Gd (III): Gd^{3+} was added to a 4 mM solution of Ca-LA in steps of 0.1, 0.2, and 0.4 equivalents. The titration was performed with a 40 mM $GdCl_3$ stock solution to achieve neglectable volume changes during the titration. After each addition, one-dimensional (1D), double quantum filtered-correlation spectroscopy (DQF-COSY (Müller et al., 1986, Piantini et al., 1982, Rance et al., 1983)) and nuclear Overhauser effect spectroscopy (NOESY (Jeener et al., 1979, Kumar et al., 1980)) spectra were acquired at 500 MHz and 45°C with the following parameters:

1D: spectral window (SW) 10,000 Hz, 128 scans with 8192 points;

DQF-COSY: standard pulse sequence, acquisition mode TPPI (time proportional phase-incrementation frequency discrimination (Marion & Wüthrich, 1983)), SW 10,000 Hz and 64 scans with 512 points (in F2), 512 increments (in F1);

NOESY: standard pulse sequence, acquisition mode TPPI, SW 10,000 Hz and 64 scans with 512 points (in F2), 512 increments (in F1), $\tau_M = 100$ ms.

Ca²⁺ depleted LA with Yb(III): $YbCl_3$ (400 mM solution in D_2O) was added to a 8 mM solution of bovine LA in D_2O in steps of 0.25 equivalents, up to a total concentration of 12 mM. After each step, two 1D spectra were acquired at 500 MHz and 25°C. The first spectrum focused in on the diamagnetic region (SW 10,000 Hz); the second covered the complete range that was expected for hyperfine shifted peaks (SW 80,000 Hz). 1024 scans with 8192 points each were accumulated for the paramagnetic region, 32 scans with 8192 points each for the diamagnetic region.

2.4 1D NMR Experiments on Yb-LA

Standard 1D experiments: A 1D spectrum of 3 mM bovine Yb-LA in D₂O was acquired at 90 MHz and 31.5°C over a SW of 10,000 Hz. Since the memory of this instrument's operating system (JEOL) is limited, 24 spectra had to be acquired and the final spectrum subsequently added up from them. Each of those spectra consisted of 256 scans with 8192 data points over a SW of 10,000 Hz. 1D spectra at various concentrations and conditions were acquired on the two high-field instruments.

Temperature Dependence of 1D Spectra: 1D spectra of 0.2 mM bovine Yb-LA and Ca-LA in D₂O were acquired at 500 MHz and different temperatures (Ca-LA: 512 scans with 8192 points each over a SW of 10,000 Hz; Yb-LA: 4096 scans with 8192 points each over a SW of 50,000 Hz). The temperature profile was as follows: 25, 35, 45, 55, 65 (75, 80, 70), 60, 50, 40, 30, 25°C; numbers in brackets only for Ca-LA. 1D spectra of 2 mM human Yb-LA in D₂O were acquired over a SW of 50,000 Hz at 500 MHz and 25, 30, 35, 40, and 45°C (16384 scans at 25 and 45°C, 2048 scans at 30, 35, and 40°C).

Comparison between human and bovine 1D spectra: long runs (at least 8192 scans) 1D spectra of 2 mM human and 4 mM bovine Yb-LA were acquired at 500 MHz and 45°C over a SW of 50,000 Hz. A long recycle delay of five seconds was chosen to allow for meaningful integration.

The following set of experiments was carried out at 400 MHz and 25°C. Samples were 4 mM Yb-LA in H₂O and D₂O solvents.

Fast repetition 1D: These spectra were acquired with the following parameters: recycle delay 80 ms, SW 125,000 Hz, 4096 scans with 8192 points. In addition to a

spectrum with the transmitter on the H₂O signal, two spectra were acquired with the transmitter moved into the up- and downfield regions in order to detect signals with very large hyperfine shifts.

1D with solvent suppression jump-return (Plateau & Guéron, 1982): SW 44,667 Hz, 512 scans with 8192 points, delay between 90° and -90° pulses of 15 ms.

Super-WEFT (Inubushi & Becker, 1983): SW 125,000 Hz, 8192 scans with 4096 points, delays between 180° and 90° pulses of 20 and 40 ms.

The following set of 1D NOE experiments was carried out on a 4 mM Yb-LA sample in H₂O at 400 MHz and 25°C.

1D NOE (Noggle & Schirmer, 1971) *in combination with WEFT presaturation* (Patt & Sykes, 1972): SW 55,555.6 Hz, 16,384 scans with 8192 points, delay between 180° and 90° pulses of 500 ms (decoupler off) plus 60 ms (decoupler on).

1D NOE (Noggle & Schirmer, 1971) *in combination with jump-return solvent suppression* (Plateau & Guéron, 1982): SW 55,555.6 Hz, 16,384 scans with 8192 points, delay between 90° and -90° pulses of 15 ms.

A summary of all one-dimensional NMR spectra performed on Yb-LA can be found in Table 1.

2.5 2D NMR Experiments on Yb-LA

Two-dimensional (2D) experiments of Yb-LA were performed at 400 MHz and 25°C. Two NOESY experiments (with τ_M values of 20 and 80 ms) were run, as well as a short and a long run COSY (Bax et al., 1981), and a TOCSY (total correlated spectroscopy, (Braunschweiler & Ernst, 1983)) spectrum on a 4 mM Yb-LA in D₂O; a

NOESY ($\tau_M = 80$ ms) and a short run COSY spectrum were acquired of a 4 mM Yb-LA in H₂O. The parameters were as follows.

NOESY: standard pulse sequence with acquisition mode TPPI, SW 55,555 Hz and 192 scans with 1024 points (in F2), 512 t_1 increments (in F1);

COSY (short): standard pulse sequence without TPPI, SW 55,555 Hz and 1024 scans with 1024 points (in F2), 300 t_1 increments (in F1);

COSY (long): standard pulse sequence without TPPI, SW 55,555 Hz and 4096 scans with 1024 points (in F2), 400 t_1 increments (in F1);

TOCSY: standard pulse sequence without TPPI, SW 10,000 Hz and 160 scans with 1024 points (in F2), 400 t_1 increments (in F1).

A summary of all two-dimensional NMR spectra performed on Yb-LA can be found in Table 2.

2.6 Determination of T_1 and T_2 values

The spin-lattice relaxation times (T_1) of the hyperfine shifted peaks in the NMR spectrum of Yb-LA were determined by the inversion recovery method (Vold et al., 1968). The sample was 4 mM in H₂O and spectra were acquired at 500 MHz and 25°C over a SW of 51,200 Hz. Each of the t_1 incremented spectra consisted of 2048 scans with 16384 points. In addition to having the transmitter on H₂O, it was moved in separate experiments into the far up- and downfield regions in order to obtain spectra of high quality over a wide SW.

The spin-spin relaxation times (T_2) of the hyperfine shifted peaks in the 1D spectrum of Yb-LA were determined from the peak widths at half-height (Abragam,

1961) in standard 1D spectra (cf. above). The line-shapes of all hyperfine shifted peaks were simulated with MacNMR and their widths were extracted.

2.7 2D Exchange Experiments

Ca/Yb-LA: Exchange spectroscopy (EXSY, (Jeener et al., 1979)) spectra of 4 mM Ca^{2+} depleted LA containing 0.5 equivalents of Ca^{2+} and Yb^{3+} were acquired at 500 MHz and 25°C and 55°C with the standard pulse sequence (identical with the NOESY sequence) and acquisition mode TPPI over a SW of 25,000 Hz (in F2) with 384 increments in the F1 dimension, 512 scans with 512 points each in the F2 dimension and various values of τ_M (15, 50, and 80 ms).

apo/Yb-LA: EXSY spectra of 4 mM Ca^{2+} depleted LA containing 0.5 equivalents Yb^{3+} were acquired at 500 MHz and 55°C with the standard pulse sequence and acquisition mode TPPI over a SW of 25,000 Hz (in F2) with 384 increments in the F1 dimension, 1024 scans with 512 points each in the F2 dimension and τ_M equal to 20 and 80 ms.

3. Results and Discussion

3.1 Studies on Gd-LA

Generally, lanthanides change the shift and the relaxation properties of resonances in NMR spectra as was outlined in the introduction. This poses a multi-dimensional problem which is hard to deal with. Gadolinium, is an exception to this rule; it exclusively enhances relaxation (Bleany, 1972). This property makes it very attractive for NMR studies, because it is much easier to interpret spectral changes, if several parameters are not varied at the same time.

In superpositions of Ca-LA with Gd-LA spectra, resonances are expected to be found at the same positions within the accuracy of the digital resolution of the experiments in this study. However, they are also expected to be broader in the Gd-LA spectrum due to enhanced spin-spin relaxation. The extent of this line-broadening depends on the distance between the protons and Gd^{3+} (Equations 4, 5, 8, and 9). Quantification of this effect is not trivial, since several factors contribute to the lanthanide's relaxation enhancing properties (cf. introduction). However, it may be possible to draw at least qualitative conclusions about metal-proton distances from line-broadening, i.e. it may be possible to distinguish between protons very close to the binding site and those further away.

Ca-LA was titrated with Gd^{3+} and the effect on the line widths was observed (Figure 6). As expected, resolution in the one-dimensional spectra was too low to detect any differential line broadening. The whole spectrum seemed to be affected equally: with each addition of Gd^{3+} all resonances got broadened further. To obtain a

more detailed view, two-dimensional spectra were recorded, which alleviate the problem of overlapping signals. The two methods of choice were DQF-COSY and NOESY (for a more detailed description of the 2D methods, cf. section 3.2.3). DQF-COSY is especially sensitive to line-broadening, because the positive and negative components of its anti-phase signals which comprise its cross-peaks tend to cancel each other out if the signal gets broad. NOESY may be useful, because a larger number of signals are detected.

A good method to compare two-dimensional spectra is the program ANSIG. This program allows overlaying of up to eight spectra. However, comparison of intensities in two-dimensional spectra is not easy, since the magnitude of signals is only visualized by a set of contour lines. Fortunately, extraction of one-dimensional spectra from two-dimensional spectra can be achieved with ANSIG (Figure 7). By this method a few cross-peaks (namely 3.18/4.95, 2.20/5.18, and 1.40/5.20) were found whose intensities in the “Gd³⁺ spectra” were reduced to a larger extent than that of most other signals. However, it was not possible to connect several of those strongly affected signals into spin systems (i.e. amino acid residues). Moreover, verification through the mirror-image signals on the opposite side of the diagonal was in most cases not very convincing.

If a large number of signals have to be compared, extraction of one-dimensional spectra becomes a tedious process. Therefore, an AppleScript was developed, which adds up two-dimensional spectra in MacNMR (appendix). Difference spectra can be obtained with this program by adding two spectra with a difference in zero-order phasing of 180°. However, even with this more systematic approach, it was not possible to get any new information as compared to the 1D ANSIG extraction method. At this point it had to be concluded that the relaxation properties of Gd³⁺ are simply too

strong to allow for a differentiation between protons in the case of Gd-LA. This method might work in a system with a smaller number of protons that also features a larger spread of proton-metal distances, but it is not sensitive enough for use as a tool in solving protein structures. Consequently, hyperfine shifting, a more discriminating method, was employed. The next section deals with the lanthanide shift reagent ytterbium.

3.2 Studies on Yb-LA

3.2.1 Temperature Stability

One of the problems to be aware of in investigations of metalloproteins with lanthanide shift reagents is a potential structural change upon exchange of the natural metal ligand for one of the lanthanides. Such changes are expected to affect, among other properties, the melting point (m_p) of the protein. The m_p (more generally the transition temperature) is defined as the midpoint of the change in a detectable physical property that is affected by the collapse of the protein's specific three-dimensional structure (Scheraga, 1961). A wide variety of physical properties have been used to determine the m_p of Ca-LA, for example, the mean residue ellipticity at 270 nm (Hiraoka et al., 1980), the aromatic absorption at 292 nm (Kuwajima & Sugai, 1978), and the fluorescence properties of tryptophan side chains (Sommers & Kronman, 1980). There seems to be agreement that the m_p of Ca-LA is between 53 and 58°C over a pH range from 5.2 to 8.1. Another observable physical property that should allow for definition of the m_p is the dispersiveness of NMR signals: native proteins feature very

dispersed spectra, whereas signals are restricted to the typical aromatic and aliphatic regions in the spectra of denatured proteins (Wüthrich, 1986).

The validity of this NMR method was confirmed by determination of the m_p of Ca-LA and comparison to the results from previous studies. One-dimensional NMR spectra were acquired at various temperatures (Figure 8). Systematic errors were minimized by varying the temperature the following way: the first spectrum was obtained at 25°C, the following spectra up to 75°C were acquired in steps of 10°C. Then the temperature was raised to 80°C, followed by lowering in steps of 10°C until 30°C were reached. A final spectrum at 25°C was acquired. Denatured proteins have some of their non-polar side chains exposed to the solvent (Dill & Shortle, 1991). This might lead to aggregation of protein molecules. A low sample concentration was chosen in order to prevent this kind of aggregation as much as possible. Nevertheless, comparison between the first and the final spectrum, both acquired at 25°C, revealed, that about 15% of the protein was denatured irreversibly during the course of the experiment, most likely at high temperatures, although no precipitation was noted. To account for this loss of sample, the spectra taken in the second half of the experiment (70, 60, 50, 40, 30°C) were multiplied by a factor of 1.15. Another interesting observation was that at least two signals (8.0 and 8.25 ppm) did not recover upon decrease of the temperature. These peaks must therefore correspond to protons that are exchangeable in the denatured protein, but protected from exchange in the native structure. The intensities of three peaks that exist as singlets in all spectra were plotted against the temperature (Figure 9a). The sigmoidal shape of the resulting curves confirmed the expected cooperativity of the folding-unfolding process. The midpoint of a sigmoidal curve is an inflection point around which the curve can be approximated by

a linear function. An equation for the determination of the m_p can therefore be derived with simple calculus:

$$\frac{m_p}{^{\circ}\text{C}} = \frac{\sum_{i=1}^N \left[\frac{T_{low,i}}{^{\circ}\text{C}} + 5 \left(\frac{I_{25,i}/2 - I_{low,i}}{I_{high,i} - I_{low,i}} \right) \right]}{N} \quad (10)$$

The half-intensities of singlet peaks in the spectrum at 25°C are computed ($I_{25}/2$). This value was compared to the intensities of the corresponding peaks in the spectra at higher temperatures. I_{low} and I_{high} denote the intensities of the peaks bracketing the $I_{25}/2$ value. The sum goes over the three peaks used in the determination. The resulting m_p at 57.9°C is in very good agreement with the results from previous studies.

After having established the validity of using the intensity of NMR signals to determine the m_p of Ca-LA, the m_p of Yb-LA was determined the same way (Figures 9b and 10). In this experiment the highest temperatures (70 - 80°C) were omitted to prevent irreversible denaturation. Plots of the intensities of three of the hyperfine shifted peaks against the temperature gave a m_p of 59.7°C which is quite close to that of Ca-LA, especially considering the limits of this method's accuracy. The similarity of the two m_p corroborates the assumption that the structures of Yb-LA and Ca-LA are closely related.

3.2.2 Assessment of Hyperfine Shifted Resonances

In order to detect hyperfine shifted resonances, a solution of Ca^{2+} depleted LA was titrated with Yb^{3+} in steps of 0.25 equivalents. One-dimensional NMR spectra were acquired after each addition (Figure 11). As expected, several peaks appeared in the far up- and downfield regions. Another interesting feature was the general broadening of the spectrum, once the Yb^{3+} concentration got beyond one equivalent, probably caused by non-specific binding of Yb^{3+} once all Ca-sites are filled. Since ions in the Zn-site of LA are coordinated by glutamate carboxylates from two neighboring molecules, the observed line broadening was probably also due to aggregation of LA caused by binding of Yb^{3+} to the Zn-site. This hypothesis is corroborated by the observation that addition of high concentrations of Yb^{3+} led to some precipitation. In the crystal structure Zn^{2+} is coordinated by amino acid side chains from two LA molecules (Ren et al., 1993). The presence of an ion in the Zn-site is therefore expected to promote aggregation.

A closer look at the baseline shape of spectra acquired with a large number of scans also revealed that there were probably additional peaks buried in the spectrum noise (not shown). For the detection of those very fast relaxing signals, more unusual NMR techniques were required. The easiest way to enhance the intensity of fast-relaxing resonances is a decrease of the recycle delay. Slow-relaxing peaks become saturated, because they do not have a chance to return to their equilibrium position in the short time intervals in between pulses. Additionally, fast pulse repetition allows for acquisition of a large number of scans in a short time. Since the signal to noise ratio increases linearly with the square root of the number of scans, this leads to better detection of fast-relaxing signals. The standard one-dimensional experiment was

performed with a short recycle delay of 80 ms (Figure 12). The resulting spectrum revealed the presence of additional peaks shifted very far up- and downfield, and gave a hint of a broad peak centered around 25 ppm. Protons that are exchangeable (most of the amide protons) cannot be detected if the sample is dissolved in D₂O. The experiment with fast pulse repetition was therefore repeated with a sample dissolved in H₂O, giving rise to additional signals (Figure 12). From here on, resonances corresponding to non-exchangeable protons will be marked by upper-case letters, whereas those corresponding to exchangeable peaks will be marked by lower-case letters.

Even better saturation of the diamagnetic region can be achieved by the combination of a short recycle delay with the so-called WEFT method (water eliminated Fourier transform spectroscopy) (Patt & Sykes, 1972). WEFT was developed, as the name suggests, to saturate the solvent peak. It is characterized by the pulse sequence:

$$180^\circ - t_1 - 90^\circ - \text{FID}(t_2)$$

The first 180° pulse inverts the total magnetization vector. During the delay time t_1 the hyperfine shifted (fast relaxing) resonances relax completely. The remaining (slower relaxing) resonances, however, are close to zero when the 90° read pulse is performed. This results in xy-magnetization of mainly the fast relaxing resonances, which is detected as FID (free induction decay). By changing t_1 to even shorter values, it is possible to distinguish between hyperfine shifted peaks with different relaxation times. The combination of WEFT with a short recycle delay is called super-WEFT (Inubushi & Becker, 1983). This experiment was carried out with t_1 delays of 20 and 40 ms (Figure 13). The short delay spectrum clearly showed the existence of the peaks at -33.6 and 25.4 ppm, and an additional peak was detected at 18.4 ppm. The super-WEFT experiments were repeated with samples in H₂O (Figure 14). Additional signals

were found in both the up- and downfield regions. In order to detect potential peaks shifted out very far, the transmitter was moved into the up- and downfield regions and super-WEFT experiments were performed. However, no additional signals were detected from 200 to -200 ppm.

A complete listing of the hyperfine shifted peaks that were detected in the experiments described above can be found in Table 3. Signals Q and R were identified clearly in the D₂O spectra; in H₂O they were obscured by amide signals. The region between 0 and -6 ppm was too crowded for interpretation in the 1D spectra. Only two peaks (P', Q') in this area could be identified by super-WEFT as fast relaxing. By comparison of peak intensities in the short and long delay super-WEFT spectra, the following order of spin-lattice relaxation times was established:

downfield region: A, B > C, d, I, M > g > H, k > E, f, J > N, O, P > l

upfield region: z' > y', x' > v' > U', W' > T' > R' > S'

One of the problems of NMR experiments in H₂O is the exchange of protons with solvent during the acquisition. The solvent peak is usually suppressed with a presaturation pulse. It is possible that saturated protons from the solvent exchange with protons on the molecule under investigation some time during the presaturation pulse and FID acquisition. Those protons are broadened and of low intensity in the NMR spectrum; if the exchange is very fast, they can be totally invisible. There are several alternative non-saturation solvent suppression methods to circumvent this problem. One of them is the application of binomial pulse sequences (binomial, because they can be derived from the binomial coefficients) (Plateau & Guéron, 1982). In binomial sequences the resonances of the molecules under investigation are excited, while the water protons are left relatively undisturbed. The read-pulse in the simplest binomial sequence (also called "jump-return") is replaced by a 90°_x - τ - 90°_{-x} pulse sequence.

The first pulse brings all spins along x in the rotating frame. During the waiting time they fan out in the xy plane, the solvent spins are at resonance and remain along x. The second pulse brings all spins back from the xy plane to positions in the zy plane, the solvent being returned to z. Consequently, there only remains a xy component of the spin magnetization of protons that resonate off the solvent resonance. This magnetization is detected as the FID. The jump-return pulse sequence was applied to Yb-LA in H₂O (Figure 15). Some of the exchangeable resonances gained intensity as compared to the spectra acquired with a conventional 90° pulse, for example, peaks f and g.

In order to establish whether all observed signals correspond to single protons or whether some of them are caused by the averaged resonances of methyl groups (rotation) or aromatic ring protons (flipping), peak intensities were integrated. All signals turned out to have about the same area with one exception: the area of the “triplet” N, O, P corresponds to five or six protons. Since integration of overlapping peaks is often ambiguous, a method to resolve this multiplet had to be found.

According to Equation 9, the spin-spin relaxation times at low field strengths are expected to be longer than at high field strengths, leading to narrower line widths (for the relation between spin-spin relaxation time and line width, see next section).

Consequently, a 1D spectrum was acquired at 90 MHz (Figure 16). Indeed, some of the broad signals sharpened up, although the signal to noise ratio was much worse. For example, M which is only visible with a fast repping pulse sequence at 500 MHz, was present in the spectrum acquired at 90 MHz with a conventional pulse sequence.

However, the narrowing effect of the lower field strength was partially made up for by the generally lower resolution at low field strengths. Especially, signals that are not shifted out far, like the “triplet”, experienced no observable resolution enhancement.

Obtaining the spectrum of LA of a different, but closely related species is another way to achieve resolution of the “triplet”. Human LA was the most obvious choice, because it is commercially available. The only difference in primary structure within the region of interest is a leucine to isoleucine mutation at position 85 (Figure 1). The two crystal structures are very similar (Figure 4). Nevertheless, the difference should be sufficient to resolve the multiplet, because hyperfine shifted chemical shifts are extremely sensitive to structural changes. The 1D NMR spectrum of human Yb-LA was acquired with a long-recycle delay of five seconds in order to obtain accurate integral values (Figure 17). Surprisingly, the “triplet” resolved into four signals. One (O) had a relative intensity of 2 and corresponds therefore probably to two protons of a fast-flipping aromatic ring side chain. In order to exclude the possibility of O corresponding to two magnetically nonequivalent protons that accidentally have the same chemical shift, its temperature behavior was observed. Resolution into two peaks was not detected in the temperature range from 25 to 45°C (data not shown). Since O appeared as singlet in the spectrum of bovine and human LA at various temperatures, the likelihood of it corresponding to nonequivalent protons is very small.

Two peaks (N and P) of the “triplet” had a combined relative intensity of 2.56, because they partially covered a broad signal, that could only be detected in the spectrum of human Yb-LA. This broad signal (Oa) was most likely totally hidden under the “triplet” in the bovine spectrum. Integration over all four signals gave an intensity of 5.58, indicating that the new peak Oa corresponds to either one or two protons:

$$\text{Int.}(Oa) = \text{Int.}(\text{triplet}) - \text{Int.}(N) - \text{Int.}(O) - \text{Int.}(P) = 5.58 - 1 - 2 - 1 = 1.58 .$$

The variation in chemical shifts upon changes in temperature serves not only to resolve overlapped signals, but can also theoretically be used to separate the diamagnetic (δ_{DIA}) from the pseudo-contact contribution (δ_{PC}). δ_{DIA} does not change significantly with temperature, whereas δ_{PC} is expected to vary with $1/T^2$ (Bleany, 1972). The chemical shifts of the hyperfine shifted resonances of Yb-LA were plotted against $1/T^2$ and extrapolated (Figure 18). δ_{DIA} were then obtained from the intercepts with the y-axis (Table 3). Unfortunately, these δ_{DIA} cannot be considered as really reliable; δ_{DIA} of all hyperfine shifted peaks in the downfield region determined by this method turned out to be somewhere between 4.1 and 8.1 ppm, whereas all hyperfine shifted peaks in the upfield region had a δ_{DIA} between -3.7 and 1.9 ppm. This separation of the diamagnetic shifts seems to be highly unlikely. One possible explanation is that the contact contribution, though smaller than the pseudo-contact contribution, is too large to be neglected in this determination of the diamagnetic chemical shift.

3.2.3 Two-dimensional Connectivities

Assignment of the hyperfine shifted resonances can be simplified dramatically through information from two-dimensional spectra. However, the detection of cross-signals by two-dimensional NMR techniques is complicated by several problems (La Mar & de Ropp, 1993). As in the case of 1D experiments, all signals are weaker in a paramagnetic than in a diamagnetic system, and relaxation occurs on a much shorter time scale. The short relaxation times require special precautions in the experimental set-up. It is crucial to acquire a large number of scans, because cross-signals between broad peaks can only be detected with a large signal to noise ratio. Fortunately, the

short spin-lattice relaxation times give rise to a fast return of the spin magnetizations to their equilibrium positions, which allows for short recycle delays and makes the acquisition of many scans possible within a reasonable time. Other problems are more experiment specific.

Correlated spectroscopy (COSY (Bax et al., 1981)) gives information about coupling which occurs between nuclei separated by only a few bonds. COSY type experiments feature dispersive cross-peaks or pure absorption cross-peaks with antiphase line structure. Those line-shapes give rise to serious problems in paramagnetic NMR with its typically broad signals; the positive and negative components of broad signals easily cancel each other out. Since the signal to noise ratio (S/N) is one of the decisive factors in paramagnetic NMR, it is advisable to use the conventional COSY pulse sequence

$$90^\circ - t_1 - 90^\circ - \text{FID}(t_2) - \text{recycle delay}$$

rather than the more sophisticated DQF-COSY (double-quantum filtered) pulse sequence (Müller et al., 1986, Piantini et al., 1982, Rance et al., 1983)

$$90^\circ - t_1 - 90^\circ - 90^\circ - \text{FID}(t_2) - \text{recycle delay}$$

because DQF-COSY, while having a better resolution for cross-peaks close to the diagonal, leads to a two-fold decrease in S/N. S/N can be further increased by acquiring the data in a non phase sensitive mode. This increase is bought with the loss of coupling information from the line shape. Since there is no information contained in the peak line-shapes of spectra acquired not phase sensitive, it makes sense to simplify the spectrum appearance by processing with magnitude calculation.

In total correlated spectroscopy (TOCSY (Braunschweiler & Ernst, 1983)) cross-peaks are theoretically found between all protons that belong to the same spin-system. The pulse sequence contains a so-called spin-lock (SL) and a composite pulse

sequence known as MLEV17 to transfer the magnetization between scalar coupled homonuclear spins during the mixing time (Bax & Davis, 1985). The signals are absorptive and of the same phase, and therefore are not as sensitive to line-broadening as the signals in COSY type spectra. However, data interpretation is less straightforward, because differentiation between protons that couple directly and those that couple via a third proton is only possible by comparison to a COSY type spectrum, or by varying the mixing time.

Cross-signals in nuclear Overhauser spectroscopy (NOESY) (Jeener et al., 1979, Kumar et al., 1980) indicate nuclei that are close in space (less than about 5 Å apart). The NOE effect in proteins is caused by cross-relaxation between nuclei. However, the electron spin in a paramagnetic system provides a much more effective relaxation mechanism which makes detection of NOE effects a difficult task. The NOESY pulse sequence includes a mixing time τ_M :

$$90^\circ - t_1 - 90^\circ - \tau_M - 90^\circ - \text{FID}(t_2) - \text{recycle delay}$$

The mixing time is usually selected to be on the order of T_1 of the nuclei under investigation. This is another complication in NMR spectroscopy of paramagnetic proteins, which feature protons with a wide variety of relaxation times. A whole series of spectra then has to be acquired in order to obtain a complete picture of NOE connectivities.

COSY and NOESY spectra ($\tau_M = 80$ ms) of Yb-LA in D_2O , as well as COSY, two NOESY ($\tau_M = 20, 80$ ms) and TOCSY spectra of Yb-LA in H_2O were acquired at 25°C and 400 MHz. COSY and three NOESY spectra ($\tau_M = 15, 50, 80$ ms) were also acquired at 45°C and 500 MHz.

Unfortunately, but expectedly, only a few COSY signals were detected between hyperfine shifted resonances (Figure 19); U'/W' and P'/R'/T' in the upfield region, as

well as O/Q in the downfield region were clearly coupled. Further, some connectivities between the peaks around 15 ppm and the diamagnetic region, and among the signals between 0 and -6 ppm were present. TOCSY spectra did not result in the desired increase in sensitivity. No additional coupling as compared to the COSY spectra was detected (not shown).

Fortunately, the sensitivity of NOESY spectra was much higher. Consequently, more NOE signals were detected (Figures 20-23). Two spin systems appeared very clearly in the upfield region (S', U', v', W' and P', R', T'). The downfield region featured many connected signals, however, identification of spin systems was less striking than in the upfield region. The only unambiguous system consisted of E, g, and H. By optimizing the mixing time, it was even possible to detect cross-peaks between the up- and downfield regions (O to S', U', W').

Detection of NOE effects between resonances with very short T_1 values and resonances with considerably longer T_1 values is particularly challenging; resonances with short T_1 values require short mixing times to prevent complete relaxation before the read pulse, whereas resonances with longer T_1 values require longer mixing times to allow for NOE build-up. Under these conditions, the steady-state one-dimensional NOE experiment (Noggle & Schirmer, 1971) is superior to the NOESY experiment. The signal under investigation (with a short T_1 value) is presaturated with a long, low-powered, selective pulse before the 90° read pulse and data acquisition. A second one-dimensional spectrum is acquired with the presaturation frequency set to an empty region of the spectrum. The difference between the two spectra shows which signals are effected by presaturation of the resonance under investigation. In order to suppress artifacts the two spectra are usually acquired in parallel (in our experiment, for example, in increments of 64 scans). Since the resonance with a short T_1 value is saturated until

directly before the read pulse is carried out, the problem of fast relaxation is less severe. The drawback to the 1D NOE experiment are the off-resonance effects (due to the width of the presaturation pulse). Reliable results can only be expected for peaks that are clearly separated from other peaks. This prerequisite is met by peaks v' and y'. A 1D NOE experiment for these two peaks was carried out in combination with presaturation of the solvent peak by WEFT (Patt & Sykes, 1972) (Figure 25). In addition to the cross signals found in the NOESY experiments, peak y' was connected to the P'/R'/T' spin system and a cross signal between U' and W' corroborated the assumption that S', U', v' and W' form a spin system. Most interestingly, another cross peak connecting the upfield with the downfield region was found between resonances v' and k.

Detection of NOE cross signals to resonance g with an one-dimensional experiment is complicated by two effects. First, the intensity of g is relatively low due to saturation transfer from the solvent. This problem can be circumvented by using a non saturation solvent suppression technique ("jump-return", cf. section 3.2.2). Second, overlapping with the neighboring resonances f and H can lead to off-resonance effects. In order to distinguish between those artifacts and real NOE signals, several difference spectra have to be acquired. In each of the "empty-region" spectra, the transmitter is set at an equal distance to the resonance under investigation on the opposite side of the overlapping resonance (Figure 25). The only true NOE signal, visible in all three spectra, connects g to the exchangeable resonance k.

A complete listing of all NOE connectivities from NOESY and 1D NOE experiments can be found in Figure 26.

3.2.4 Measurement of Relaxation Times

The next logical step after assessment of the hyperfine shifted resonances and their connection into spin systems, is the determination of the properties of the resonances, in particular their relaxation times. Spin-lattice relaxation times (T_1) were obtained by the most commonly used method, inversion-recovery (Vold et al., 1968), the pulse sequence of which is

$$180^\circ - \tau - 90^\circ - \text{FID}(t_2) - \text{recycle delay}$$

The first 180° pulse turns the total magnetization vector to the negative z-axis. During the time interval τ , spin-lattice relaxation leads to return of this magnetization to the equilibrium position. The progress of this process can be monitored by applying a 90° pulse, which turns the z-magnetization into a detectable y-magnetization. This experiment is performed several (at least five to ten) times with incremented τ values. The recycle delay between single scans must be several times longer than the longest T_1 under investigation to allow for complete return to equilibrium in between scans. The peak intensities (I) in the Fourier transformed spectra depend on the delay time τ according to the equation

$$I(\tau) = I(\infty)(1 - 2e^{-\tau/T_1}) \quad (11)$$

where $I(\infty)$ is the peak intensity in a 1D spectrum acquired with a single 90° pulse.

Equation 11 rearranges to

$$\ln[I(\infty) - I(\tau)] = \ln 2 + \ln I(\infty) - \frac{\tau}{T_1} \quad (12)$$

which allows for determination of T_1 from the slope of a plot of $\ln[I(\infty)-I(\tau)]$ vs. τ . One of the crucial factors to obtain accurate results from the linear regression are flip angles larger than 90° . Time and frequency domain are connected by Fourier transformation. This means that short pulses cover a broad spectral window (SW), long pulses cover only a narrow SW. Consequently, to get an even distribution of pulse power throughout the frequency domain, short, high-powered pulses are desirable. In paramagnetic NMR one has to deal with a very wide SW. Unfortunately, NMR instrumentation sets a limit to the pulse power. It is not possible to reduce the pulse length far enough to achieve approximately even excitation over the SW necessary to cover all hyperfine shifted peaks. The pulse power is, of course, highest at the transmitter frequency; it drops with a $\text{sine}(x)/x$ function in both directions and reaches zero at a distance of $(1/\text{pulse length})$ from the transmitter (Sanders & Hunter, 1993). In our experiment, for example, it was not possible to reduce the length of the 180° pulse to less than $21.4 \mu\text{s}$, corresponding to 46.7 kHz or $\pm 93.5 \text{ ppm}$ on the 500 MHz instrument. Therefore, it was necessary to determine the T_1 values in three separate experiments, with the transmitter being at three different frequencies (Figures 27-29). The signal intensities were extracted and plotted according to Equation 12 (Figure 30). The T_1 values obtained with least square fits are listed in Table 4. In trying to find a linear fit function for the experimental data points, it became obvious that an initial slope had to be determined, because data points corresponding to long τ values ($\tau > T_1$) usually fell off the least square fit curves. Unfortunately, it turned out to be impossible to determine T_1 values for the signals shifted out furthest. They simply relaxed too fast and returned even with very short delay times τ to their equilibrium position before the 90° read pulse was applied, their T_1 values must be shorter than 10 ms .

The determination of spin-spin relaxation times (T_2) can be performed more easily than the determination of T_1 times, however, it is less accurate. In the Bloch vector model (Bloch, 1946), the real part of the NMR spectrum in the frequency domain consists of absorptive Lorentzian signals:

$$v(\omega) = \lambda M_0 \frac{R_2}{R_2^2 + (\Omega - \omega)^2} \quad (13)$$

where λ is an experimental constant of proportionality, M_0 the magnitude of the equilibrium magnetization, ω the transmitter frequency, Ω the offset of the chemical shift, and R_2 the spin-spin relaxation rate constant ($T_2 = 1/R_2$). The line width (defined as the full-width at half-height, FWHH) of this Lorentzian signal is given by:

$$\Delta\nu_{FWHH} = \frac{R_2^*}{\pi} = \frac{1}{\pi T_2^*} \quad (14)$$

T_2 values can therefore simply be obtained from measurement of the signals' line-widths. However, one additional factor has to be considered in the determination of T_2 times: field inhomogeneities lead to line-broadening; R_2 values determined from experimental line widths (R_2^*) differ slightly from theoretical R_2 values:

$$R_2^* = R_2 + R_{2,inhom} \quad (15)$$

In paramagnetic NMR this complication is usually neglectable, because the theoretical R_2 values of the very fast-relaxing hyperfine shifted peaks are much larger than the contribution from field inhomogeneities, especially in spectra obtained with today's

super-conducting magnets. In this case, paramagnetism works in the experimentalists' favor.

A one-dimensional NMR spectrum of Yb-LA in H₂O was acquired. After processing, the line-shapes were simulated with MacNMR (Figure 31). This allows for the most accurate determination of line-widths. Before those line widths could be transformed into T₂ times, the line-broadening factor which was used before the Fourier transformation had to be subtracted. The resulting T₂ values are listed in Table 4.

3.2.5 Correlation to the Crystal Structure

As has been outlined in the introduction, it is not trivial to obtain absolute distance information from relaxation times. Several mechanisms contribute to relaxation, and all of them depend on many factors. However, it is possible to simplify the distance-relaxation time correlation by concentrating on the two mechanisms that are most important in lanthanide complexes, dipolar relaxation (Equations 4 and 5 (Solomon, 1955)) and Curie relaxation (Equations 8 and 9 (Guéron, 1975, Vega & Fiat, 1976)). In both mechanisms the relaxation times are proportional to the inverse of the sixth power of the proton-lanthanide distance. Although the proportionality factors are different (c_M and c_χ), the two sets of equations can be combined:

$$\frac{1}{T_1} = \frac{1}{T_{1M}} + \frac{1}{T_{1\chi}} = \frac{c_{1M}}{r^6} + \frac{c_{1\chi}}{r^6} = \frac{c_1}{r^6} \quad (16)$$

$$\frac{1}{T_2} = \frac{1}{T_{2M}} + \frac{1}{T_{2\chi}} = \frac{c_{2M}}{r^6} + \frac{c_{2\chi}}{r^6} = \frac{c_2}{r^6} \quad (17)$$

For nuclei that are close to the metal-binding site the paramagnetic contributions to relaxation summarized in Equations 16 and 17 are much stronger than relaxation through other nuclei. The overall relaxation times of the hyperfine shifted resonances are therefore expected to be proportional to $1/r^6$. If it is possible to assign an absolute proton-metal distance to one of the resonances, distances for all other hyperfine shifted resonances can be calculated. A crystal structure should be very useful in this process. The region around the metal-binding site is not expected to change dramatically upon solvation of the protein beyond its extent in the crystals, because it is stabilized by the coordination of side chains and backbone carbonyl groups to the metal.

A crystal structure of a recombinant form of bovine LA (additional N-terminal residue and a M90V mutation) with a bound Ca^{2+} is available from the protein data bank (1hfs, (Pike et al., 1996)). From inspection of the crystal structure in the Swiss-Pdb Viewer (Guex & Peitsch, 1997), it was concluded that the mutations probably do not influence the structure of the Ca-site dramatically. Crystal structures do not include the positions of protons. The proton coordinates in 1hfs were therefore calculated with the program MOLMOL (Karadi et al., 1996). The resulting coordinates were extracted and fed into a FORTRAN program (Appendix A) which assesses systematically all proton-metal distances (Table 5). In correlating distances from the crystal structure to NMR data one has to be aware of the fact that the solution structure is not static. In particular, methyl groups are rotating fast on the NMR time scale, giving rise to a single averaged NMR signal. The same is true for some protons such as HD1 and HD2 of Phe from aromatic side chains whose flexibility is not restricted by other residues. Taking those considerations into account, Table 5 was modified; distances were averaged weighed by $1/r^6$, because according to equations (16) and (17) the relaxation time values are

expected to depend on the inverse of the sixth power of the lanthanide to proton distances (Table 6).

The proton-metal distances exhibit an interesting pattern: the ratio of exchangeable to non exchangeable protons is very high among protons which are relatively close to the binding site. This is in quite good agreement with the NMR spectra which feature a relatively high number of exchangeable resonances with short relaxation times. The assignments described in the following seemed obvious at first, however, as will become clear later, they cannot be taken for granted. Since d, x', y', and z' are fastest relaxing among the exchangeable peaks, they could correspond to the amide protons of Asp 88, Asp 82, Asp 87, and Asp 84, which feature similar distances to the metal binding site (3.84-4.17 Å). z' is most likely part of either Asp 88 or Asp 82, while d is most likely part of Asp 87 or Asp 84.

There is a gap in metal-proton distances between the amide protons of Asp 84 (4.17 Å) and Thr 86 (4.76 Å) which is reflected in the relaxation times: T_1 of d, the slowest of the four fastest relaxing resonances, is about 16 ms, whereas T_1 of H, the fifth fastest relaxing resonance, is larger than 30 ms. The next group of amide protons (Thr 86, Leu 81, Phe 80, and Leu 85) gives rise most likely to resonances g, v', k, and f, with f or k probably corresponding to Leu 85. The remaining hyperfine shifted exchangeable resonance l has a markedly longer relaxation time, which reflects the second gap in exchangeable proton to metal distances (H Leu 85 at 5.35 Å vs. H Asp 83 at 5.84 Å). l most likely corresponds to the amide proton of Asp 83.

Interpretation of the non-exchangeable resonances is even more ambiguous. Resonances A, B, C, I, M, and probably Oa are the fastest relaxing. However, it is not possible to quantify the extent of relaxation enhancement of I, M, and Oa, because they are overlapped by slower relaxing resonances. It is also unclear whether HA Phe 80

(proton nomenclature in amino acids according to the nomenclature used in pdb files) is too close to the metal binding site to give rise to an observable signal. Further, the HD protons of Phe 80 might cause two resonances corresponding to the two protons 1HD and 2HD at distances of 3.57 Å and 7.53 Å, or average out as one proton at a distance of 5.55 Å with double intensity. Finally, the region between 0 and -6 ppm is too crowded for relaxation-based interpretation. However, super-WEFT experiments showed that at least two resonances in this region are fairly fast relaxing, neither of which is exchangeable.

These complications prevented more detailed assignments of resonances from relaxation data alone. This study was set out to investigate the feasibility of assignments based on the combination of relaxation and two-dimensional NMR data. Thus, further assignments were sought with the help of NOE connectivities. Resonance l has an NOE cross peak with J. The identity of l has been established as being most likely H Asp83 from relaxation data. Since all non-exchangeable protons that are close to both the metal and H Asp83, belong to Asp 82, J is probably part of this spin system (either 1HB or 2HB). Another cross peak connects l to f, which can therefore be assigned to H Asp84, because this is the only amide proton close to H Asp83. f has more NOE cross signals to N and P, which are also connected among each other by cross peaks. f, N, and P are therefore probably all part of the same spin system, meaning that N and P can be assigned to HA and 1HB of Asp 84.

Another starting point for the interpretation of two-dimensional connectivities is O. From the comparison between bovine and human Yb-LA 1D spectra O has been shown to have an intensity of two, therefore probably corresponding to the averaged signal of two protons on a flipping aromatic ring system. Phe 80 is the only residue of the Ca²⁺ binding loop with an aromatic side chain. The HD Phe 80 protons are quite

close to the metal binding site, their signal is expected to relax faster than O. Therefore O corresponds most likely to the HE protons of Phe 80. There also exists an outside chance that signal O is caused by two non-equivalent protons. Their resonances would have to show the same temperature behavior (likely) and the same change in shifts upon going from bovine to human LA (less likely, but possible). Further, O shows three cross peaks to the S', U', v', W' spin system. Only the protons of Asp 87 are close enough to the HE protons of Phe 80 to account for those cross peaks; U' and W' probably correspond to 1HB and 2HB of Asp 87 (they are also mutually connected by COSY cross peaks), and S' can be assigned to HA Asp 87. v' has been connected in a 1D NOE experiment to k which in turn shows a cross signal to g. If v' is assigned to the amide proton of Asp 87, then k and g have to correspond to the amide protons of Thr 86 and Leu 85, respectively.

Although the assignments described above must be seen as tentative, none of the other possible assignment scenarios works without such assumptions as changes in the crystal structure upon going to the solution state or large errors in the measured T_1 times. Those could be justified relatively easy for exchangeable protons: signal intensities are used in the T_1 determination by inversion recovery. Signal intensities are decreased by exchange with solvent protons if the solvent signal is saturated with a presaturation pulse and saturation transfer occurs as observed for example in Figure 15. It can be shown that this decrease in signal intensity leads to a concomitant decrease in the calculated T_1 times (Cutnell et al., 1981). However, if large errors are assumed in the T_1 values and one relies mainly on the information from the 2D spectra, the system is underdetermined, several assignment models become possible. In particular, the spin systems identified in the upfield region could correspond to any of the five Asp residues in the binding loop.

Since none of the assignment scenarios which relied on the protons closest to the metal binding site was very convincing, an additional explanation had to be considered. The relaxation properties of Yb^{3+} might be strong enough to broaden the signals of the closest protons to such an extent, that they become invisible in the NMR spectrum. This would require an expansion of the region of protons that are considered in the interpretation of hyperfine shifted peaks. Unfortunately, it is not trivial to figure out to what extent this shell might have to be expanded. Further, since the volume of a sphere increases with the third power of its radius, the number of protons that have to be considered increases dramatically upon expansion of the region under investigation. Those two factors prevented a successful assignment of resonances based on an extended shell around the metal binding site.

3.2.6 Exchange Studies

Before realizing the full extent of the difficulties associated with the assignment of the hyperfine shifted resonances, it seemed like a good idea to look for a method to connect them to their positions in the spectrum of Ca-LA. This would have given reliable “diamagnetic” chemical shifts, another piece of information that would have helped in assigning them. LA has a relatively small dissociation constant of about 10^{-7} M (Eberhard & Erne, 1991). Nevertheless, it might be possible to force exchange to at least a medium time scale by raising the temperature. A sample containing 0.5 equivalents of each Ca^{2+} and Yb^{3+} and one equivalent of LA (Yb,Ca-LA) should be suitable for 2D exchange spectroscopy (EXSY, (Jeener et al., 1979)). The EXSY pulse sequence is identical to that of NOESY. In order to detect cross-signals, exchange has

to happen fast enough that during the mixing time nuclei resonate for a while at the two different frequencies in each conformation. Since the NOESY and EXSY pulse sequences are identical, one has to be careful not to mistake NOE for exchange signals. They can be discriminated by their temperature behavior: NOE signals lose intensity with increasing temperature due to shortened rotational correlation times, while exchange signals gain intensity due to increased exchange rates.

EXSY spectra of Yb,Ca-LA in D₂O were recorded at 25 and 55°C. The few cross peaks present in the 25°C spectrum turned out to be NOE signals, because they vanished with increasing temperatures. Exchange at 55°C proved to be still too slow to produce any cross peaks. Unfortunately, the exchange could not be accelerated any further, because at temperatures beyond 55°C the protein denatures (cf. section 3.2.1). In order to establish whether the metal ions dissociate at a reasonable rate at 55°C, the same experiment was carried out with a sample containing 0.5 equivalents of Yb³⁺ and one equivalent of LA, which should give rise to cross-signals between the resonances in apo- and Yb-LA. But again no cross-signals were detected; the metal ion must be bound very strongly to the protein.

4. Conclusion

This study was designed to investigate the feasibility of paramagnetic NMR for the elucidation of the structure of metal binding sites of proteins. Particular interest was laid on whether the relatively newly developed two-dimensional paramagnetic techniques would allow for assignments in metalloproteins in which the metal is not part of a prosthetic group, but is coordinated exclusively by amino acid side chains of the protein itself. LA which was used as a model system in this study is one of those metalloproteins and the solution structure of its binding site has until now not been solved.

Two different, but related approaches were taken. The first approach relied solely on the relaxation enhancing properties of paramagnetic agents, Ca^{2+} was exchanged for Gd^{3+} . It rapidly became obvious that this approach is not feasible, because the relaxation enhancing properties of Gd^{3+} are too strong to allow for detection of differential effects on protons depending on their distance to the metal binding site. The second approach combined relaxation enhancement and hyperfine shifting, and Ca^{2+} was exchanged for Yb^{3+} . Yb-LA was shown to have a similar melting point and therefore probably also a similar structure as Ca-LA. Yb-LA provided a very nice set of one- and two-dimensional NMR spectra, as well as relaxation enhancement data. However, even with the help of LA's crystal structure, it turned out to be impossible to develop a consistent model of resonance assignments. One or several of three main reasons may be responsible. First, the relaxation enhancing properties of Yb^{3+} , while being weaker than those of Gd^{3+} , are probably still too strong: resonances corresponding to protons very close to the metal binding site are broadened to such an extent that they become invisible in the NMR spectrum. Second, it is possible that the

contact contribution has a stronger influence on the relaxation time values than originally expected. Third, the crystal and solution structures might differ significantly. The side chains directly coordinated are expected to have limited flexibility. However, resonances from these residues might be invisible for reasons stated above. Side chains that are part of the metal binding loop, but are not coordinated to the metal are probably conformationally less restricted. They might change their orientation in solution as compared to the crystal, especially considering the position of the metal binding loop at the protein surface. This would make a correlation between NMR and crystal structure data hard, if not impossible.

LA has been notorious for the problems associated with the elucidation of its solution structure (Alexandrescu et al., 1992). Nevertheless, because the stability of its molten globule state under certain conditions promises insights into the process of protein folding, it remains a potentially important system to study. So, although the investigation of LA's binding site by paramagnetic NMR turned out not to be feasible, this approach should not be disregarded in the future. In order to better judge over the feasibility of this technique, it should be applied to a system in which previous NMR studies have demonstrated that it is more accessible than LA.

Run	Sample	Experiment	T/°C	B ₀ /Tesla*	SW/Hz	scans	points
1	3 mM D ₂ O	standard 1D	31.5	2.11	10,000	24x256	8192
2 a-j	0.2 mM D ₂ O	standard 1D	various	11.74	50,000	4096	8192
3	4 mM D ₂ O, human	standard 1D	45	11.74	50,000	8192	8192
4 a-c	4 mM H ₂ O	standard 1D, short recycle delay (80 ms); transmitter different pos.	25	9.39	125,000	4096	8192
5	4 mM D ₂ O	standard 1D, short recycle delay (80 ms)	25	9.39	125,000	4096	8192
6	4 mM H ₂ O	jump-return	25	9.39	44,667	512	8192
7	4 mM H ₂ O	SUPERWEFT (t ₁ = 20 ms)	25	9.39	125,000	8192	4096
8	4 mM D ₂ O	SUPERWEFT (t ₁ = 20 ms)	25	9.39	125,000	8192	4096
9	4 mM H ₂ O	SUPERWEFT (t ₁ = 40 ms)	25	9.39	125,000	8192	4096
10	4 mM D ₂ O	SUPERWEFT (t ₁ = 40 ms)	25	9.39	125,000	8192	4096
11	4 mM H ₂ O	1D NOE/WEFT	25	9.39	55,556	8192	16,384
12	4 mM H ₂ O	1D NOE/ jump-return	25	9.39	55,556	8192	16,384

Table 1 Summary of one-dimensional NMR experiments.

* corresponds in ¹H-NMR to 90, 400, and 500 MHz, respectively ($\nu = \gamma B_0 / 2\pi$)

Run	Sample	Experiment	SW (F1) in Hz	SW (F2) in Hz	t1 increments	scans in F2	points in F2
1	4 mM H ₂ O	NOESY/TPPI $\tau_M = 80$ ms	55,556	27,778	512	192	1024
2	4 mM H ₂ O	NOESY/TPPI $\tau_M = 20$ ms	55,556	27,778	512	192	1024
3	4 mM H ₂ O	COSY no TPPI	55,556	55,556	300	300	1024
4	4 mM H ₂ O	COSY no TPPI	55,556	55,556	400	400	1024
5	4 mM H ₂ O	TOCSY no TPPI	55,556	55,556	400	400	1024
6	4 mM D ₂ O	NOESY/TPPI $\tau_M = 80$ ms	10,000	5,000	512	192	1024
7	4 mM D ₂ O	COSY no TPPI	10,000	10,000	300	300	1024

Table 2 Summary of two-dimensional NMR experiments (400 MHz, 25°C, pH 6.8).

downfield region			upfield region		
	shift	δ_{DIA}^a		shift	δ_{DIA}^a
A	80.1		P'	-4.1	
B	75.6		Q'	-5.9	
C	48.0		R'	-9.3	1.9
d	45.4		S'	-10.7	1.5
E	34.8	8.1	T'	-12.8	-1.0
f	33.6		U'	-17.4	-3.7
g	31.9		v'	-27.2	
H	30.2	4.8	W'	-31.7	-1.1
I	25.4		x'	-33.6	
J	23.8	4.7	y'	-52.2	
k	20.5		(Ya') [†]		
l	19.6		z'	-103.7	
M	18.4				
N	16.3	4.2			
O	15.9	6.4			
(Oa) [‡]	≈ 14.5				
P	15.1	4.1			
Q	13.0	7.0			
R	11.7	4.5			

Table 3 Complete listing of the hyperfine shifted peaks detected in the 1D NMR spectra of Yb-LA (25°C, pH 6.8, 500 MHz).

^a determined by extrapolation

[†] very broad, might be artifact

[‡] only detected in the spectrum of human Yb-La

transmitter	on H ₂ O		upfield	downfield
resonance	T ₁ in ms	T ₂ in ms	T ₁ in ms	T ₁ in ms
C	15.6	0.52		16.1
d	≈ C			≈ C
E	49	2.05		51.4
f	68.8			48.1
g	35.9			27
H	32.3	2.04		34.2
J	41.3	1.17		54.4
k	54.8			59.2
l	107.5			96
N	81.9	3.50		
O	83.9	4.13		
P	67.2	3.12		
R'	126.4	5.40	121.9	
S'	158.2	6.01	138.2	
T'	104.9	2.77	105	
U'	79	1.83	75.1	
v'	45.1		47.3	
W'	104.3	1.62	70.7	
y'			17.1	

Table 4 T₁ and T₂ values of the hyperfine-shifted resonances in the 1D NMR spectrum of Yb-LA (25°C, pH 6.8, 500 MHz).

HA	PHE	80	3.03	1HB	PHE	80	6.02
1HD	PHE	80	3.57	2HB	LEU	85	6.04
HA	LEU	85	3.66	1HG	LYS+	79	6.10
2HB	ASP	84	3.73	1HD2	LEU	85	6.14
<u>H</u>	ASP	88	3.84	3HD1	ILE	75	6.16
<u>H</u>	ASP	82	3.85	<u>H</u>	ILE	89	6.26
<u>H</u>	ASP	87	4.06	HA	ASP	87	6.26
<u>H</u>	ASP	84	4.17	HG	LEU	85	6.27
2HB	LYS+	79	4.17	HA	LEU	81	6.27
3HD2	LEU	85	4.46	HA	ASP	83	6.37
HA	LYS+	79	4.60	<u>H</u>	LYS+	79	6.44
<u>H</u>	THR	86	4.76	1HB	LEU	85	6.57
<u>H</u>	LEU	81	4.92	HB	THR	38	6.67
<u>H</u>	PHE	80	5.07	HA	THR	86	6.92
1HB	ASP	88	5.18	2HD1	ILE	75	6.97
2HB	ASP	82	5.20	2HG	LYS+	79	6.97
1HE	PHE	80	5.26	2HA	GLY	51	7.05
1HB	ASP	82	5.30	1HB	LEU	81	7.12
<u>H</u>	LEU	85	5.35	2HG2	THR	38	7.17
1HB	LYS+	79	5.36	2HG2	THR	86	7.25
HA	ASP	88	5.37	2HD	LYS+	79	7.28
1HB	ASP	84	5.38	<u>H</u>	LEU	52	7.31
1HB	ASP	87	5.39	1HG1	ILE	75	7.31
HA	ASP	84	5.40	1HG2	THR	38	7.39
2HB	PHE	80	5.47	1HE	LYS+	79	7.40
2HB	ASP	87	5.51	3HD1	ILE	89	7.45
1HD1	ILE	75	5.66	HG	LEU	81	7.50
2HD2	LEU	85	5.69	2HD	PHE	80	7.53
HB	THR	86	5.76	2HD	PHE	53	7.53
2HB	ASP	88	5.79	2HD1	ILE	55	7.54
<u>H</u>	ASP	83	5.84	HZ	PHE	80	7.59
1HD	LYS+	79	5.95	<u>H</u>	VAL	90	7.59
HA	ASP	82	6.01	2HG1	VAL	90	7.64

Table 5 Distances between Ca^{2+} and nearby protons in the crystal structure of bovine LA (from pdb file 1hfv), exchangeable protons underlined.

HA	PHE	80	3.03
HA	LEU	85	3.66
2HB	ASP	84	3.73
H	ASP	88	3.84
H	ASP	82	3.85
H	ASP	87	4.06
H	ASP	84	4.17
2HB	LYS+	79	4.17
HD	PHE	80	4.23
HA	LYS+	79	4.60
H	THR	86	4.76
HD2	LEU	85	4.84
H	LEU	81	4.92
H	PHE	80	5.07
1HB	ASP	88	5.18
2HB	ASP	82	5.20
1HB	ASP	82	5.30
H	LEU	85	5.35
1HB	LYS+	79	5.36
HA	ASP	88	5.37
1HB	ASP	84	5.38
1HB	ASP	87	5.39
HA	ASP	84	5.40
2HB	PHE	80	5.47
2HB	ASP	87	5.51
HB	THR	86	5.76
2HB	ASP	88	5.79
H	ASP	83	5.84
HE	PHE	80	5.85
1HD	LYS+	79	5.95
HA	ASP	82	6.01
1HB	PHE	80	6.02
2HB	LEU	85	6.04
1HG	LYS+	79	6.10
HD1	ILE	75	6.11
H	ILE	89	6.26
HA	ASP	87	6.26
HG	LEU	85	6.27
HA	LEU	81	6.27
HA	ASP	83	6.37
H	LYS+	79	6.44
1HB	LEU	85	6.57
HB	THR	38	6.67
HA	THR	86	6.92
2HG	LYS+	79	6.97
2HA	GLY	51	7.05
1HB	LEU	81	7.12
2HD	LYS+	79	7.28
H	LEU	52	7.31
1HG1	ILE	75	7.31
1HE	LYS+	79	7.40
HG2	THR	38	7.58
HG	LEU	81	7.50
HZ	PHE	80	7.59
H	VAL	90	7.59
HG1	THR	86	7.74
HG2	THR	86	7.78
1HA	GLY	51	7.82
HA	ASP	78	7.87
HD1	ILE	89	7.89
HB	ILE	89	7.91
1HB	ASP	83	7.92
2HB	LEU	81	7.93
2HG1	ILE	75	8.00
HD1	LEU	85	8.00
1HB	CYS	91	8.05

Table 6 Modification of Table 5 by taking the average distances for equivalent methyl and ring-protons (bold print) as described in Section 3.2.5.

LYS	GLN	LEU	THR	LYS	CYS	ALA	LEU	SER	HIS	GLU	LEU	ASN	ASP	LEU
LYS	GLN	PHE	THR	LYS	CYS	GLU	LEU	SER	GLN	LEU	LEU	LYS	ASP	ILE
GLU	GLN	LEU	THR	<u>LYS</u>	<u>CYS</u>	<u>GLU</u>	<u>VAL</u>	<u>PHE</u>	<u>ARG</u>	<u>GLU</u>	LEU	<u>LYS</u>	<u>ASP</u>	<u>LEU</u>
1	2	3	<u>4</u>	<u>5</u>	<u>6</u>	7	8	9	10	11	12	13	14	15
ALA	GLY	TYR	ARG	ASP	ILE	THR	LEU	PRO	GLU	TRP	LEU	CYS	ILE	ILE
ASP	GLY	TYR	GLY	GLY	ILE	ALA	LEU	PRO	GLU	LEU	ILE	CYS	THR	MET
LYS	GLY	<u>TYR</u>	<u>GLY</u>	<u>GLY</u>	VAL	SER	<u>LEU</u>	<u>PRO</u>	<u>GLU</u>	<u>TRP</u>	<u>VAL</u>	<u>CYS</u>	<u>THR</u>	<u>THR</u>
16	17	<u>18</u>	19	20	21	22	<u>23</u>	<u>24</u>	<u>25</u>	26	27	<u>28</u>	29	30
PHE	HIS	ILE	SER	GLY	TYR	ASP	THR	GLN	ALA	ILE	VAL	LYS	ASN	SER
PHE	HIS	THR	SER	GLY	TYR	ASP	THR	GLN	ALA	ILE	VAL	GLU	ASN	ASN
<u>PHE</u>	<u>HIS</u>	<u>THR</u>	<u>SER</u>	GLY	TYR	ASP	THR	GLN	ALA	<u>ILE</u>	<u>VAL</u>	<u>GLN</u>	ASN	ASN
<u>31</u>	<u>32</u>	<u>33</u>	<u>34</u>	<u>35</u>	36	37	<u>38</u>	39	40	41	<u>42</u>	43	44	45
ASP	HIS	LYS	GLU	TYR	GLY	LEU	PHE	GLN	ILE	ASN	ASP	LYS	ASP	PHE
GLU	SER	THR	GLU	TYR	GLY	LEU	PHE	GLN	ILE	SER	ASN	LYS	LEU	TRP
ASP	SER	<u>THR</u>	<u>GLU</u>	<u>TYR</u>	GLY	LEU	PHE	GLN	<u>ILE</u>	<u>ASN</u>	ASN	LYS	ILE	TRP
46	47	<u>48</u>	<u>49</u>	<u>50</u>	<u>51</u>	52	<u>53</u>	<u>54</u>	<u>55</u>	<u>56</u>	57	58	59	60
CYS	GLU	SER	SER	THR	THR	VAL	GLN	SER	ARG	ASN	ILE	CYS	ASP	ILE
CYS	LYS	SER	SER	GLN	VAL	PRO	GLN	SER	ARG	ASN	ILE	CYS	ASP	ILE
CYS	LYS	ASP	ASP	GLN	ASN	PRO	HIS	SER	SER	ASN	ILE	CYS	ASN	ILE
<u>61</u>	62	63	64	65	66	67	68	<u>69</u>	70	71	<u>72</u>	<u>73</u>	74	75
SER	CYS	ASP	LYS	LEU	LEU	ASP	ASP	ASP	LEU	THR	ASP	ASP	ILE	MET
SER	CYS	ASP	LYS	PHE	LEU	ASP	ASP	ASP	ILE	THR	ASP	ASP	ILE	MET
SER	<u>CYS</u>	<u>ASP</u>	<u>LYS</u>	<u>PHE</u>	LEU	ASP	ASP	ASP	LEU	<u>THR</u>	<u>ASP</u>	<u>ASP</u>	<u>ILE</u>	<u>MET</u>
76	<u>77</u>	78	79	80	<u>81</u>	82	83	84	85	86	87	88	89	90
CYS	VAL	LYS	LYS	ILE	LEU	ASP	ILE	LYS	GLY	ILE	ASP	TYR	TRP	LEU
CYS	ALA	LYS	LYS	ILE	LEU	ASP	ILE	LYS	GLY	ILE	ASN	TYR	TRP	LEU
<u>CYS</u>	<u>VAL</u>	<u>LYS</u>	<u>LYS</u>	<u>ILE</u>	<u>LEU</u>	<u>ASP</u>	<u>LYS</u>	VAL	GLY	<u>ILE</u>	ASN	<u>TYR</u>	TRP	<u>LEU</u>
<u>91</u>	92	93	<u>94</u>	<u>95</u>	96	97	98	99	<u>100</u>	<u>101</u>	102	103	<u>104</u>	<u>105</u>
ALA	HIS	LYS	PRO	LEU	CYS	SER	ASP	LYS	LEU	GLU	GLN	TRP	TYR	CYS
ALA	HIS	LYS	ALA	LEU	CYS	THR	GLU	LYS	LEU	GLU	GLN	TRP	LEU	CYS
<u>ALA</u>	<u>HIS</u>	<u>LYS</u>	<u>ALA</u>	<u>LEU</u>	CYS	SER	GLU	LYS	<u>LEU</u>	<u>ASP</u>	<u>GLN</u>	<u>TRP</u>	LEU	CYS
<u>106</u>	<u>107</u>	<u>108</u>	109	<u>110</u>	<u>111</u>	112	113	114	<u>115</u>	116	<u>117</u>	<u>118</u>	119	120
GLU	ALA	GLN												
GLU	LYS	LEU												
GLU	LYS	LEU												
121	122	123												

Figure 1 Primary structures of guinea pig, human and bovine LA (top, middle and bottom row, respectively);
Secondary structure of bovine LA: α -helix, 3_{10} -helix, β -sheet;
Underlined numbers indicate residues conserved in all known primary structures of LA.



Figure 2 Ribbon drawing of the crystal structure of bovine LA from pdb file 1hfz; the calcium ion is seen as the small sphere in the upper left.

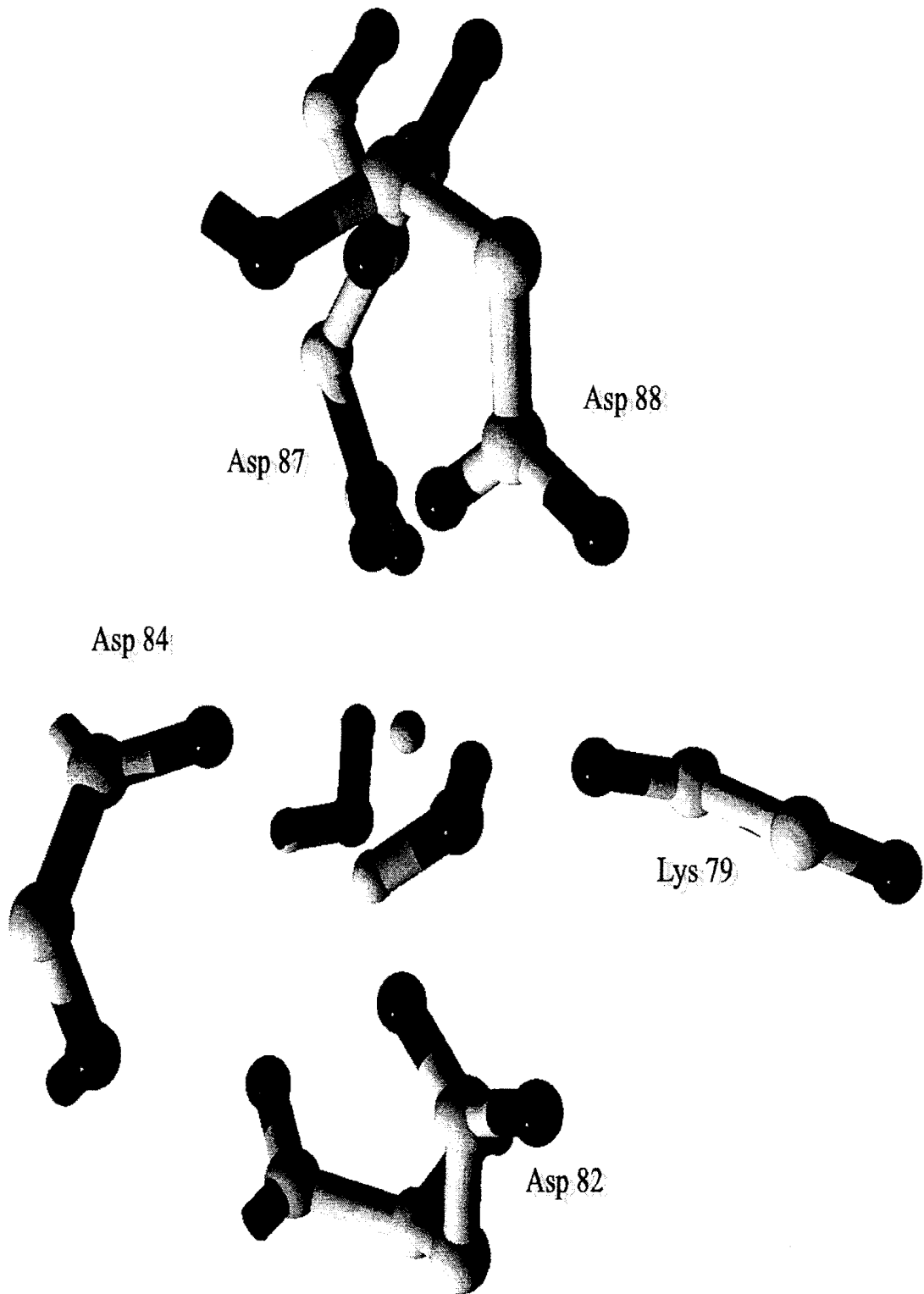


Figure 3 The Ca²⁺ binding site of bovine LA from pdb file 1hfz.

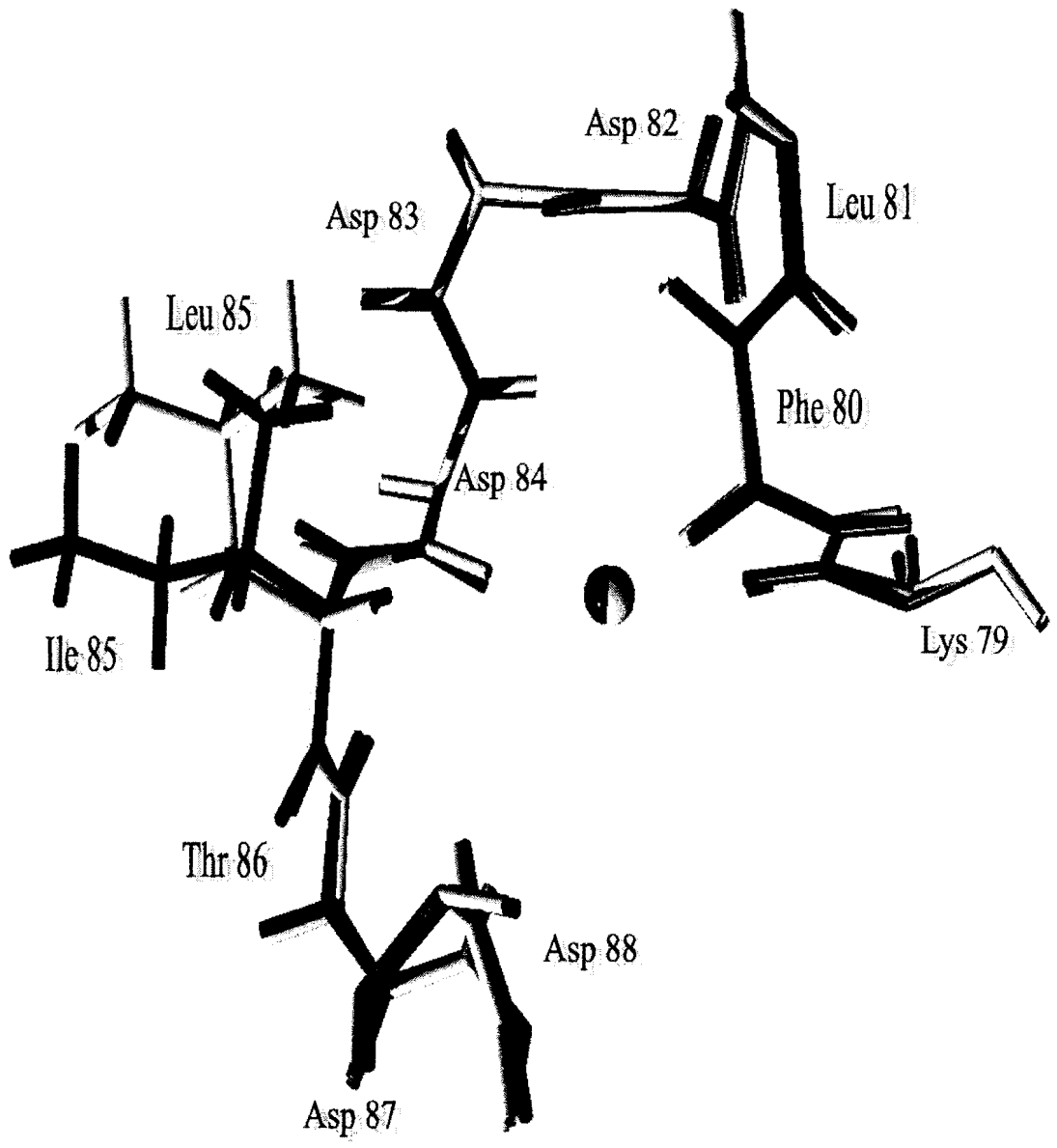


Figure 4 Superposition of the Ca²⁺ binding loops of human (dark) and bovine LA (light) from the pdb files 1hml (human) and 1hfz (bovine).

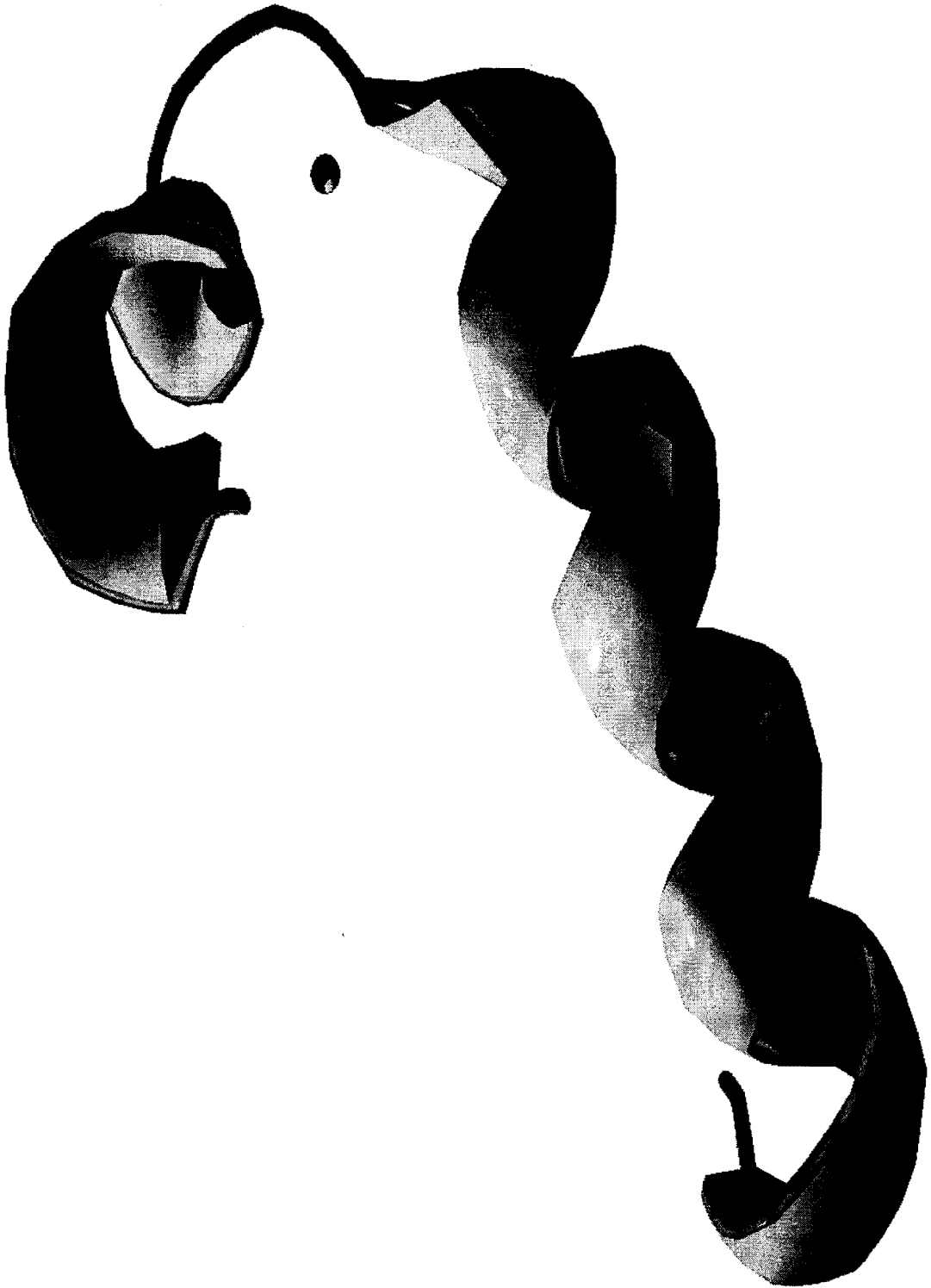


Figure 5 The "Calcium Elbow" in LA.

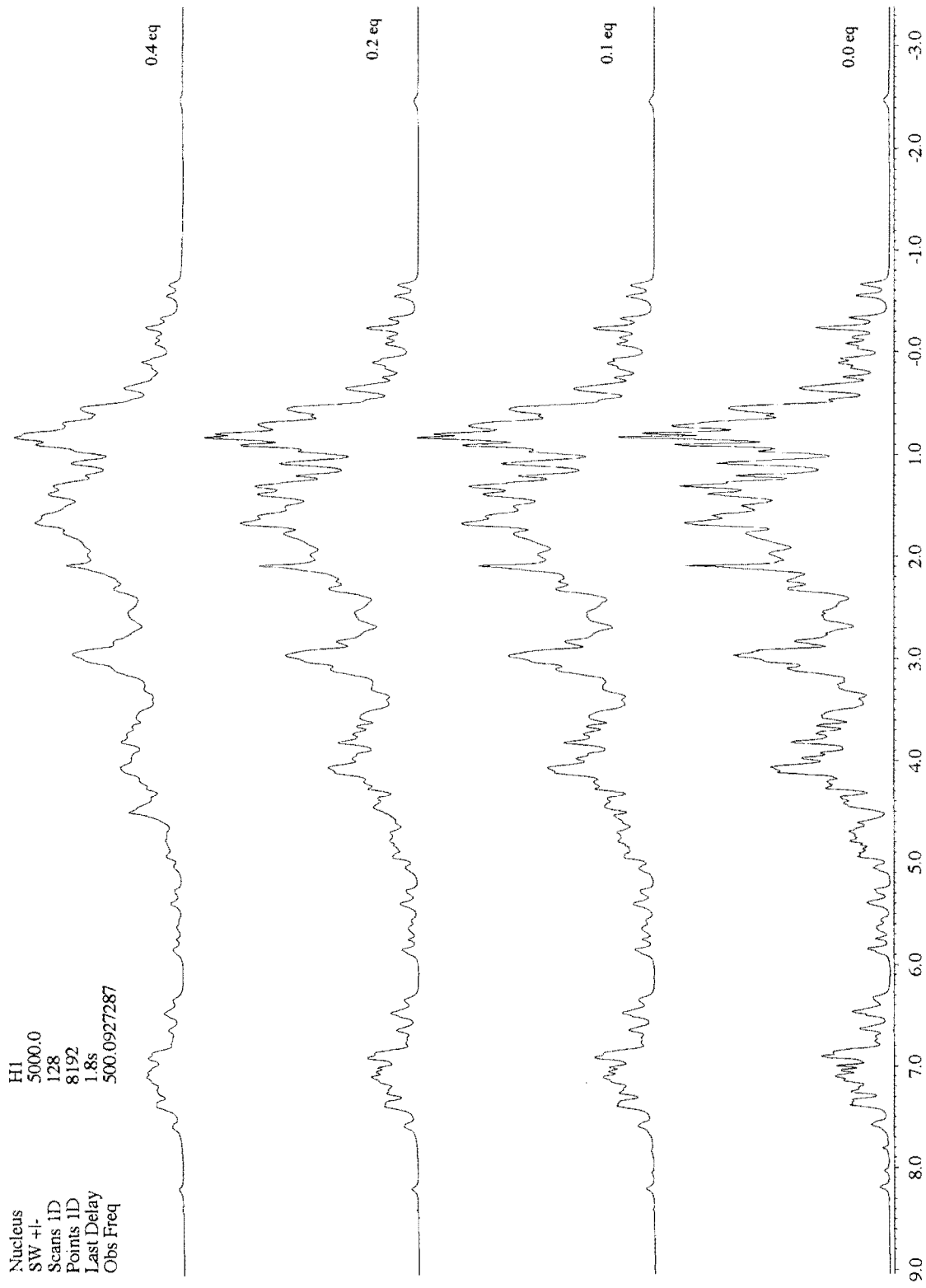


Figure 6 Titration of Ca-LA with Gd^{3+} ($[Ca-LA] = 4 \text{ mM}$ in D_2O , pH 6.8, $45^\circ C$).

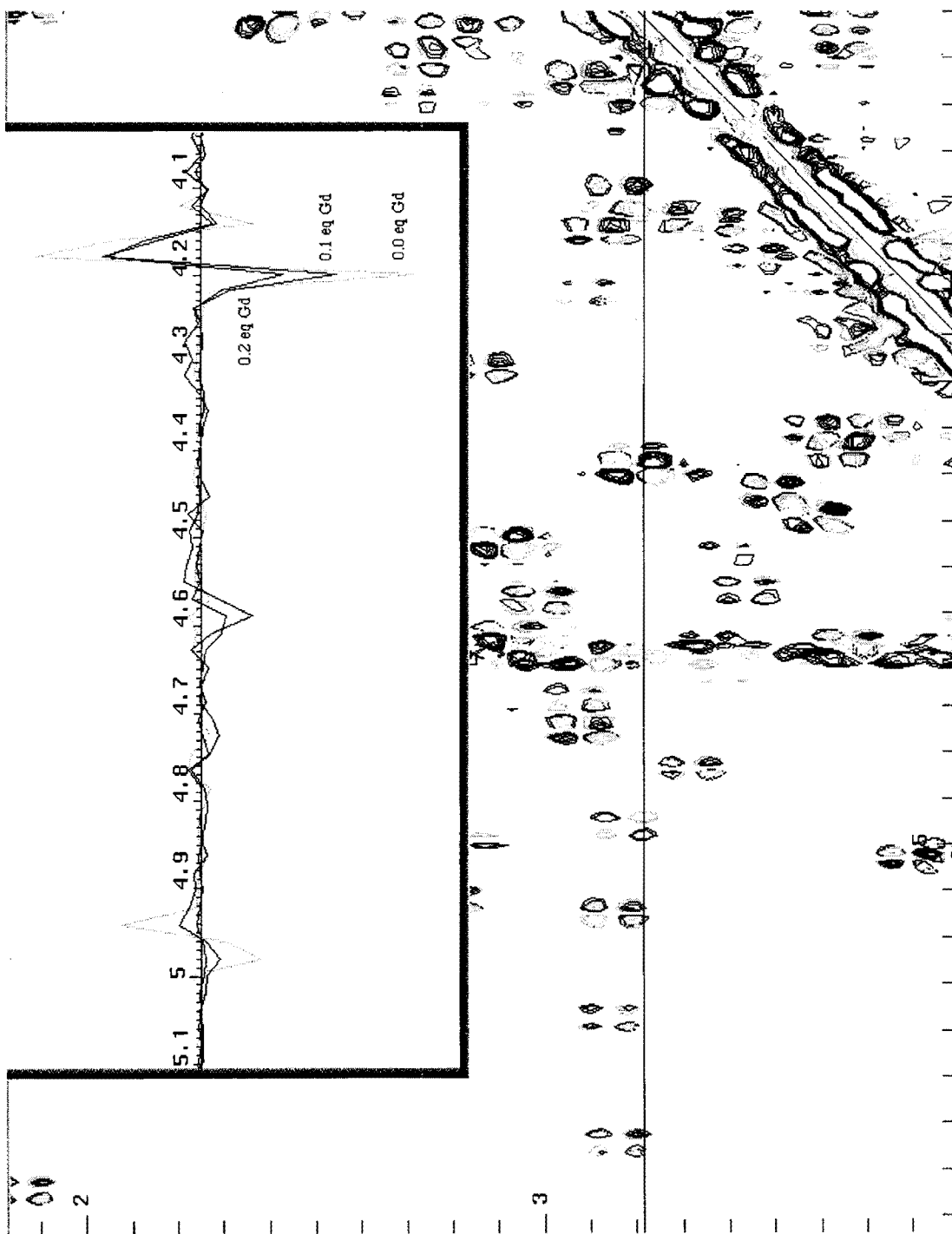


Figure 7 Superposition of three COSY spectra in ANSIG ($[\text{Ca-LA}] = 4 \text{ mM}$ in D_2O , pH 6.8, 45°C); slices were extracted at 3.22 ppm for display in the inset.

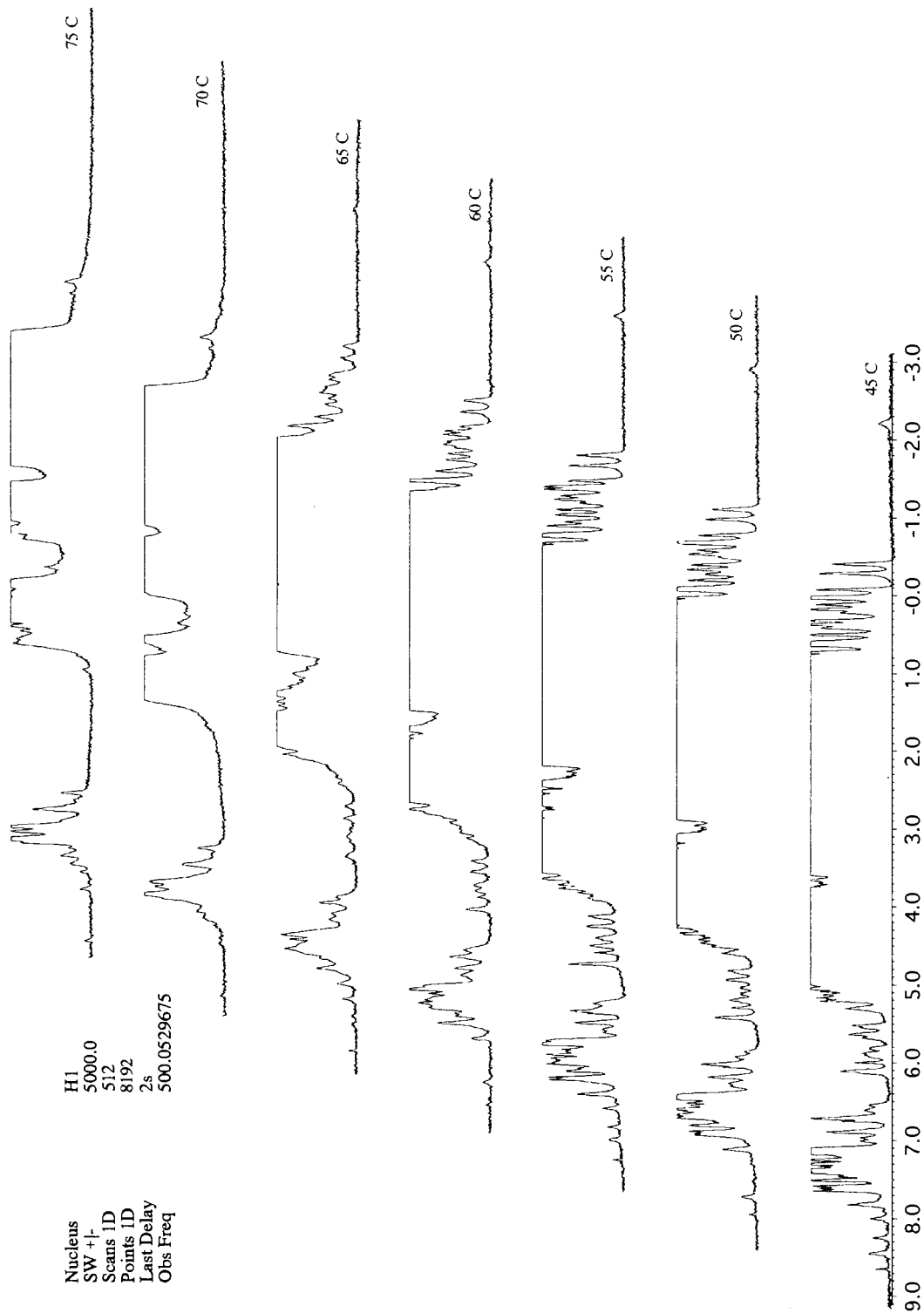


Figure 8 Temperature dependence of the 1D NMR spectrum of Ca-LA ($[\text{Ca-LA}] = 0.2 \text{ mM}$ in D_2O , pH 6.8).

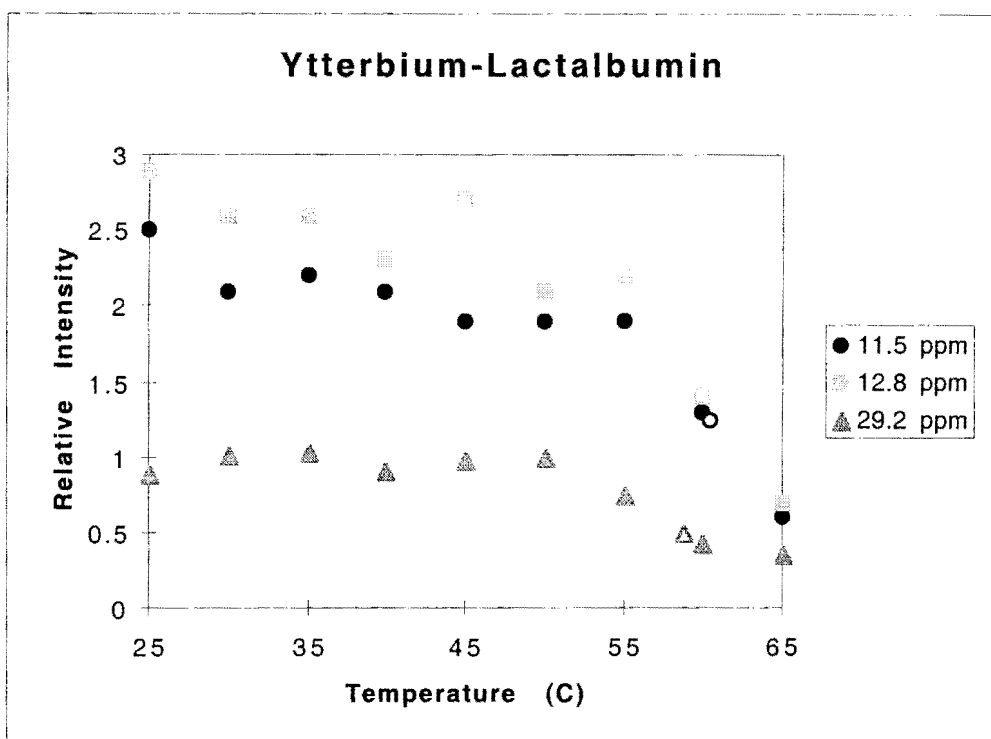
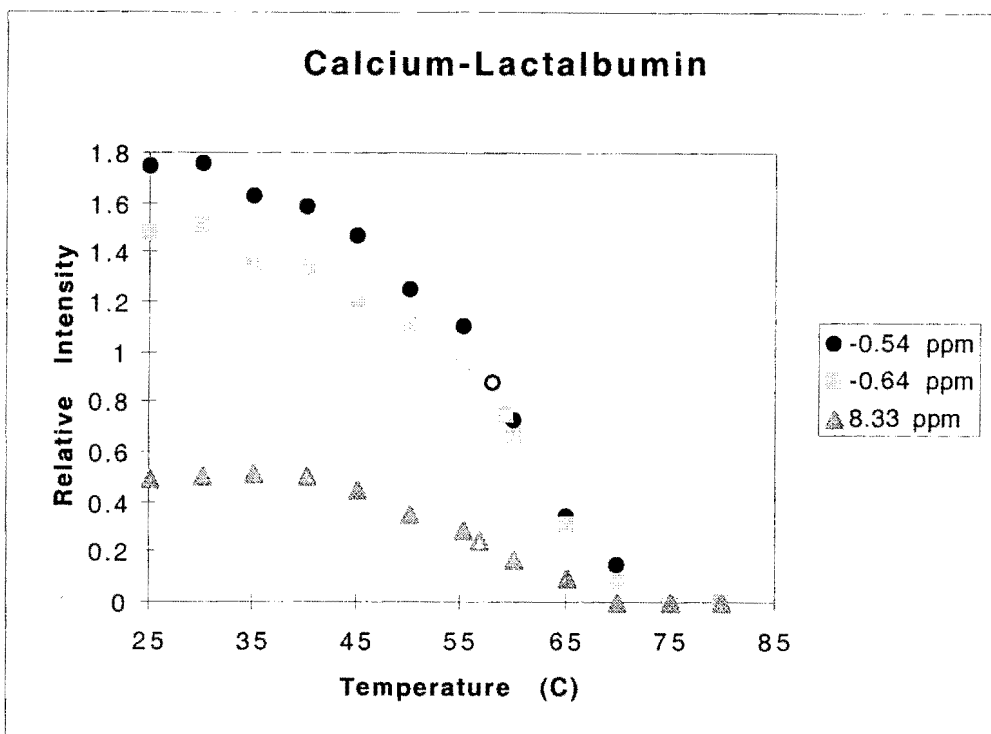


Figure 9 Temperature dependence of peak intensities in the 1D NMR spectra of (a) calcium and (b) ytterbium LA (empty markers indicate the midpoints of the transition curves).

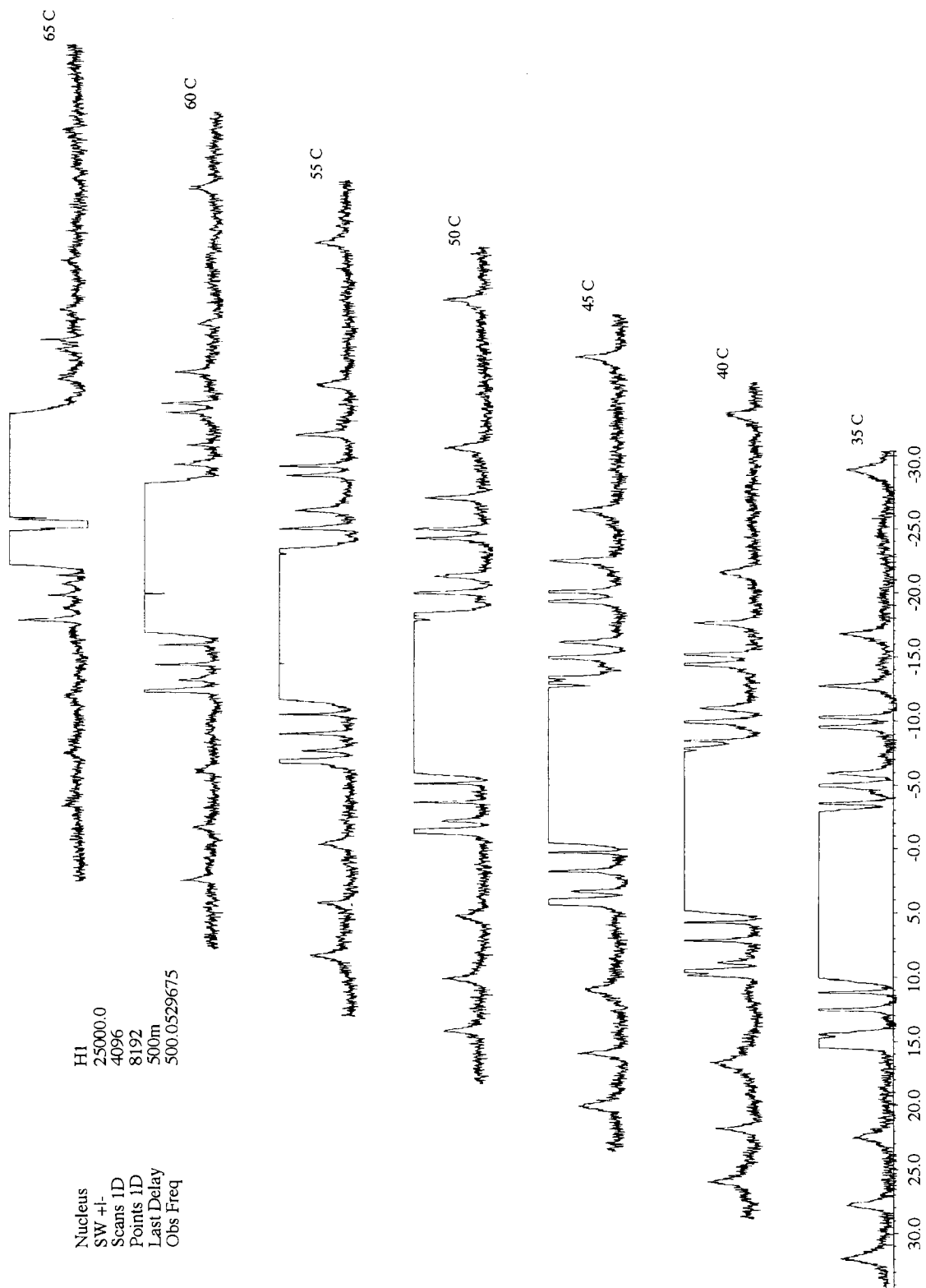


Figure 10 Temperature dependence of the 1D NMR spectrum of Yb-LA ([Yb-LA] = 0.2 mM in D₂O, pH 6.8).

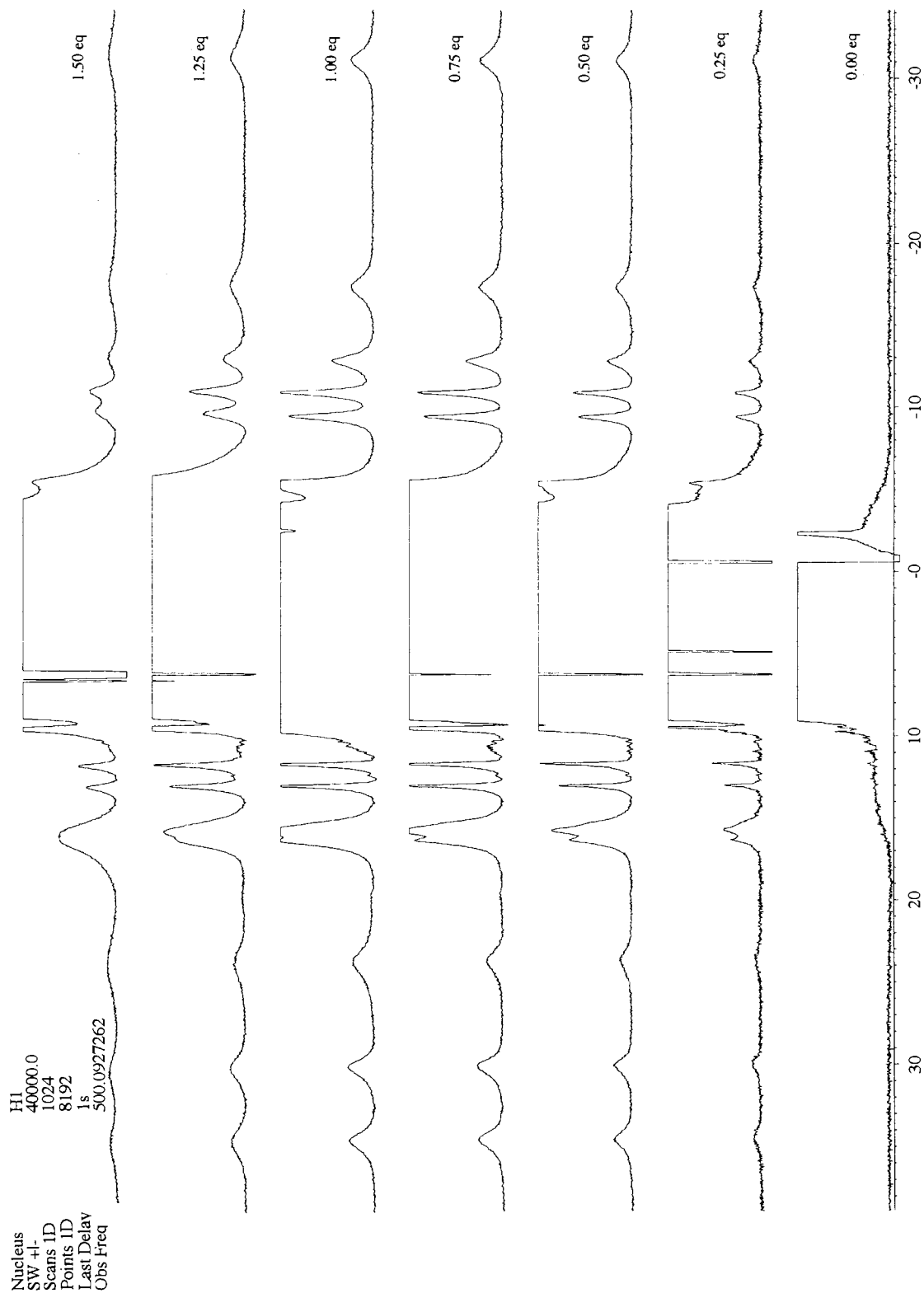


Figure 11 Titration of Ca^{2+} depleted bovine LA with Yb^{3+} ($[\text{LA}] = 8 \text{ mM}$ in D_2O , pH 6.8, 25°C).

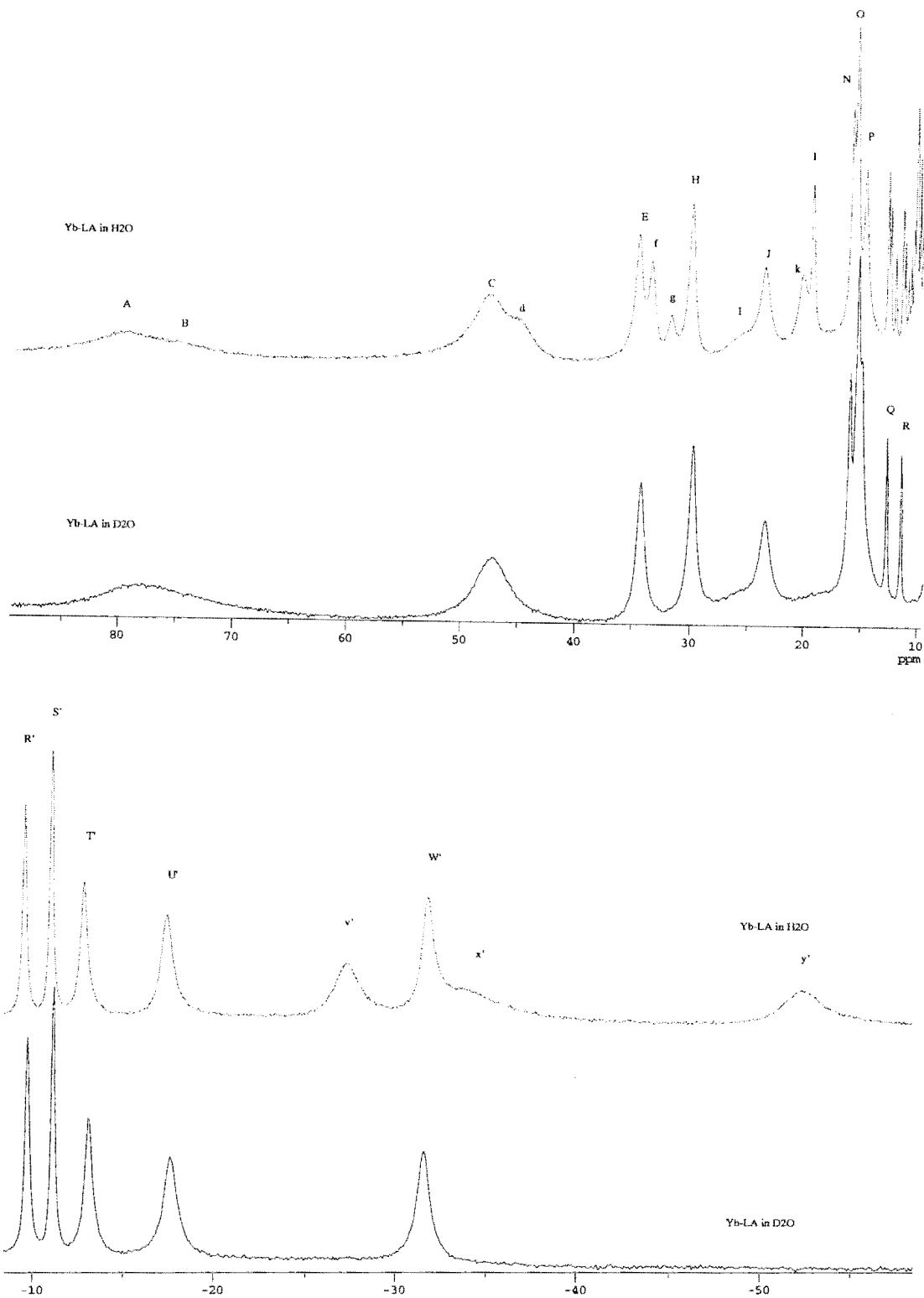


Figure 12 1D spectra of Yb-LA with short recycle delays ($[Yb-LA] = 4 \text{ mM}$, pH 6.8, 25°C , 400 MHz, recycle delay 80 ms).

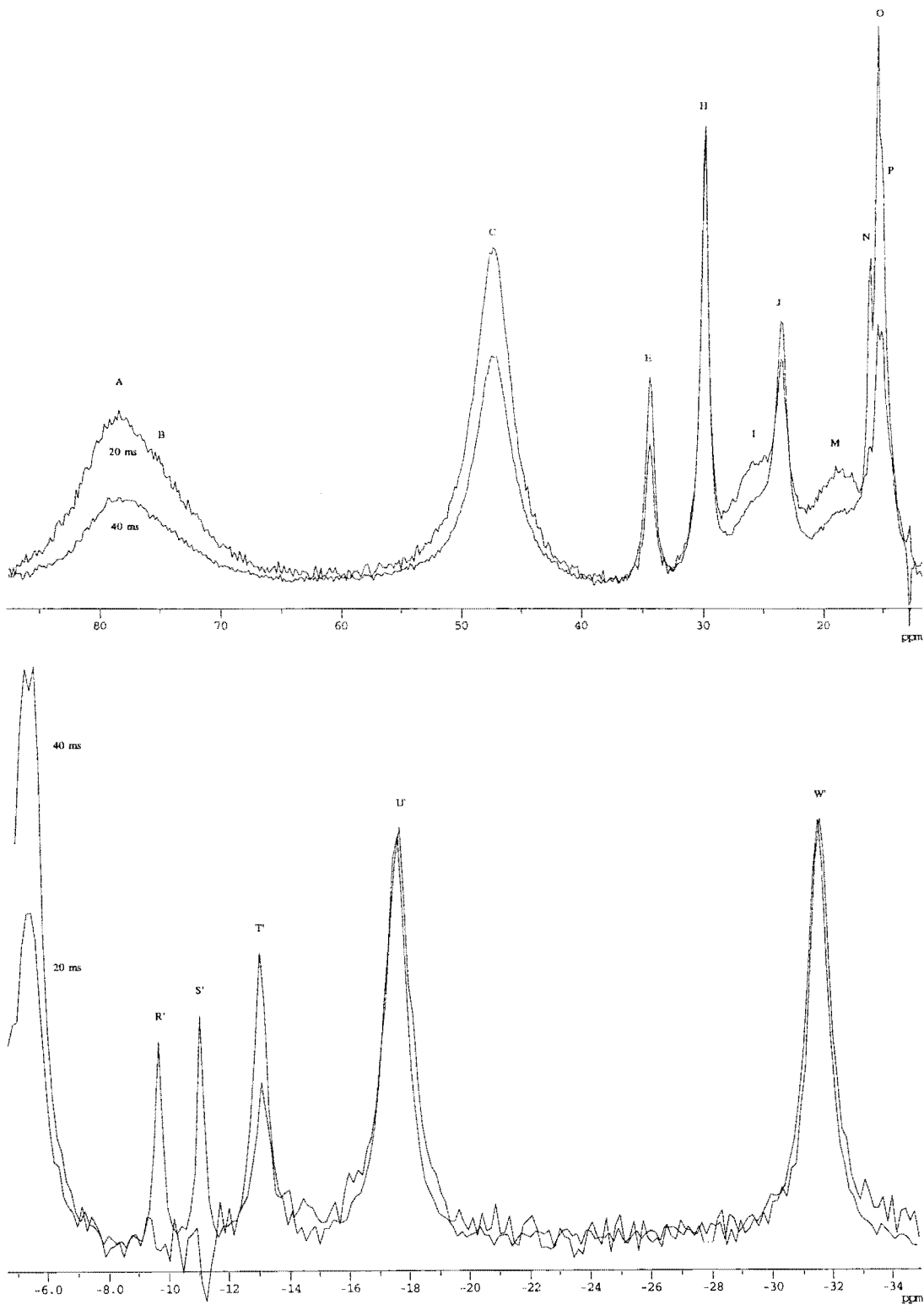


Figure 13 Super-WEFT spectra of Yb-LA in D₂O ([Yb-LA] = 4 mM, pH 6.8, 25°C, 400 MHz).

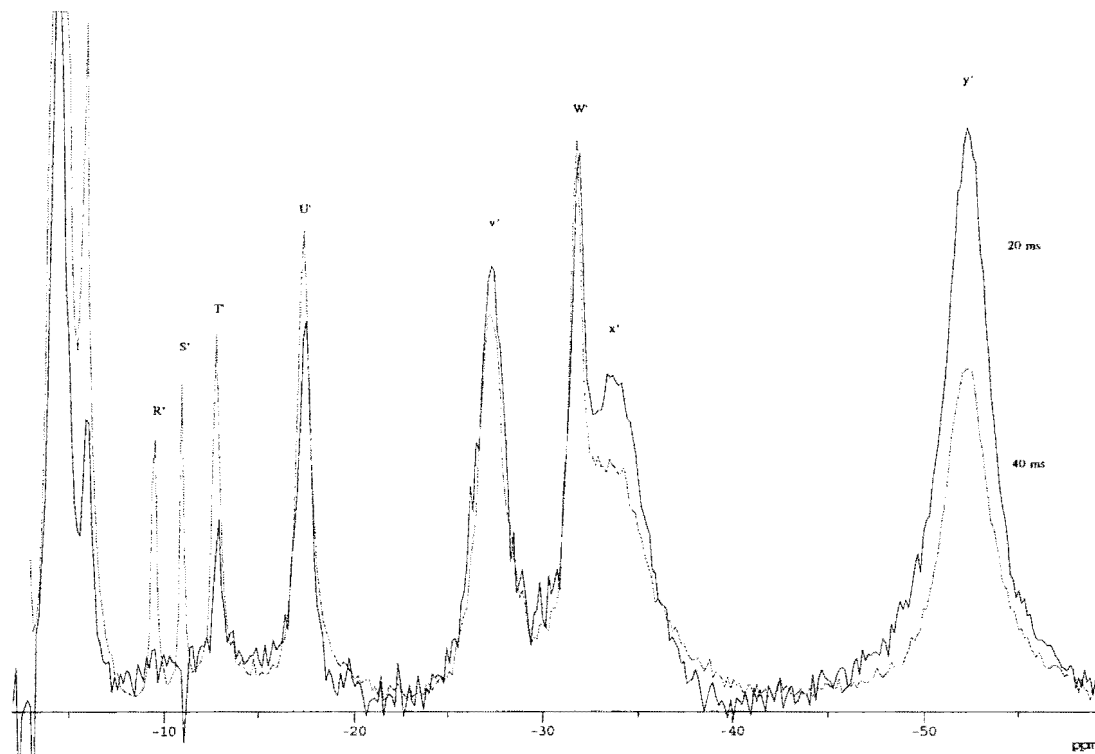
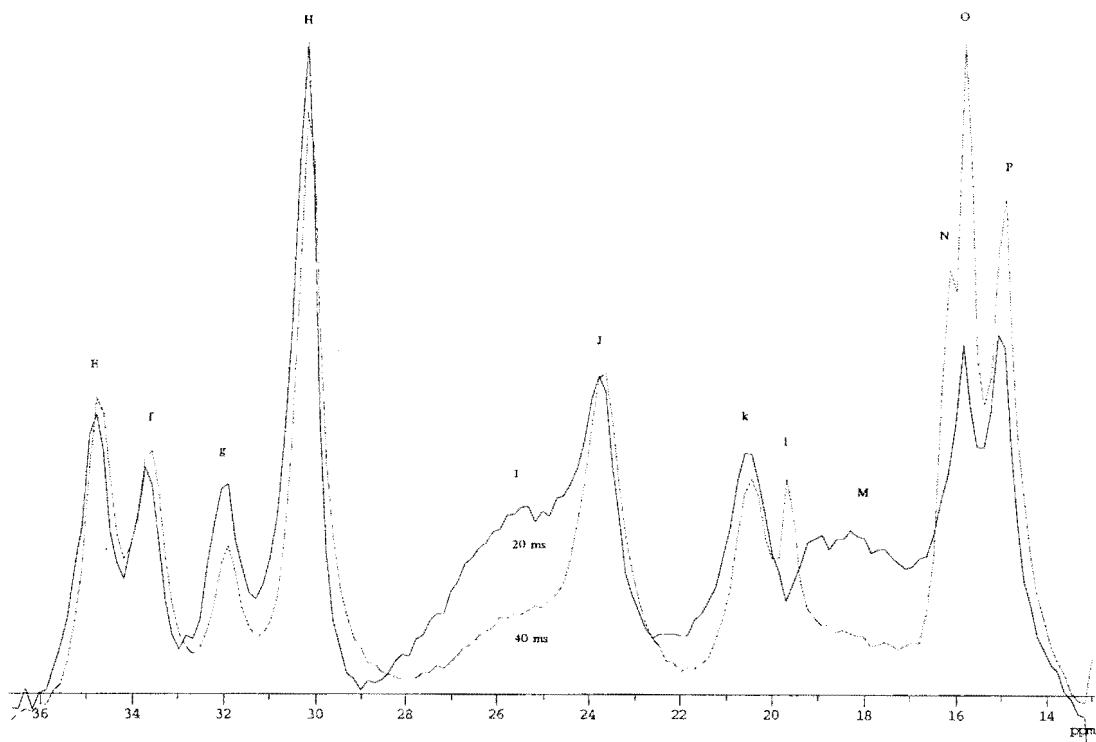


Figure 14 Super-WEFT spectra of Yb-LA in H₂O ([Ca-LA] = 4 mM, pH 6.8, 25°C, 400 MHz).

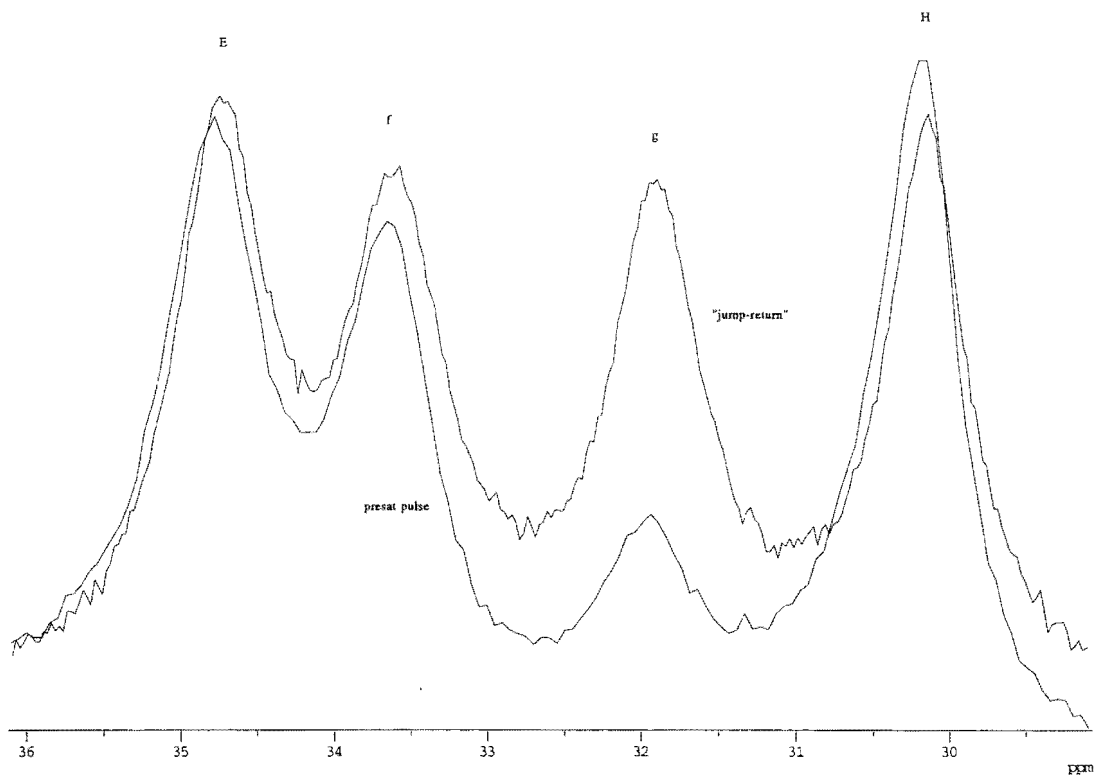


Figure 15 1D spectra of Yb-LA with different solvent suppression ($[Ca-LA] = 4$ mM in H_2O , pH 6.8, $25^\circ C$, 400 MHz).

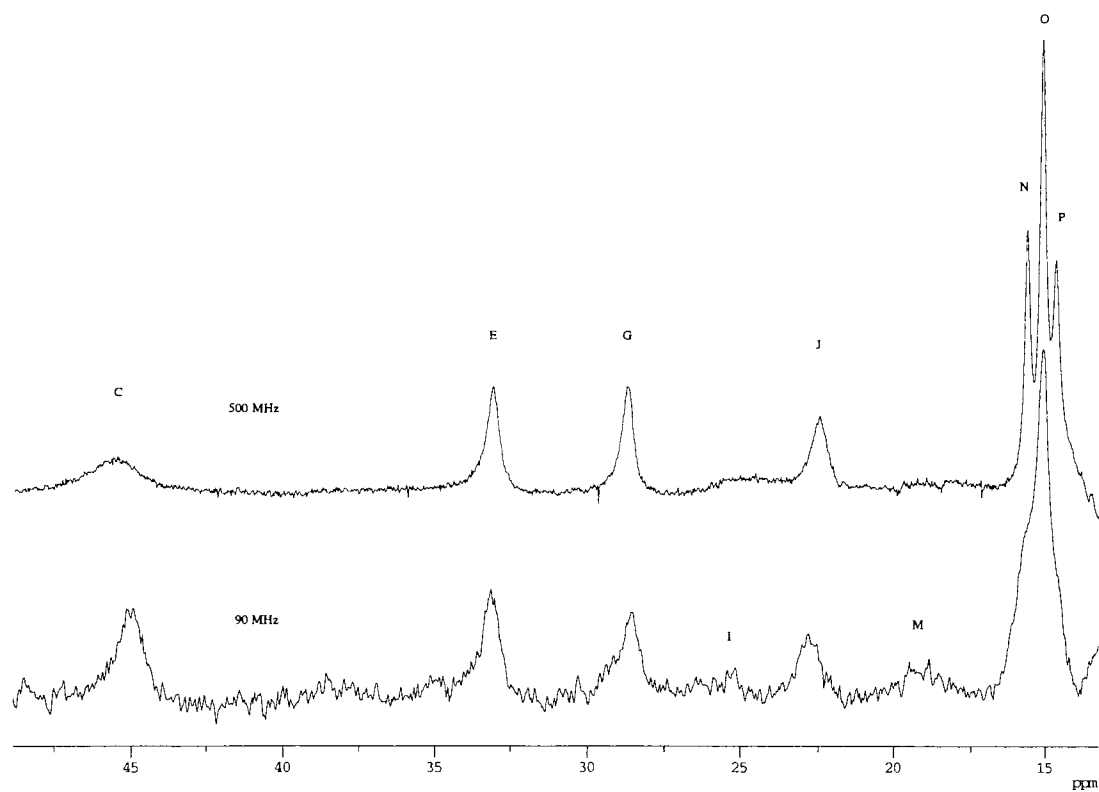


Figure 16 1D Spectra of Yb-LA at 90 MHz and 500 MHz ([Ca-LA] = 4 mM in D₂O at 500 MHz and 3 mM in D₂O at 90 MHz, pH 6.8, 31.5°C).

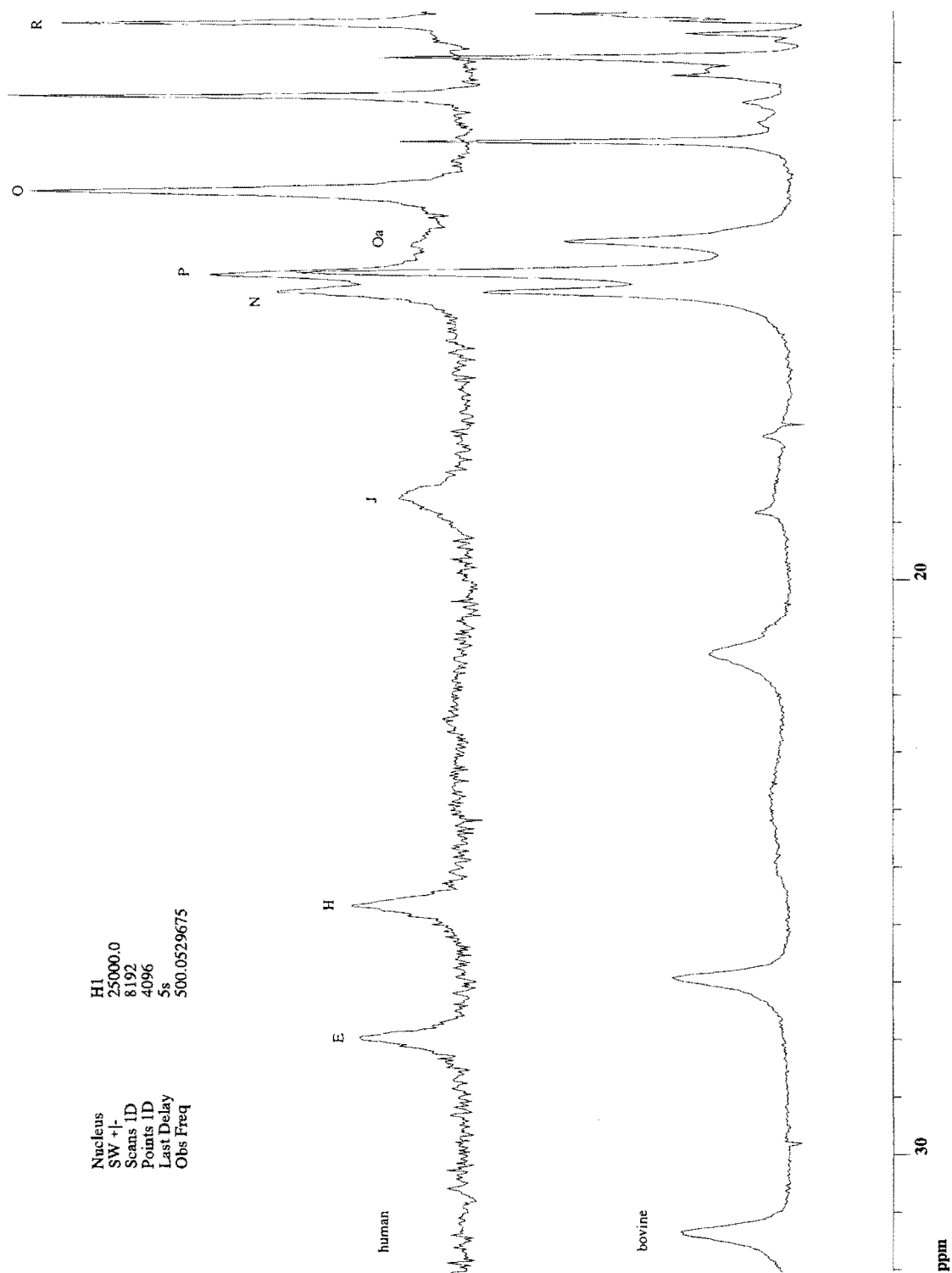


Figure 17 1D Spectra of human and bovine Yb-LA ([Yb-LA] = 4 mM in D₂O for bovine and 2 mM in D₂O for human LA, pH 6.8, 45°C)

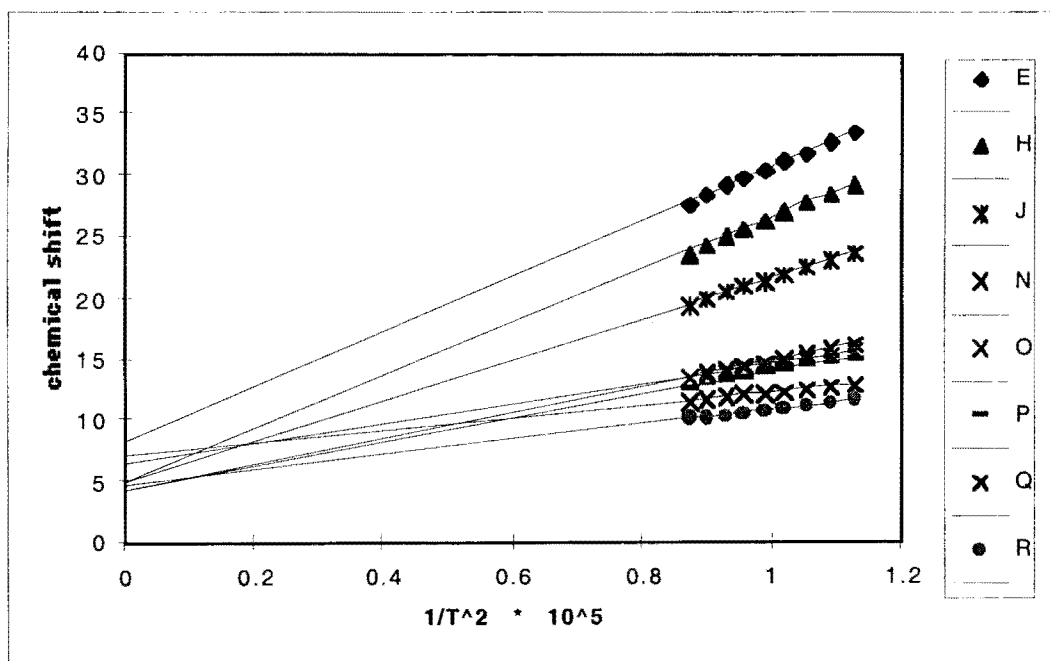
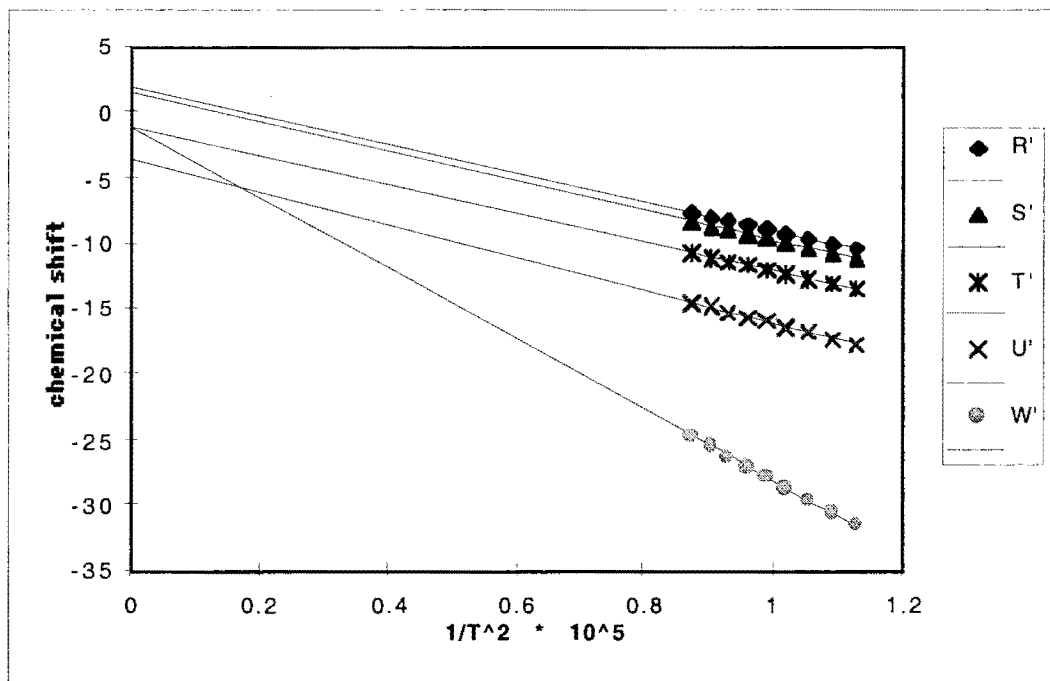


Figure 18 Extrapolation of the temperature behavior of the hyperfine shifted resonances of Yb-LA for the determination of diamagnetic chemical shifts.

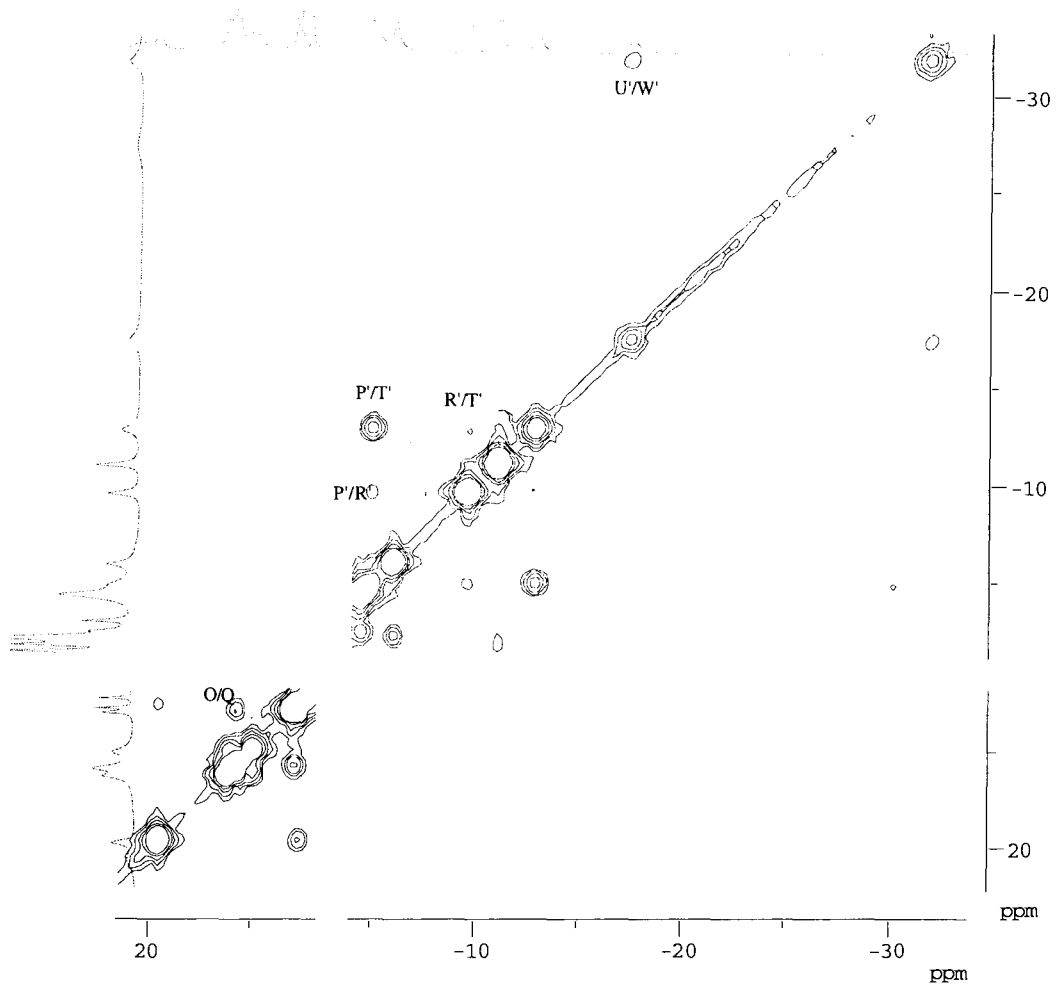


Figure 19 COSY spectrum of Yb-LA ([Yb-LA] = 4 mM in H₂O, 25 °C, pH 6.8, 400 MHz, apodized with a sine bell square function shifted by 0°).

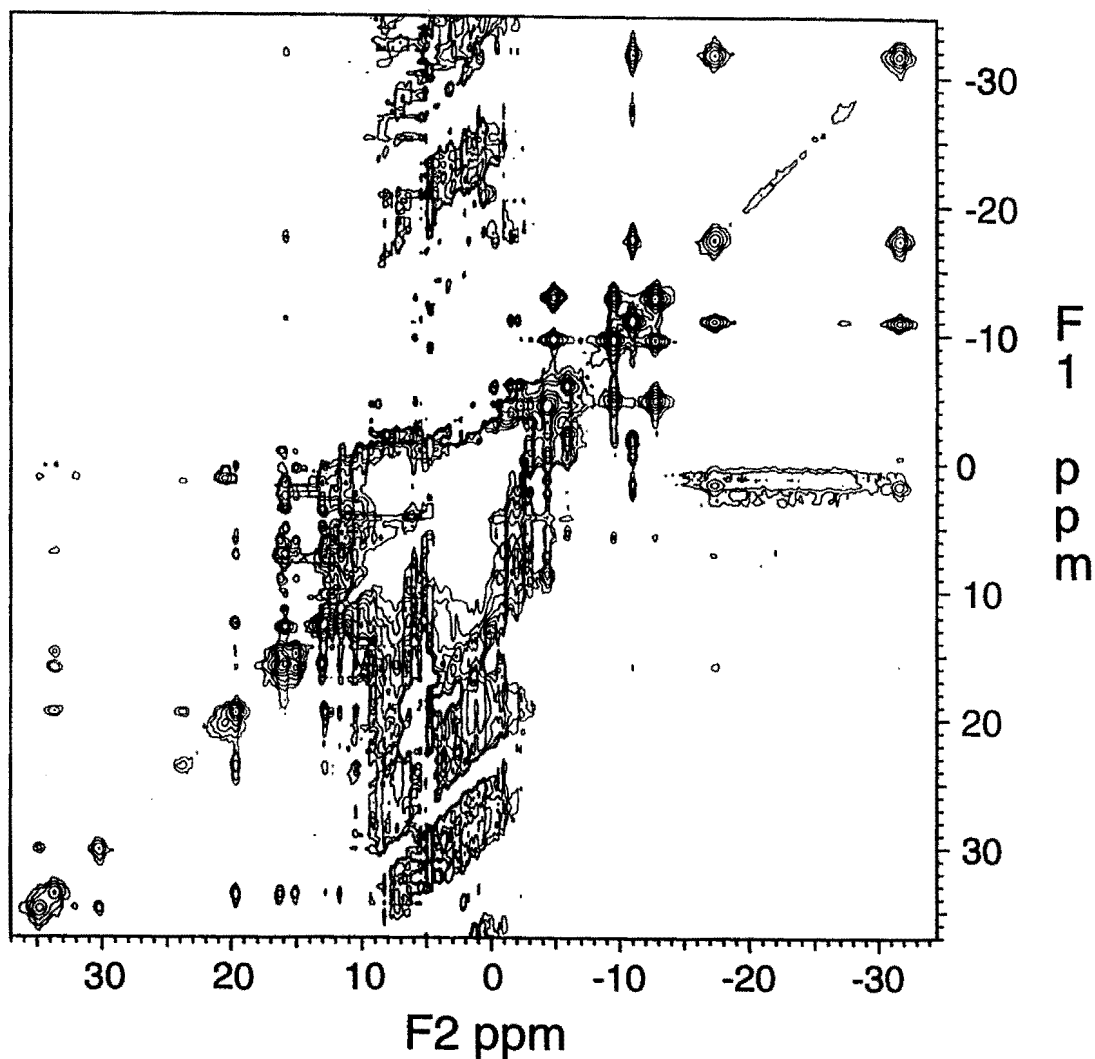


Figure 20 NOESY spectrum ($\tau_M = 80$ ms) of Yb-LA ([Yb-LA] = 4 mM in H₂O, 25 °C, pH 6.8, 400 MHz, apodized with a sine bell square function shifted by 54°).

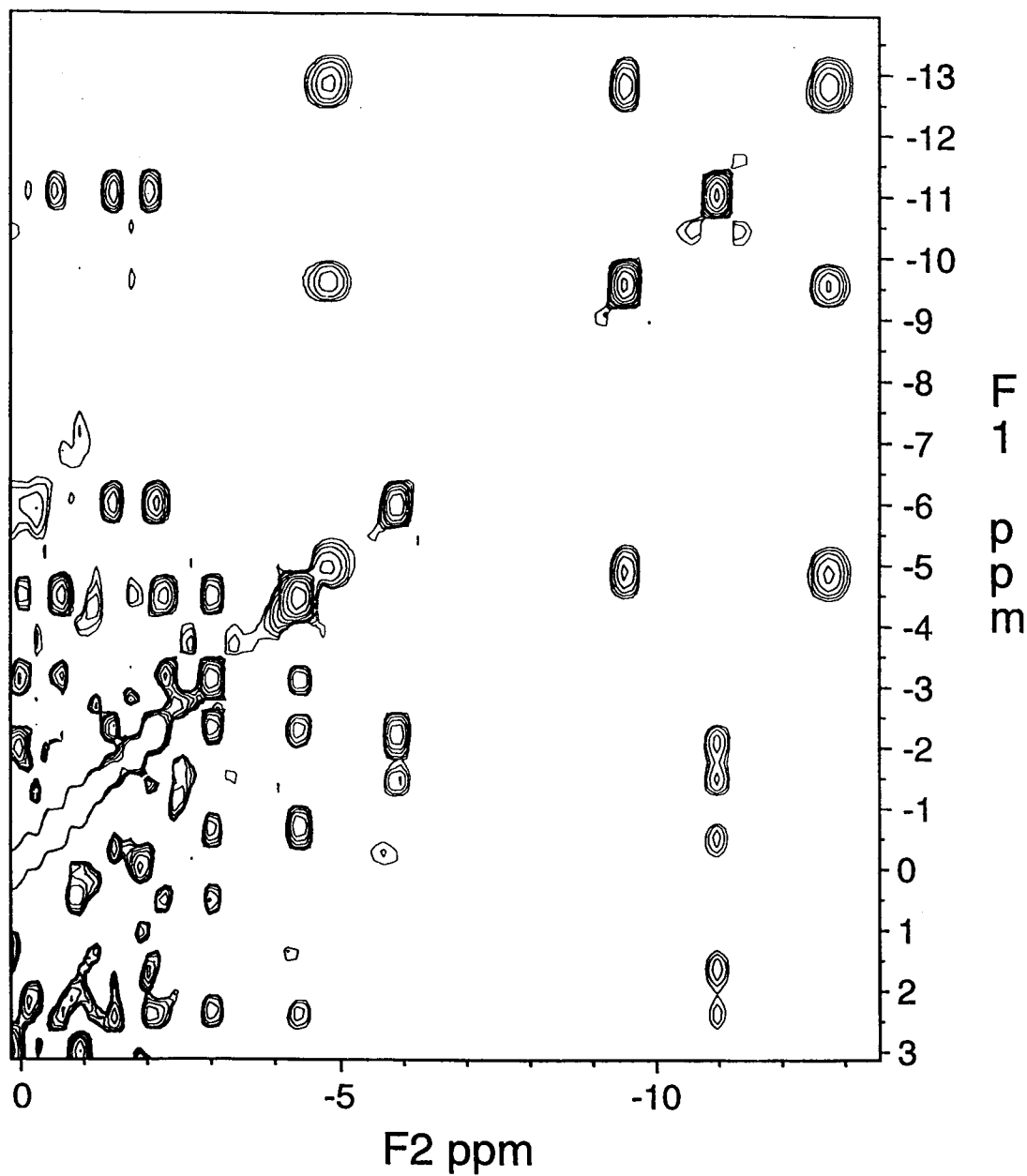


Figure 21 Upfield region of Figure 20 (apodized with a sine bell square function shifted by 18°).

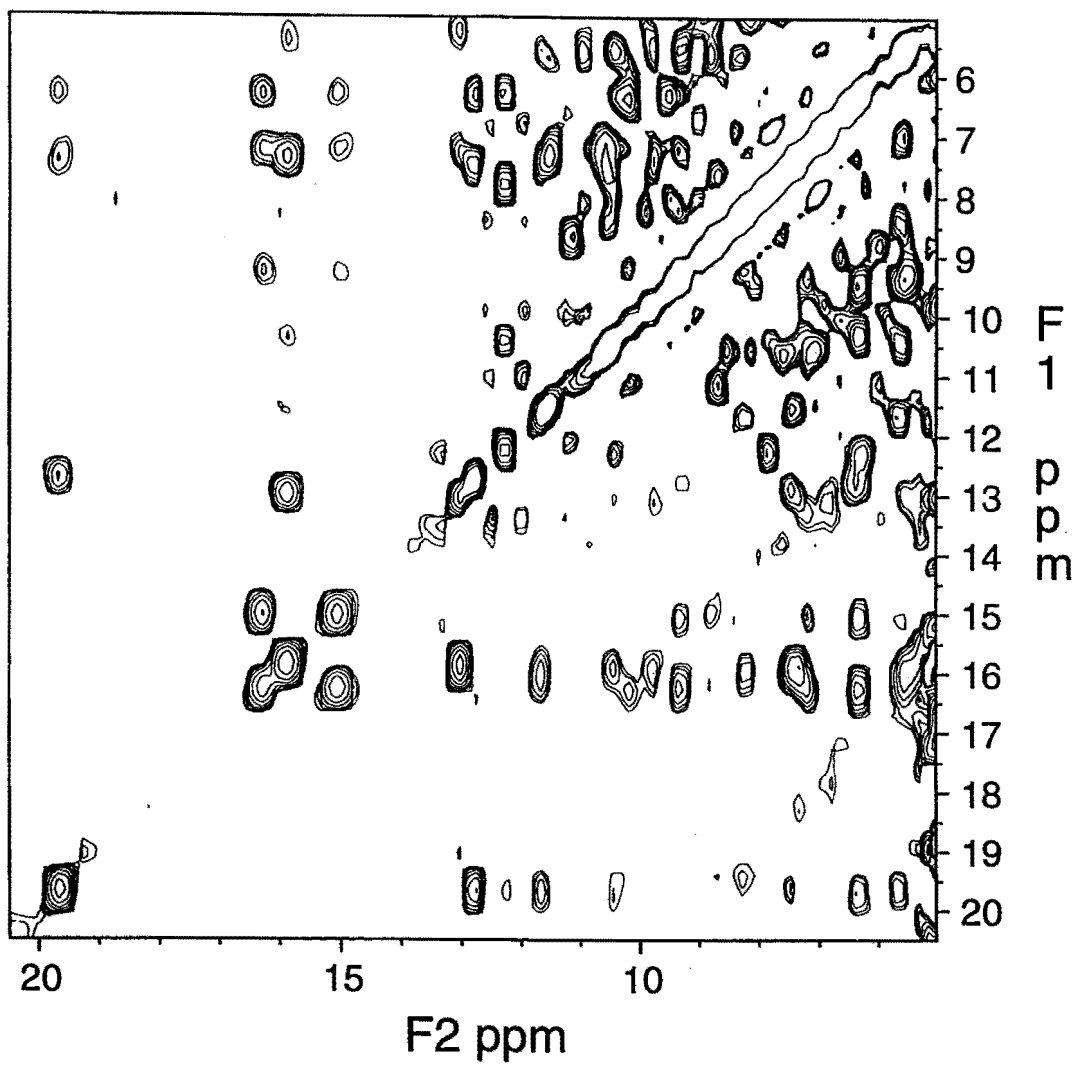


Figure 22 Downfield region of Figure 20 (apodized with a sine bell square function shifted by 18°).

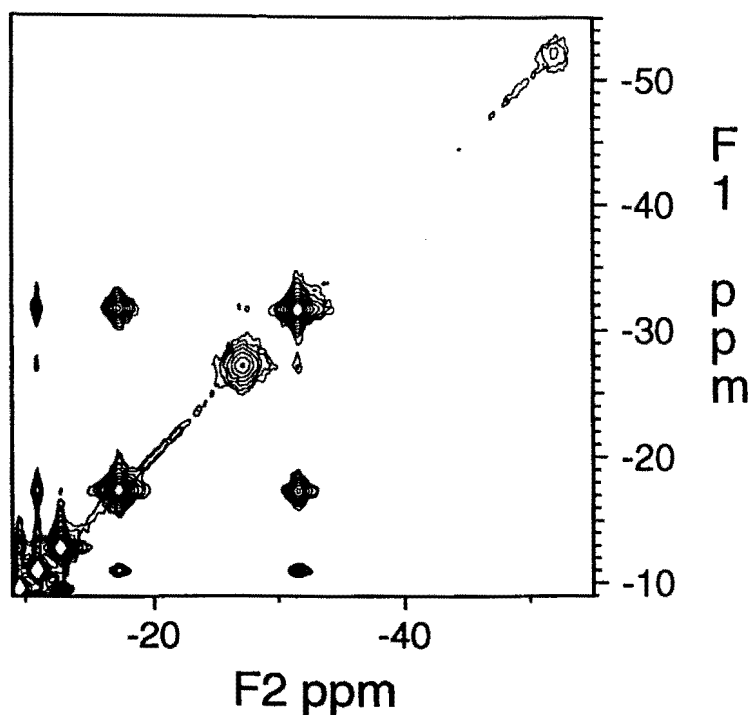
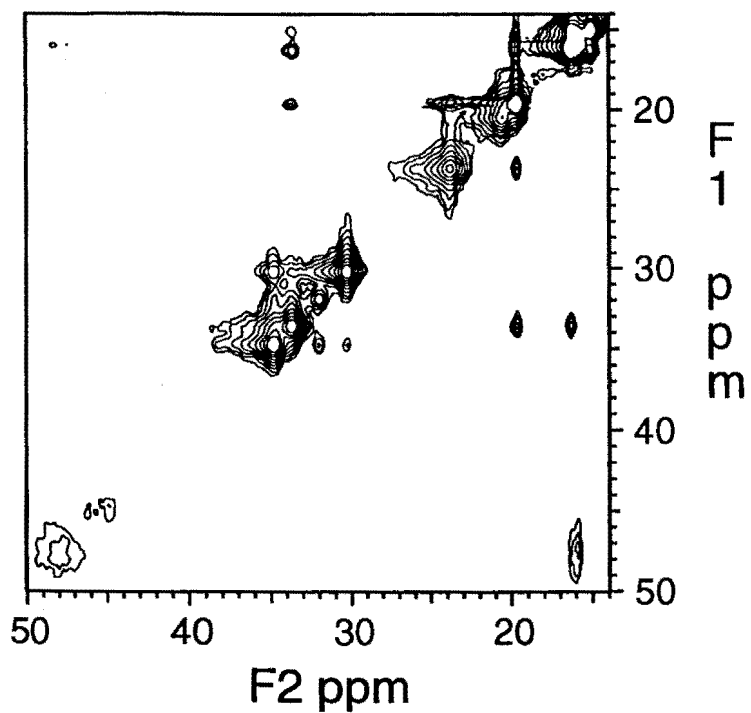


Figure 23

NOESY spectrum ($\tau_M = 20$ ms) of Yb-LA ([Yb-LA] = 4 mM in H₂O, 25 °C, pH 6.8, 400 MHz, apodized with a sine bell square function shifted by 54°).

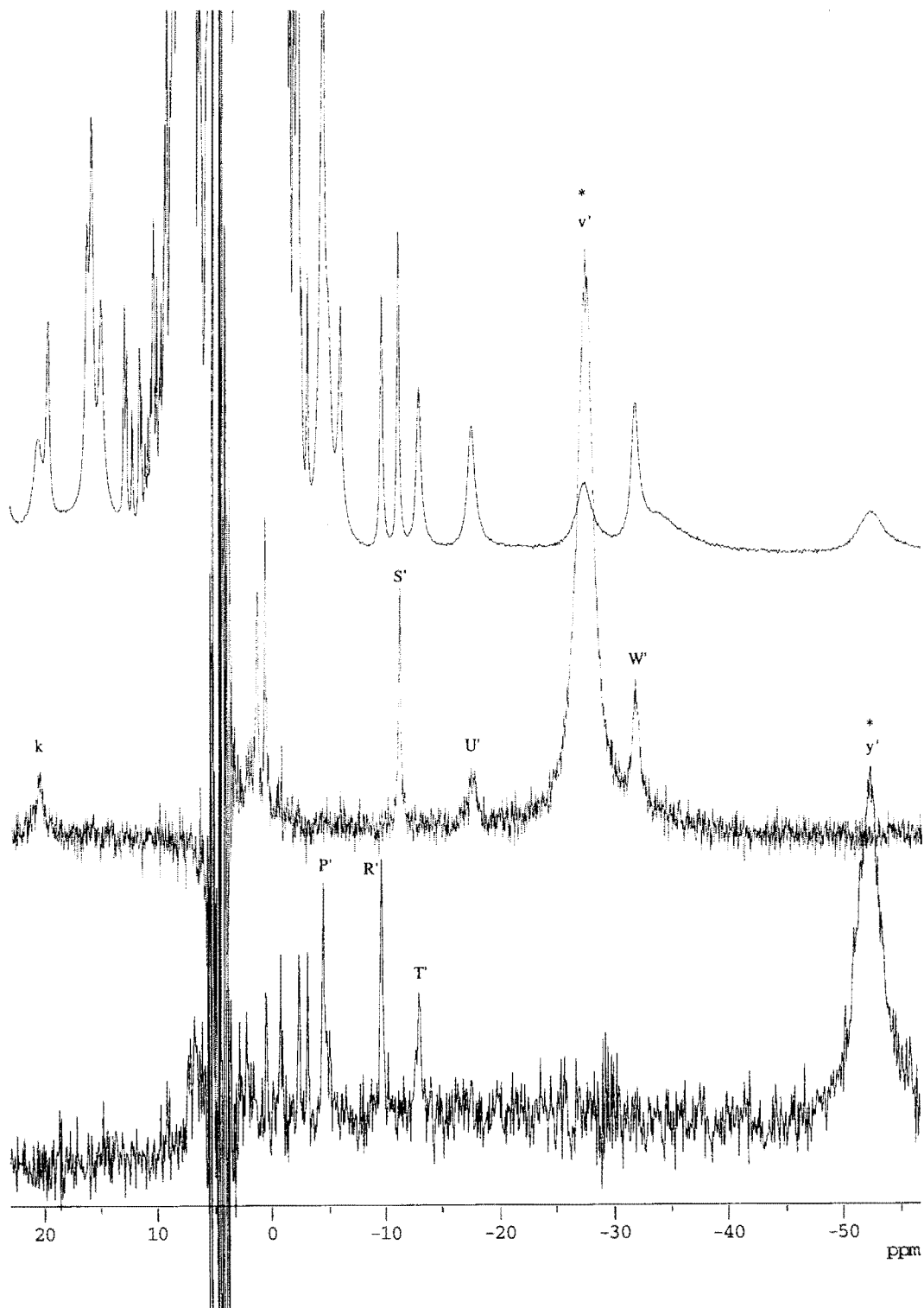


Figure 24 1D NOE experiment of Yb-LA ([Yb-LA] = 4 mM in H₂O, 25 °C, pH 6.8, 400 MHz); * indicates presaturated resonances; top spectrum is reference (from Figure 12).

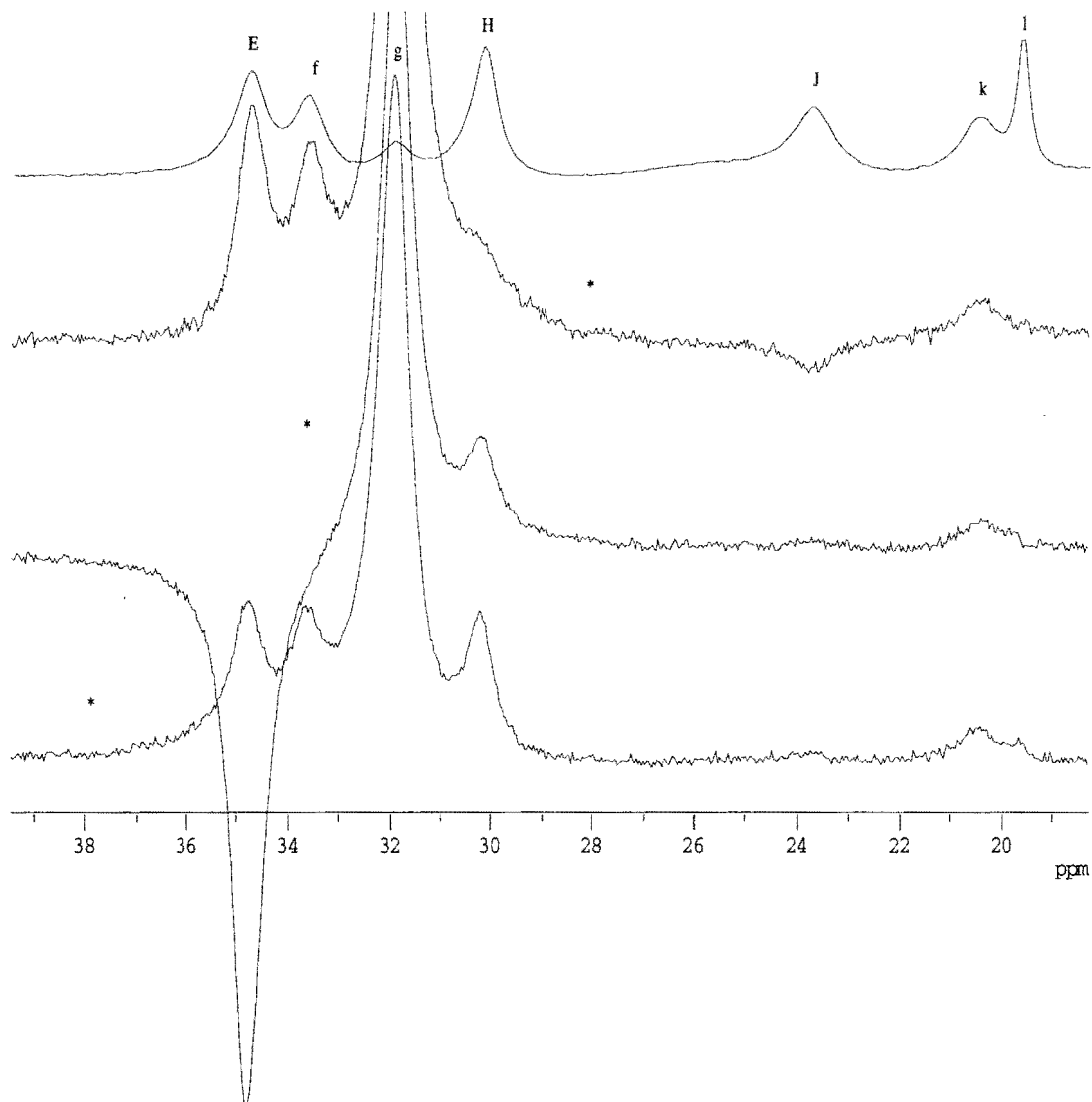
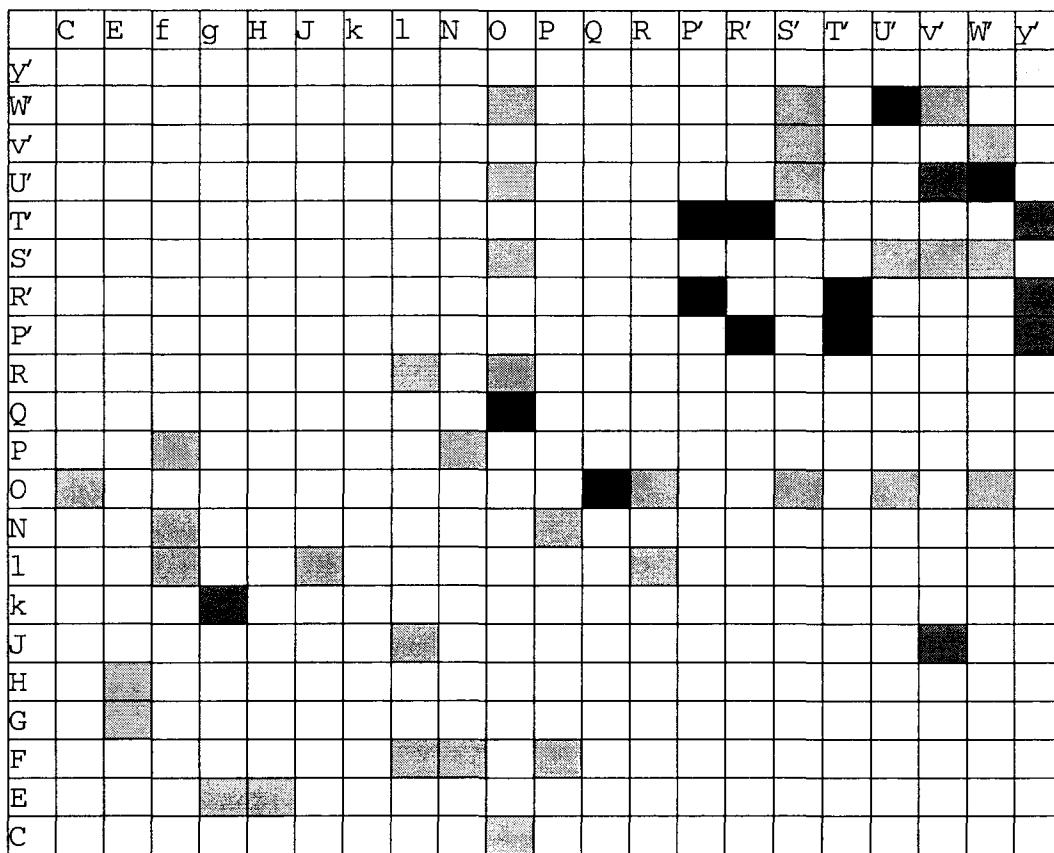


Figure 25 1D NOE experiment of resonance g of Yb-LA ([Yb-LA] = 4 mM in H₂O, 25 °C, pH 6.8, 400 MHz), solvent suppression "jump-return"; * indicates presaturation; top spectrum is reference (from Figure 12).



NOESY
 NOESY+COSY
 Diagonal Peaks
 1D NOE

Figure 26 Summary of cross signals between hyperfine shifted resonances in the 2D NMR spectra of Yb-LA.

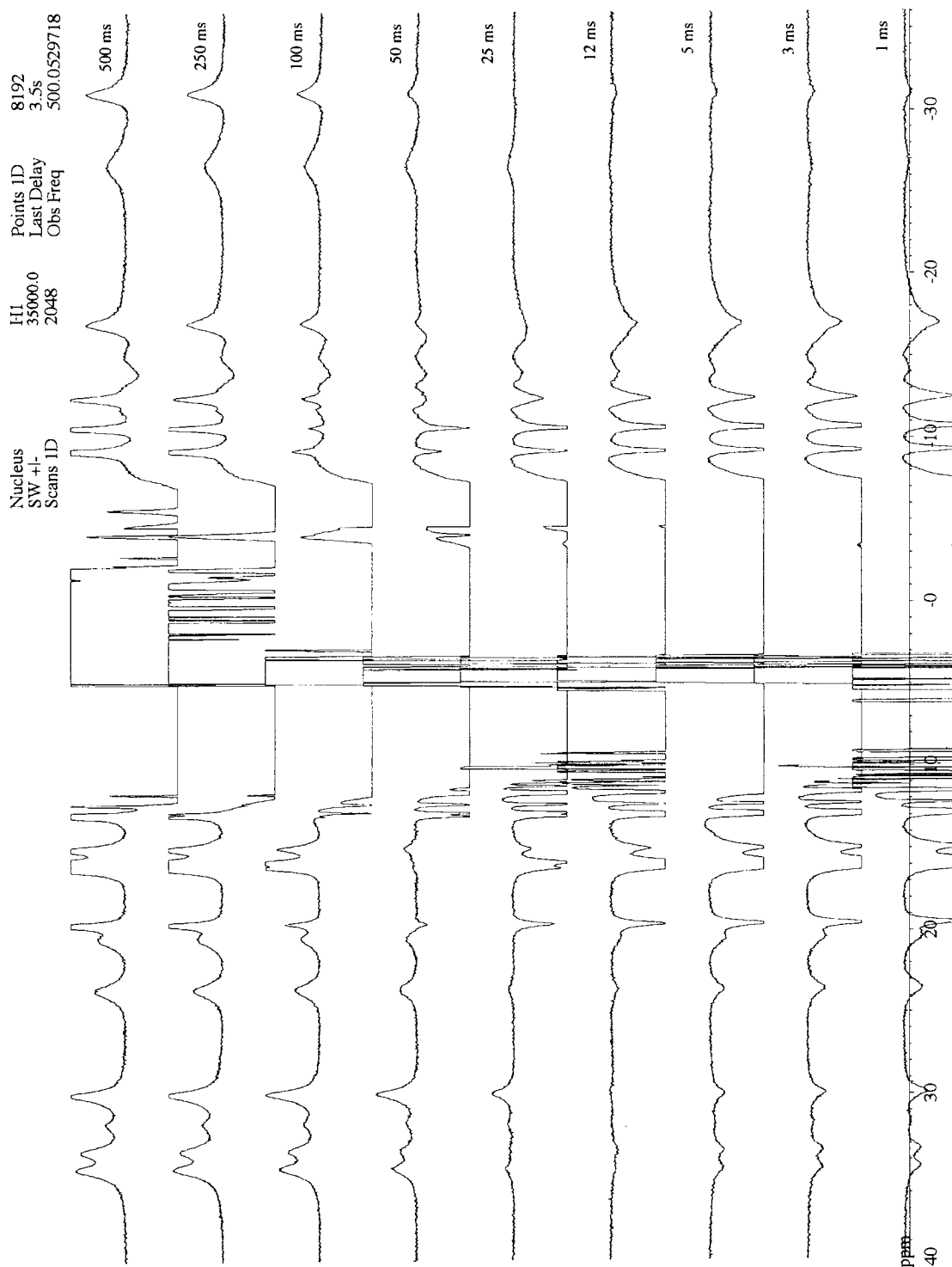


Figure 27 T1 IR experiment of Yb-LA ([Yb-LA] = 4 mM in H₂O, 25°C, pH 6.8, transmitter at 4.76 ppm).

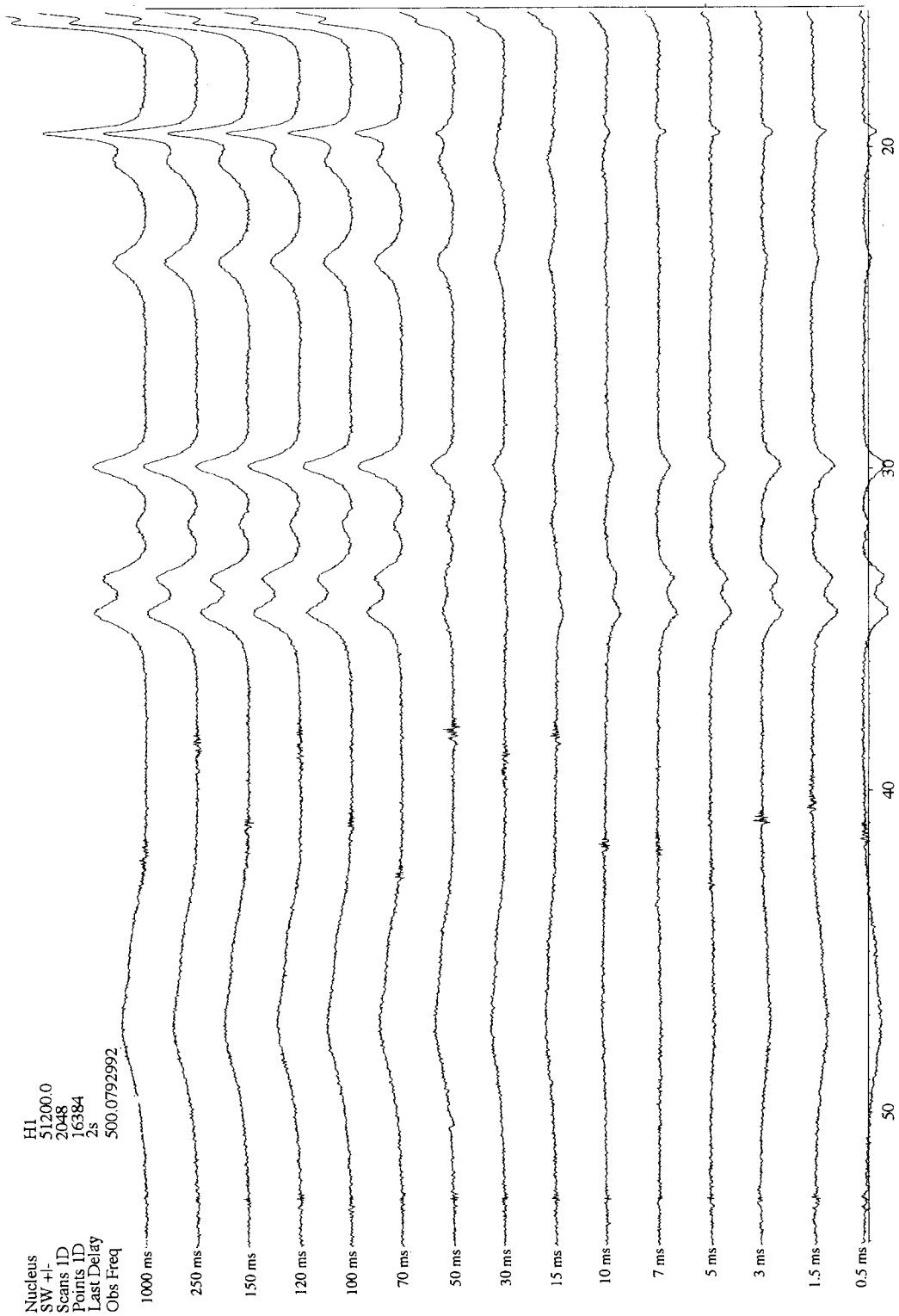


Figure 28 T1 IR experiment of Yb-LA ([Yb-LA] = 4 mM in H₂O, 25°C, pH 6.8, transmitter at 57.4 ppm).

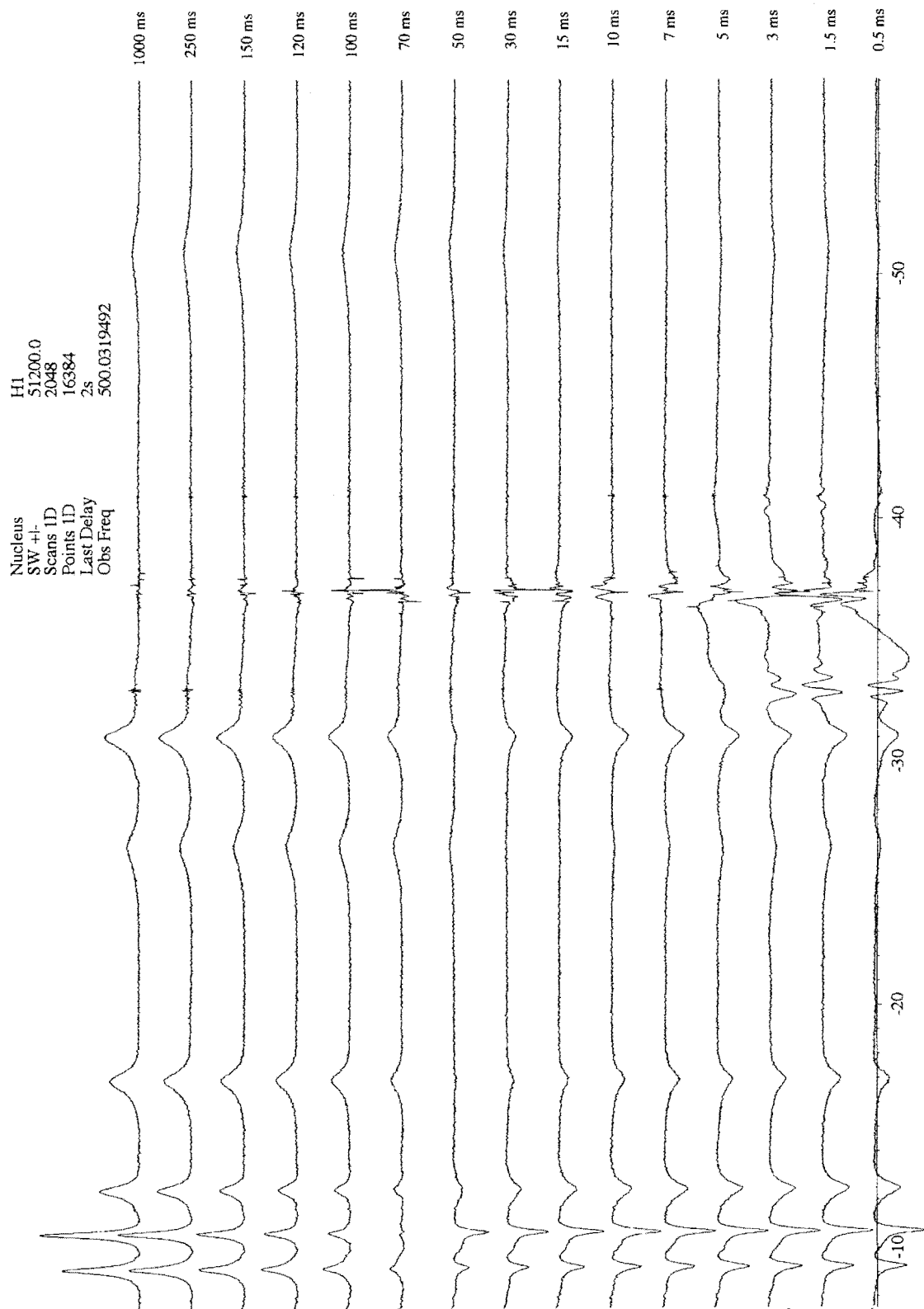


Figure 29 T1 IR experiment of Yb-LA ([Yb-LA] = 4 mM in H₂O, 25°C, pH 6.8, transmitter at 37.3 ppm).

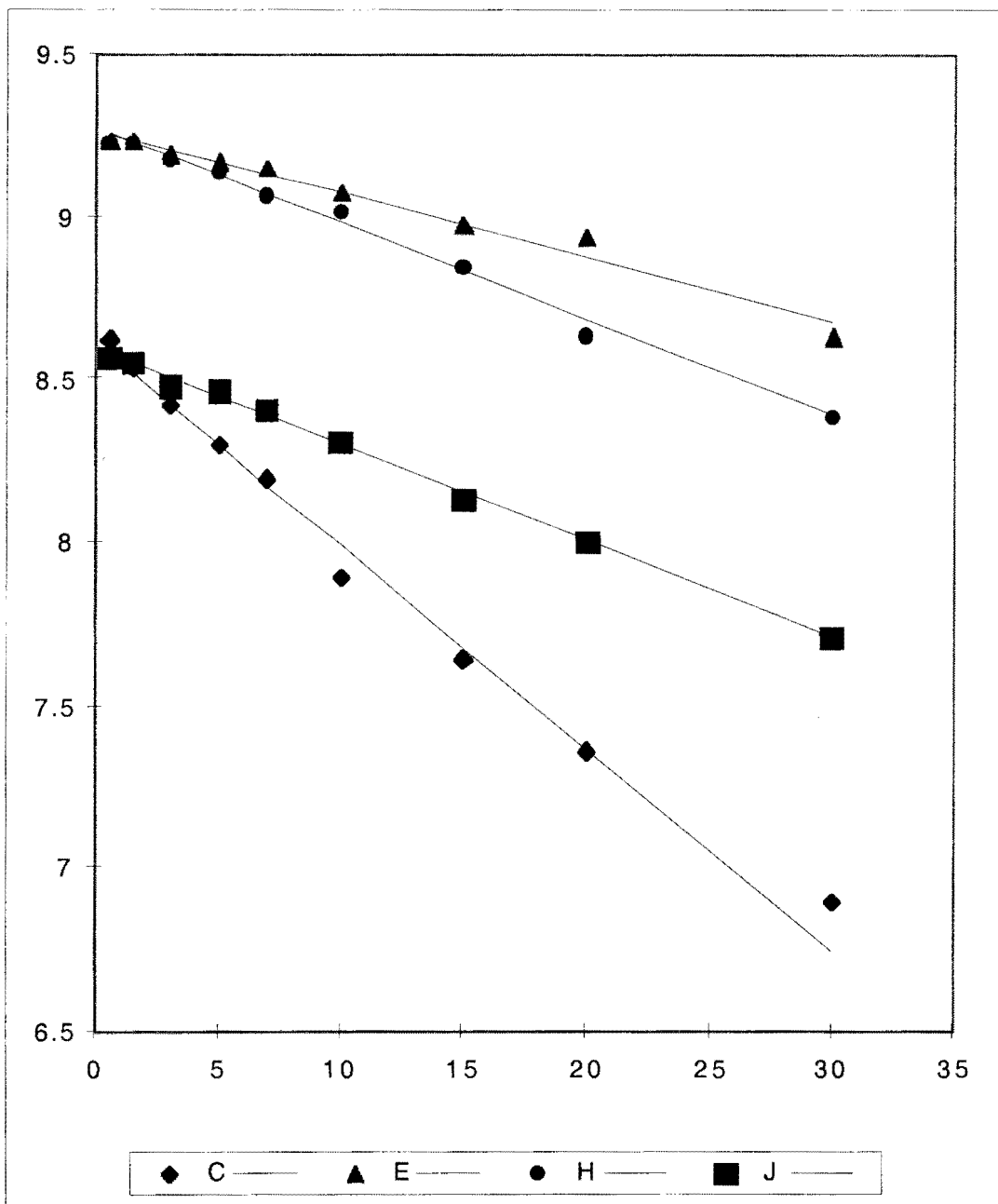


Figure 30 Linear regression of peak intensities of some resonances of Yb-LA for T_1 determinations by inversion recovery.

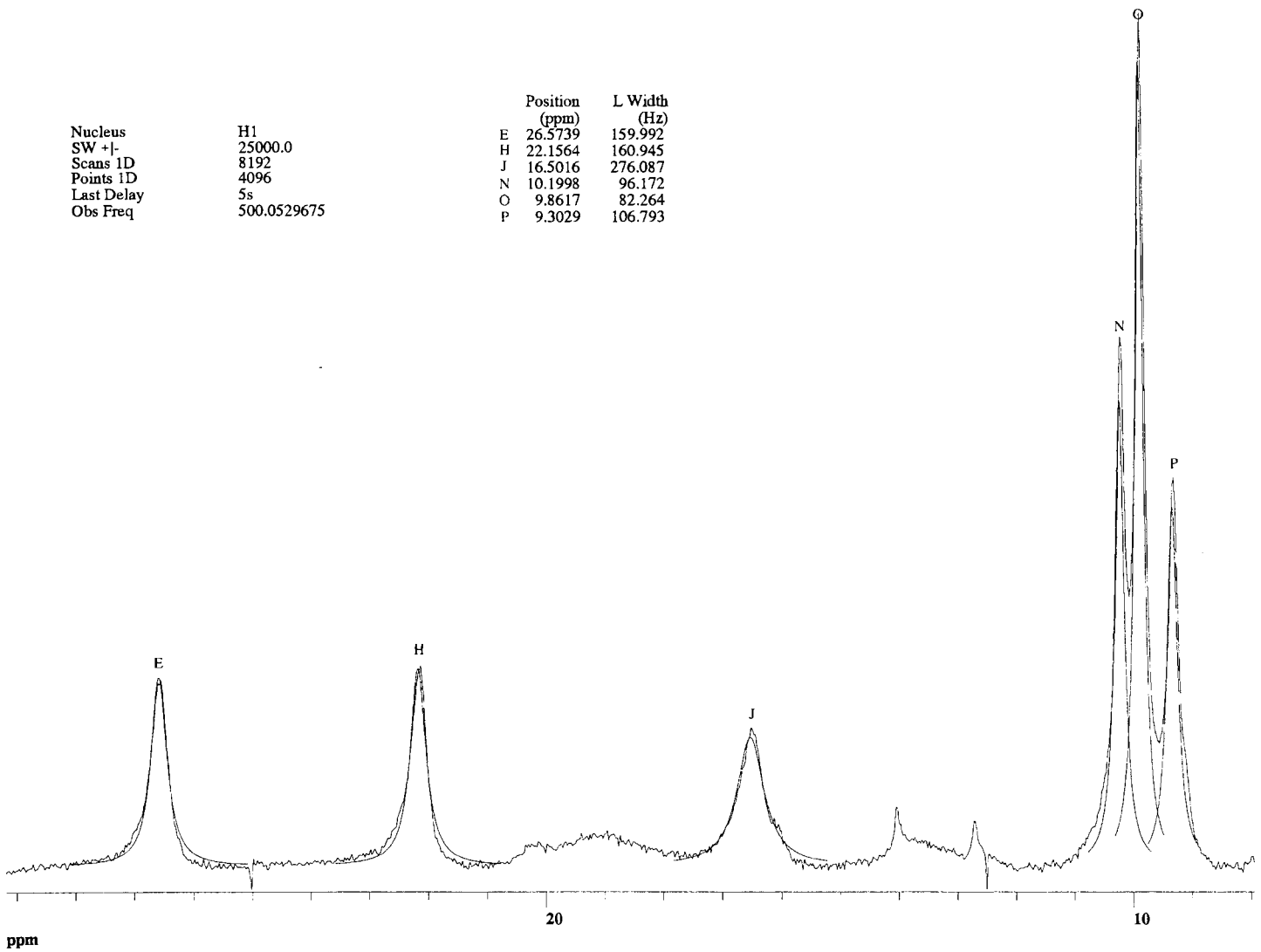


Figure 31 Peak simulations of some resonances of Yb-LA for T_2 determinations from line-widths ([Yb-LA = 4 mM in D_2O , 25 °C, pH 6.8).

REFERENCES

- Abragam, A. (1961) in *The principles of nuclear magnetism* pp 47, Oxford University Press, London and New York.
- Acharya, K. R., Ren, J., Stuart, D. I., & Phillips, D. C. (1991) *J. Mol. Biol.* 221, 571-581.
- Acharya, K. R., Stuart, D. I., Walker, N. P. C., Lewis, M., & Philips, D. C. (1989) *J. Mol. Biol.* 208, 99-127.
- Alexandrescu, A. T., Broadhurst, R. W., Wormald, C., Chyan, C., Baum, J., & Dobson, C. M. (1992) *Eur. J. Biochem.* 210, 699-709.
- Aramini, J. M., Hiraoki, T., Grace, M. R., Swaddle, T. W., Chiancone, E., & Vogel, H. J. (1996) *Biochim. Biophys. Acta* 1293, 72-82.
- Balacco, G. (1994) *J. Chem. Int. Comput. Sci.* 34, 1235-1241.
- Banci, L., Bertini, I., & Luchinat, C. (1991) *Nuclear and electron relaxation. The electron nucleus hyperfine coupling in diluted systems*, VCH, Weinheim.
- Baum, J., Dobson, C. M., Evans, P. A., & Hanley, C. (1989) *Biochemistry* 28, 7-13.
- Bax, A., & Davis, D. G. (1985) *J. Magn. Res.* 65, 355.
- Bax, A., Freeman, R., & Harris, G. (1981) *J. Magn. Res.* 42, 164-168.
- Berliner, L. J., Ellis, P. D., & Murakami, K. (1983) *Biochemistry* 22, 5061-5063.
- Berliner, L. J., Koga, K., Nishikawa, H., & Sheffler, J. (1987) *Biochemistry* 26, 5769-5774.
- Bernstein, F. C., Koetzle, T. F., Williams, G. J. B., Meyer, E. F., Brice, M. D., Rogers, J. R., Kennard, O., Shimanouchi, T., & Tasumi, M. (1977) *J. Mol. Biol.* 112, 535-542.
- Bleany, B. (1972) *J. Magn. Res.* 8, 91-100.

- Bloch, F. (1946) *Phys. Rev.* 70, 460-474.
- Braunschweiler, L., & Ernst, R. R. (1983) *J. Magn. Res.* 53, 521-528.
- Brodbeck, U., Denton, W. L., Tanahashi, N., & Ebner, K. E. (1967) *J. Biol. Chem.* 242, 1391-1397.
- Brodbeck, U., & Ebner, K. E. (1966) *J. Biol. Chem.* 241, 762-764.
- Campbell, I. D., Dobson, C. M., & Williams, R. J. P. (1975) *Proc. Roy. Soc. Lond. Ser. A* 345, 42-59.
- Chyan, C., Wormald, C., Dobson, C. M., Evans, P. A., & Baum, J. (1993) *Biochemistry* 32, 5681-5691.
- Cutnell, J. D., LaMar, G. N., & Kong, S. B. (1981) *J. Am. Chem. Soc.* 103, 3567-3572.
- Delaglio, F., Grzesiek, S., Zhu, G., Vuister, G. W., Pfeiffer, J., & Bax, A. (1995) *J. Biomol. NMR* 6, 277-293.
- Dill, K. A., & Shortle, D. (1991) *Annu. Rev. Biochem.* 60, 795-826.
- Dolgikh, D. A., Abaturon, L. V., Bolotina, I. A., Brazhnikov, E. V., Bychkova, V. E., Gilmanshin, R. I., Lebedev, Y. O., Semisotnov, G. V., Tiktopulo, E. I., & Ptitsyn, O. B. (1985) *Eur. Biophys. J.* 13, 109-121.
- Eberhard, M., & Erne, P. (1991) *Eur. J. Biochem.* 202, 1333-1338.
- Gansow, D. A., Loeffler, P. A., Davis, R. E., Lenkinski, R. E., & Willcott, M. R. I. (1976) *J. Am. Chem. Soc.* 98, 4250-4258.
- Guéron, M. (1975) *J. Magn. Res.* 19, 58.
- Guex, N., & Peitsch, M. C. (1997) *Electrophoresis* 18, 2714-2723.
- Hill, R. L., & Brew, K. (1975) *Adv. Enzymol. Relat. Areas Mol. Biol.* 43, 411-490.
- Hiraoka, Y., Segawa, T., Kuwajima, K., Sugai, S., & Murai, N. (1980) *Biochem. Biophys. Res. Commun.* 95, 1098-1104.

- Improta, S., Molinari, H., Pastore, A., Consonni, R., & Zetta, L. (1995) *Eur. J. Biochem.* 227, 87-96.
- Inubushi, T., & Becker, E. D. (1983) *J. Magn. Res.* 51, 128-133.
- Jeener, J., Meier, B. H., Bachmann, P., & Ernst, R. R. (1979) *J. Chem. Phys.* 71, 4546-4553.
- Karadi, R., Billeter, M., & Wüthrich, K. (1996) *J. Mol. Graphics* 14, 51-55.
- Kraulis, P. J. (1989) *J. Magn. Res.* 84, 627-633.
- Kumar, A., Ernst, R. R., & Wüthrich, K. (1980) *Biochem. Biophys. Res. Commun.* 95, 1-6.
- Kuwajima, K. (1989) *Proteins* 6, 87-103.
- Kuwajima, K., & Sugai, S. (1978) *Biophysical Chem.* 8, 247-254.
- LaMar, G. N., & deRopp, J. S. (1993) *Biol. Magn. Res.* 12, 1-78.
- Lee, L., & Sykes, B. D. (1980a) *Adv. Inorg. Biochem.* 2, 183-210.
- Lee, L., & Sykes, B. D. (1980b) *Biochemistry* 19, 3208-3214.
- Lee, L., & Sykes, B. D. (1980c) *Biophys. J.* 32, 193-210.
- Lee, L., & Sykes, B. D. (1980d) *J. Magn. Res.* 41, 512-513.
- Lee, L., & Sykes, B. D. (1981) *Biochemistry* 20, 1156-62.
- Lee, L., & Sykes, B. D. (1982) in *Biochemical Structure Determination by NMR* (Bothner-By, A. A., Glickson, J. D., & Sykes, B. D., Eds.) pp 169-185, Dekker, New York.
- Lee, L., & Sykes, B. D. (1983) *Biochemistry* 22, 4366-73.
- Levinthal, C. (1968) *J. Chim. Phys. Phys. Chim. Biol.* 65, 44-45.
- Luo, Y. (1996) *M.S. Thesis*, Portland State University, Portland, OR.
- Marion, D., & Wüthrich, K. (1983) *Biochem. Biophys. Res. Commun.* 113, 967-974.

- McDonald, C. C., & Phillips, W. D. (1969) *Biochem. Biophys. Res. Commun.* 35, 43-51.
- Müller, N., Ernst, R. R., & Wüthrich, K. W. (1986) *J. Am. Chem. Soc.* 108, 6482-6496.
- Musci, G., & Berliner, L. J. (1985) *Biochemistry* 24, 3852-3856.
- Musci, G., Reed, H. G., & Berliner, L. J. (1986) *Inorg. Biochem.* 26, 229-236.
- Patt, S. L., & Sykes, B. D. (1972) *J. Chem. Phys.* 56, 3182.
- Piantini, U., Sörensen, O. W., & Ernst, R. R. (1982) *J. Am. Chem. Soc.* 104, 6800-6801.
- Pike, A. C., Brew, K., & Acharya, K. R. (1996) *Structure* 4, 691.
- Plateau, P., & Guéron, M. (1982) *J. Am. Chem. Soc.* 104, 7310-7311.
- Prasad, R. V., Butkowski, R. J., Hamilton, J. W., & Ebner, K. E. (1982) *Biochemistry* 21, 1479-1482.
- Ptitsyn, O. B. (1991) *FEBS Letters* 285, 176-181.
- Rance, M., Sörensen, O. W., Bodenhausen, P., Wagner, G., Ernst, R. R., & Wüthrich, K. (1983) *Biochem. Biophys. Res. Commun.* 117, 479-485.
- Rao, K. R., & Brew, K. (1989) *Biochem. Biophys. Res. Commun.* 169, 1390-1396.
- Ren, J., Stuart, D. I., & Acharya, K. R. (1993) *J. Biol. Chem.* 268, 19282-19292.
- Reuben, J. (1973) *J. Magn. Res.* 11, 103-104.
- Richardson, R. M., & Brew, K. (1980) *J. Biol. Chem.* 255, 3377-3385.
- Sanders, J. K. M., & Hunter, B. K. (1993) *Modern NMR Spectroscopy. A Guide for Chemists*, 2nd ed., Oxford University Press, Oxford and New York.
- Scheraga, H. A. (1961) *Protein Structure*, Academic Press Ltd., New York and London.
- Shewale, J. G., Sinha, S. K., & Brew, K. (1984) *J. Biol. Chem.* 259, 4947-4956.

Shimizu, A., Ikeguchi, M., & Sugai, S. (1993) *Biochemistry* 32, 13198-13203.

Solomon, I. (1955) *Phys. Rev.* 99, 559-565.

Sommers, P. B., & Kronman, M. J. (1980) *Biophysical Chem.* 11, 217-232.

Stuart, D. I., Acharya, K. R., Walker, N. P. C., Smith, S. G., Lewis, M., & Phillips,
D. C. (1986) *Nature* 324, 84-87.

Tanford, C. (1968) *Advan. Protein Chem.* 23, 121-282.

Vega, A. J., & Fiat, D. (1976) *Mol. Phys.* 31, 347-355.

Vold, R. L., Wangh, J. S., Klein, M. P., & Phelps, D. E. (1968) *J Chem Phys* 48,
3831-3832.

Wider, G., Hosur, R. V., & Wüthrich, K. (1983) *J. Magn. Res.* 52, 130-135.

Widman, A. (1899) *Z. Physiol. Chem.* 27, 575.

Wüthrich, K. (1986) *NMR of proteins and nucleic acids*, John Wiley & Son Inc, New
York.

APPENDIX A

Program used for distance calculations between metal ion and protons in LA (written by David H. Peyton).

```

c234567891123456789212345678931234567894123456789512345678961234567
c ***** DISTANCES *****
c Calculates the distance between 1 fixed points and N fixed
c points
c input: PDIST.IN, pdb format, be sure to kill all lines that
c are not atoms.
c EXCEPT: 1st line is the number of atoms (points) to be included
c in the calculation!
c 1000 atoms maximum!
c *****
  DIMENSION X1(1000),Y1(1000),Z1(1000)
  DIMENSION X2(1000),Y2(1000),Z2(1000)
  DIMENSION DIST(1000)
  DIMENSION atomname1(1000),resname1(1000),res1(1000)
  DIMENSION atomname2(1000),resname2(1000),res2(1000)
  OPEN (UNIT=1,FILE='PDIST.IN',STATUS='OLD')
  OPEN (UNIT=2,FILE='PDIST.OUT',STATUS='NEW')
  WRITE(9,*)'ENTER THE MAX DIST TO GIVE OUTPUT (5.0 may be OK) '
  DMAX=5.0
  READ(9,*)DMAX
  READ(1,5)N
  DO 100 I=1,N
    READ(1,80)atomname1(I),resname1(I),res1(I),X1(I),Y1(I),Z1(I)
100 CONTINUE
  DO 150 I=1,N
    atomname2(I)=atomname1(I)
    resname2(I)=resname1(I)
    res2(I)=res1(I)
    X2(I)=X1(I)
    Y2(I)=Y1(I)
    Z2(I)=Z1(I)
150 CONTINUE
  DO 170 I=1,N
    WRITE(2,20)'  '
    WRITE(2,30)' PT NUMBER', ' ATOM', ' X', ' Y', ' Z', ' DISTANCE'
    WRITE(2,20)'  '
    WRITE(2,10)' FIXED  ',atomname1(I),resname1(I),res1(I)
      1 ,X1(I),Y1(I),Z1(I)
    WRITE(2,20)'  '
  DO 200 L=1,N
    DIST(L)=SQRT((X1(I)-X2(L))**2+(Y1(I)-Y2(L))**2
      1          +(Z1(I)-Z2(L))**2)
    A=DIST(L)-DMAX
    IF (A) 300,200,200
300 CONTINUE
    WRITE(2,40)L,atomname2(L),resname2(L),res2(L)

```

```
1          ,X2(L) ,Y2(L) ,Z2(L) ,DIST(L)
200 CONTINUE
170 CONTINUE
  STOP
5  FORMAT(I3)
10 FORMAT(A12,2X,a4,1x,a3,3x,a3,4x,3(F7.3,4X),4X,A5)
20 FORMAT(A4)
30 FORMAT(A12,6X,a6,6x,3(4X,A,5X),3X,A10)
40 FORMAT(4X,I3,7X,A4,1x,a3,3x,a3,4x,3(F7.3,4X),2X,F7.2)
80 FORMAT(12x,a4,1x,a3,3x,a3,4x,3f8.3)
  END
```

APPENDIX B

AppleScript developed for adding two-dimensional NMR spectra.

```
set my_file_path to "Macintosh HD:test"    -- folder w/ files to be
                                           added
set my_list to list folder my_file_path
set my_creator to "MNM5"                  -- "MNM5" for MacNMR

tell application "MacNMR 5.4"
    activate
    Wait For Script

    -- define output file
    Get File Name
    set my_target_file to (Get File Specification) as string
    Get File Name {file my_target_file} with replacing

    repeat until my_list is {}

        set file_name to (my_file_path & ":" & first item of my_list)

        --make sure object is no folder
        set is_folder to folder of (info for alias file_name)
        if is_folder = false then

            set my_file_info to file creator of (info for alias file_name)

            --make sure file was created by MacNMR 5.*
            if my_file_info = my_creator then

                open {file file_name}
                Set Data Pointer 1
                set final to Get NMR Parameter name "Scans 2D"
                repeat with i from 1 to final
                    Add To File at record i without replacing
                    Increment Data Pointer
                end repeat

            end if

        end if

        close Window 1
        set my_list to rest of my_list

    end repeat

    open {file my_target_file}
    Script Done
end tell
```